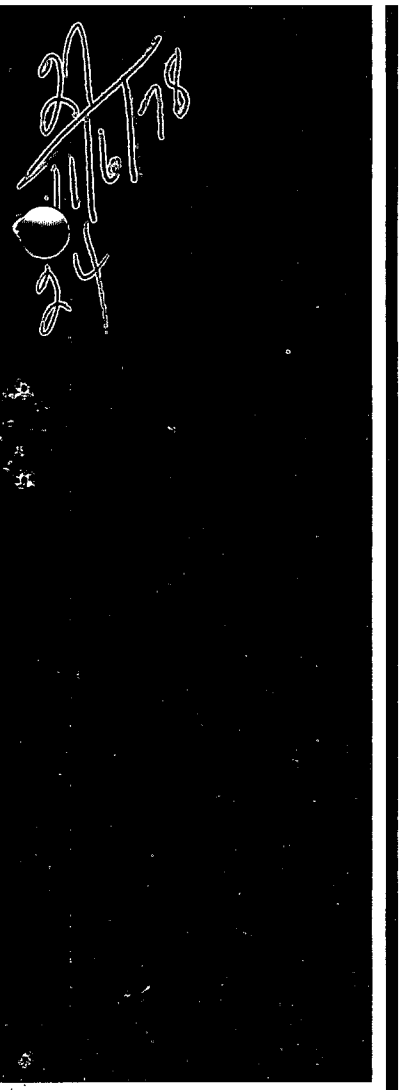

NUREG/CR-0274
ORNL/NUREG/TM-154

Fission Product Release from Simulated LWR Fuel

R. A. Lorenz
J. L. Collins
S. R. Manning

Prepared for the U.S. Nuclear Regulatory Commission
Office of Nuclear Regulatory Research
Under Interagency Agreements DOE 40-551-75 and 40-552-75

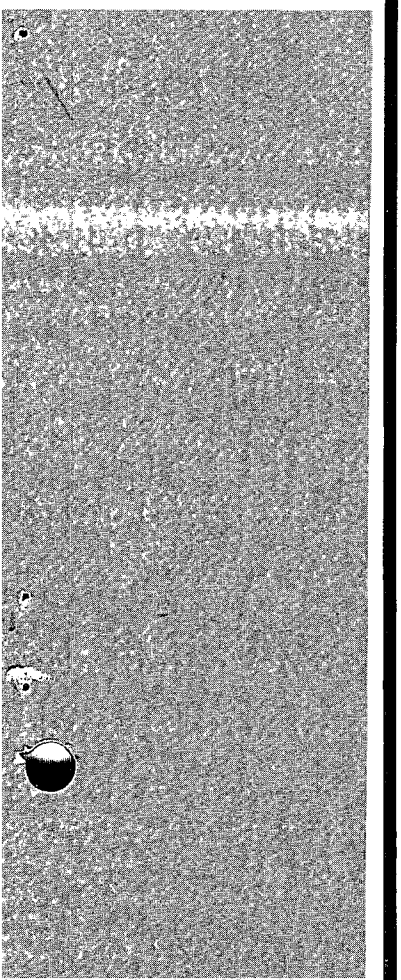

OAK RIDGE NATIONAL LABORATORY
OPERATED BY UNION CARBIDE CORPORATION · FOR THE DEPARTMENT OF ENERGY

Printed in the United States of America. Available from
National Technical Information Service
U.S. Department of Commerce
5285 Port Royal Road, Springfield, Virginia 22161

DISCLAIMER

The enclosed document has not received any secondary reviews by the U.S. Department of Energy's Office of Scientific and Technical Information (OSTI) for public releasability Post 9/11. It is being made available with the understanding that any further distribution, beyond the requesting organization, is the responsibility of the receiving organization/individual. Any distribution outside the DOE community may require additional reviews by the originating site in compliance with Secretary Abraham's May 30, 2002, memorandum titled "Safeguarding Information Pertaining to Weapons of Mass Destruction and Other Sensitive Information."

NUREG/CR-0274
ORNL/NUREG/TM-154
Dist. Category R3

Contract No. W-7405-eng-26

CHEMICAL TECHNOLOGY DIVISION

FISSION PRODUCT RELEASE FROM SIMULATED LWR FUEL

R. A. Lorenz
J. L. Collins
S. R. Manning

Manuscript Completed: July 1978
Date Published: October 1978

Prepared for the
U.S. Nuclear Regulatory Commission
Office of Nuclear Regulatory Research
Washington, D.C. 20555
Under Interagency Agreements DOE 40-551-75 and 40-552-75

NRC FIN No. B0127

Prepared by the
OAK RIDGE NATIONAL LABORATORY
Oak Ridge, Tennessee 37830
operated by
UNION CARBIDE CORPORATION
for the
DEPARTMENT OF ENERGY

TABLE OF CONTENTS

FISSION PRODUCT RELEASE FROM SIMULATED LWR FUEL

R. A. Lorenz
J. L. Collins
S. R. Manning

ABSTRACT

A series of tests has been conducted with simulated LWR fuel as part of a program for determining the quantities and characteristics of radiologically significant fission products that can be released under postulated spent-fuel transportation accident (SFTA) conditions and successfully terminated loss-of-coolant accident (LOCA) conditions. These tests were performed in either flowing-steam or dry-air atmospheres with Zircaloy-4-clad fuel-rod segments that contained unirradiated UO_2 pellets coated with radioactively traced CsOH, CsI, and TeO_2. A brief summary of the test conditions and amounts released are given below.

Implant test	Temp. (°C)	Atmosphere	Test period (hr)	Percent of inventory released		
				Cs	I	Te
1	700	steam	1.0	10.8	22.5	-
2	700	steam	1.5	7.3	16.5	-
3	900	steam	2.0	7.7	25.6	1.6
4	1100	steam	1.0	25.2	32.9	0.1
5	700	steam	2.0	5.5	17.8	6.5
6	500	steam	20.0	$\leq$0.4	0.65	0.50
7	700	air	5.0	1.1	11.6	<0.015
8	1100	steam	1.0	35.9	65.8	3.3
9	500	air	20.0	0.30	8.6	0.003
10	700	steam	5.0	0.07	1.8	0.16
11	1300	steam	0.25	28.0	4.5	1.0
12	900	steam	2.0	24.9	60.3	1.6

Cesium release associated with the implanted CsOH appeared to be limited by the formation of low-volatility uranate compounds. Iodine release was observed primarily as CsI, but also as I_2; in addition, at test temperatures of 900°C and above, significant migration of the CsI to the cooler ends of the fuel-rod segments was noted. Tellurium release was markedly restricted by rapid reaction with the Zircaloy cladding. The tests in air yielded enhanced releases of cesium and iodine, and considerable

swelling of the oxidized UO_2. As anticipated, measured release fractions were greater when the test rods were ruptured at temperature by internal pressure than when the cladding failures were machined in the rods prior to testing.

---

1. INTRODUCTION

Fission products that accumulate in the fuel-to-cladding gap region of light water reactor (LWR) fuel rods during the several years of normal operation are the principal source of radionuclides that can be released from defected rods under controlled loss-of-coolant accident (LOCA) and spent-fuel transportation accident (SFTA) conditons. As part of a program to characterize the release of fission products from the gap region, a series of experiments was performed in which the gap inventories of the volatile fission products--cesium, iodine, and tellurium--were simulated by coating unirradiated UO_2 pellets with suitably radiotracer-tagged amounts of CsOH, CsI, and TeO_2. This series of experiments, which is designated as the Implant Test Series, followed the Control Test Series in which individual species were introduced directly into the test apparatus.[1] These two series were preliminary to release studies currently being conducted with low-burnup fuel capsules [$\sim$1000 MWd/metric ton (MT)] irradiated in the General Electric Test Reactor, and with high-burnup fuel segments ($\sim$30,000 MWd/MT) from the H. B. Robinson reactor, a commercial pressurized water reactor (PWR).

The primary objectives of the experimental program are to determine the quantities of radiologically significant fission products released from defected fuel rods in steam and air at temperatures characteristic of SFTA (700°C, max) and controlled LOCA (1200°C, max cladding temperature) conditions, and to identify their chemical and physical forms. (Most previous fission product work was performed at higher temperatures, many including the melting of UO_2, with emphasis on mixed steam-air atmospheres.) The information derived from this program will provide source-term data for use in computer models of a variety of accident scenarios currently being assembled in the Fission Product Transport Analysis Program

by Battelle Columbus Laboratories, also under the sponsorship of the United States Nuclear Regulatory Commission. The experiments in the program are not intended to simulate any particular postulated accidents; rather, the observed physicochemical behavior will be translated into specific accident behavior by means of the computer models.

The use of fission product simulants has permitted flexibility in the parameters under study and ease of post-experiment analysis at less cost and greater safety than with tests involving highly irradiated fuel rods. The parameters investigated in the Implant Test Series include nuclide concentration, behavior of isolated compounds, nature of defect opening (drilled and ruptured), atmosphere (steam or air), and temperature. Moreover, if the results obtained in this series are validated by the irradiated fuel experiments, simulated studies can be readily extended at some future date, if needed, to include detailed examination of the following additional parameters: (1) fuel-rod length, (2) defect size (in more detail), (3) pellet-to-cladding gap clearance, (4) realistic thermal gradients and their effects (which may be locally large during emergency coolant application), and (5) transient (temperature) studies.

2. DEVELOPMENT OF AN IMPLANTATION TECHNIQUE

Because of the costs and experimental difficulties associated with the use of fully irradiated fuel in studies of fission product behavior, most researchers seek to develop fuel preparation methods and experimental techniques which simulate as closely as possible typical conditions. Although the extent to which the simulant accurately corresponds to the actual situation is open to examination, a recent review[2] of the use of simulants vis-a-vis irradiated fuel has concluded that, if essential differences in fission product behavior are indeed present, these are insignificant when viewed in terms of the sensitivity to experimental conditions. It must be kept in mind, however, that this conclusion applies strictly to conditions of meltdown, wherein the high temperatures involved tend to minimize the importance of kinetics in determining chemical from.

Similarly, for reasons of experimental convenience and economy, we have developed a method of simulating fission product behavior in the fuel-clad gap of unirradiated fuel. The objective was to distribute the fission product simulants on the surfaces of the UO_2 pellets, since additional release from the pellet matrix is inconsequential under the present set of test conditions.

A typical fuel rod used in an Implant Test is sketched in Fig. 1, and the method of implanting the fission products is outlined. Note that three pellets at each end of the test fuel rod were not treated so that axial migration within the fuel rod could be examined.

Only CsI was employed in Implant Tests 1 and 2, whereas the remaining tests utilized cesium as both CsI and CsOH. Cesium iodide, which contained $\sim$10% ^{129}I, was first irradiated to provide the ^{134}Cs and ^{130}I radiotracers. The crystalline CsI was then dissolved in a few drops of water and (for tests using CsOH also) mixed with dissolved CsOH under an argon atmosphere to minimize exposure to CO_2. After placing the UO_2 pellets on a large petri dish and warming them with a hot plate to $\sim$90°C (the pellets will not become wetted if cool), the pellets were coated with the simulant aqueous solution. In the experiments in which water-insoluble TeO_2 was employed, the ^{123m}Te-traced powder was divided into 24 aliquots that were applied to the concave ends of the pellets while the UO_2 was cool. Adhesion of the TeO_2 to the fuel was accomplished by adding a drop of water to the TeO_2 within the concave face of the pellet and heating the resultant slurry to dryness on a hot plate.

The pellets were then assembled in the Zircaloy rod and, after being subjected to a 1-hr heat treatment of 200°C under vacuum conditions, the rod was filled with argon. Afterwards, the assembly was maintained at 400°C for 16 hr to permit an approach to chemical equilibrium within the assembly prior to actual experimentation. The amounts of fission product simulants used generally correspond to a 3% release to the gap space within a spent-fuel-rod segment of the size employed in the test.

ORNL DWG 76-71

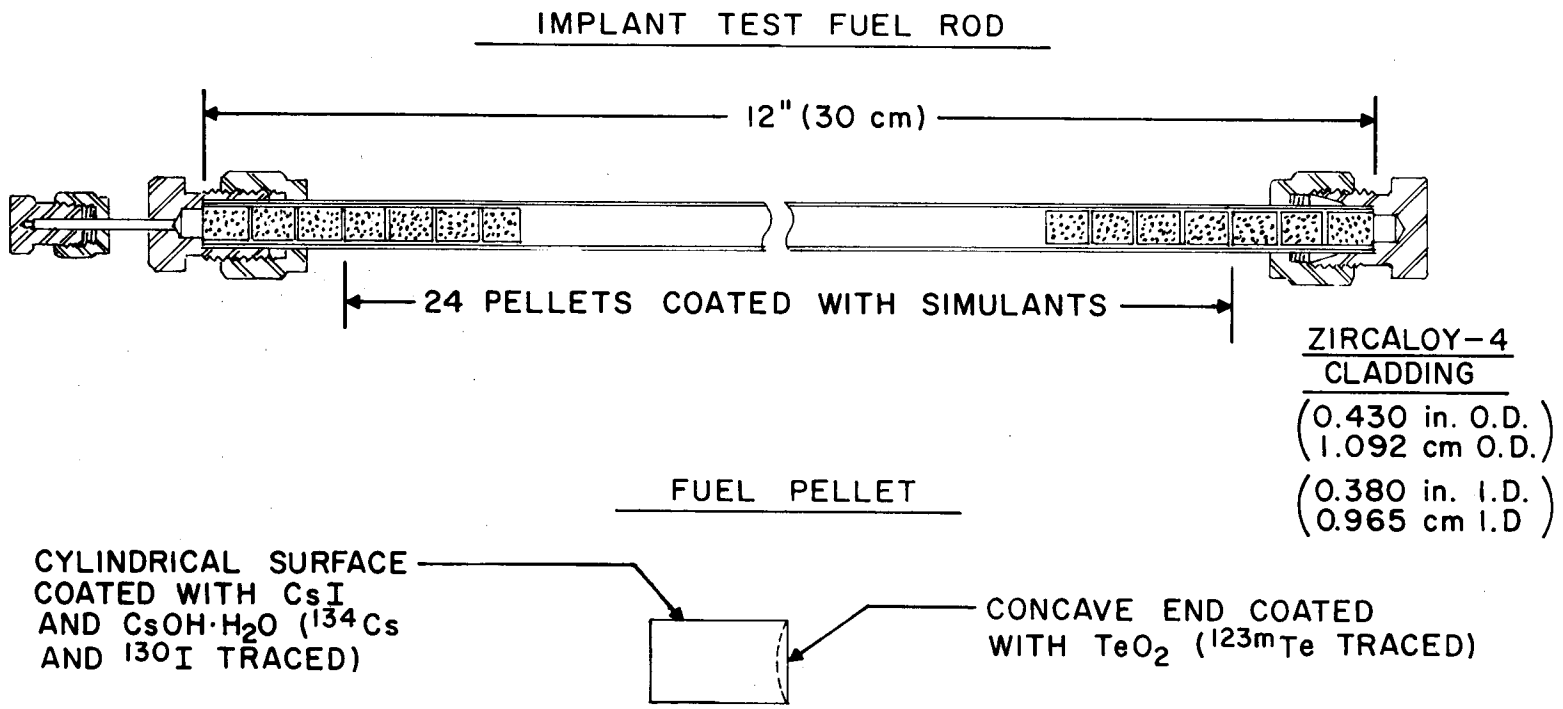

Fig. 1. Implant test fuel rod.

3. EXPERIMENTAL APPARATUS

The apparatus arrangement shown in Fig. 2 was used in the Implant Test Series. It was developed on the basis of the experience acquired during the conduct of the Control Test Series.[1] The actual components of the system are shown in Fig. 3.

In a typical Implant Test, the fuel specimen (5) was placed in a quartz liner (4) which was positioned within the quartz furnace tube (2) and heated by an induction coil (8) or resistance heater (1) to the desired temperature. The defect opening was provided by drilling a 1/16-in.-diam hole through the cladding at mid-capsule or by applying internal argon gas pressure (6) to the capsule (at 700 or 900°C) to cause rupture. A flowing-steam--argon mixture [300 cm^3/min (STP) steam + 75 cm^3/min (STP) argon] was generated by bubbling argon through a steam generator (Fig. 2) at 95.6°C. (Dry air was employed in Implant Tests 7 and 9.) The flowing gas swept away those species that were vented from the capsule. Released material that did not condense or react with the quartz liner of the furnace tube was transported to the gold-lined quartz thermal gradient tube (10), where released species condensable above 125°C were deposited. Particles capable of being transported by the carrier gas beyond the thermal gradient tube were separated into five decreasing particle-size fractions (1.3 to 0.1 μ aerodynamic diam) on Teflon membranes on the stages (14) within an all-aluminum low-pressure cascade impactor (13). The low pressure was provided by a vacuum pump (see Fig. 2) and an aluminum orifice plate (12) held in a stainless steel housing (11). Downstream, a stainless steel filter pack assembly (15) containing three high-efficiency filter papers (16) (Reeve Angel 934 AH pure borosilicate glass fiber) completed the collection of particulates. The assembly also contained fine-mesh silver-plated screens (17) to collect the reactive forms of iodine such as I_2 and HI. The next component in the apparatus train was an aluminum adsorber housing assembly (18) which contained three charcoal cartridges (19) (fine grain, -12+16 mesh, 5% TEDA-impregnated charcoal) and one silver-exchanged zeolite adsorber cartridge, -12+16 mesh, to collect the less-reactive, more-penetrating chemical forms of iodine. An ice-bath-cooled condenser (20)

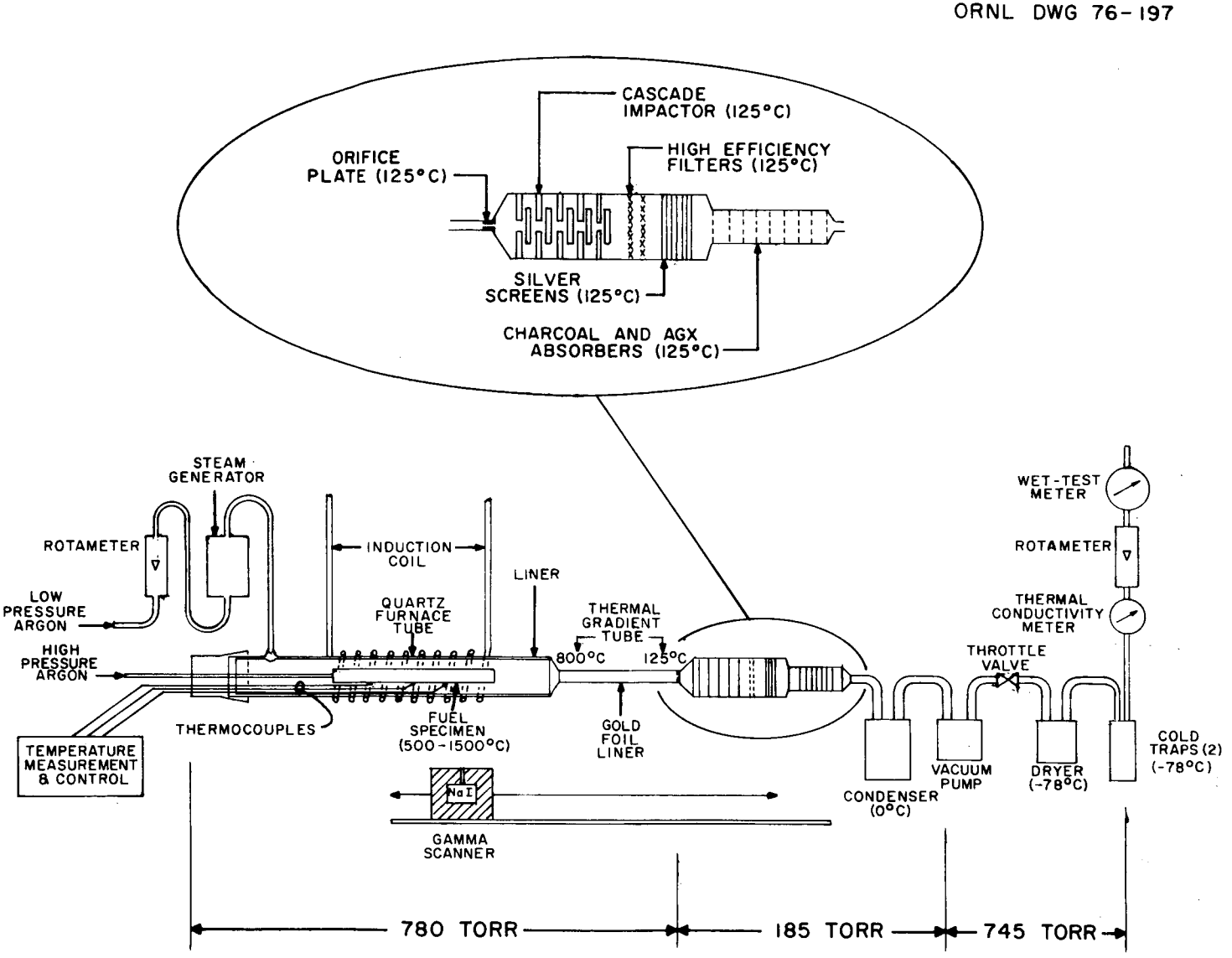

Fig. 2. Apparatus for studies of fission product release from LWR fuel-rod segments.

ORNL PHOTO: 0834-76A

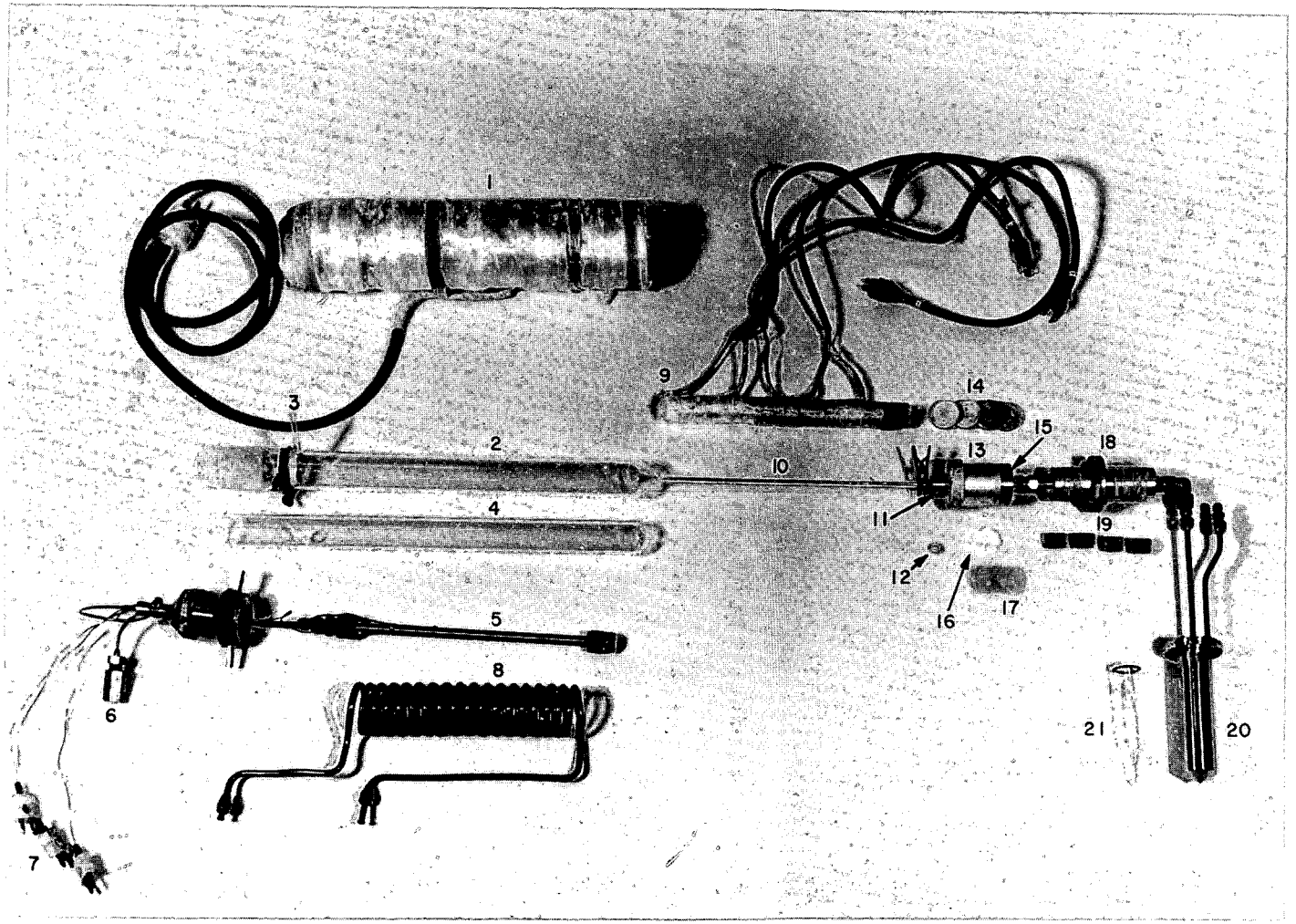

Fig. 3. The experimental apparatus used in the Implant Test Series (components identified on pp. 6 and 9 in the text).

containing a Pyrex graduate (21) was used to condense and collect the steam. Also, the apparatus was equipped with a dry-ice-cooled freeze trap (Fig. 2) to remove the last traces of moisture, with two charcoal traps at dry-ice temperatures (which will be used to trap fission product noble gases in tests with irradiated fuel), with a thermal conductivity meter for monitoring hydrogen produced from the steam-Zircaloy reaction, and lastly, a wet-test meter for measuring effluent argon and monitoring large amounts of hydrogen. Other components identified in Fig. 3 are a blank end cap and steam inlet location (3), connectors for thermocouples on the fuel rod (7), and the thermal gradient tube heater (9).

A mobile NaI (Tl activated) gamma scanner, as shown in Fig. 2, was employed in Implant Tests 1 through 5 to monitor the iodine released. In Implant Tests 6 through 12, two stationary NaI(Tl) crystals were used: one monitored the radiotracers as they were deposited on the thermal gradient tube; the other monitored these species as they accumulated in the cascade impactor and filter-pack assemblies.

4. IMPLANT TESTS

A detailed description of each of the implant tests is presented in this section. The experimental operating conditions of each of the tests are summarized in Table 1.

4.1 Cesium Iodide Behavior at High Concentration at 700°C (Implant Test 1)

The primary purpose of this test was to determine the behavior and release of CsI implanted within the gap of the simulated LWR fuel-rod capsule. As is shown in Table 1, the test was conducted at 700°C for 1 hr under a steam-argon atmosphere. A photograph of the ruptured capsule is shown in Fig. 4. The rupture, about 0.41 mm^2 in size, was located in the midcapsule region where the wall had been thinned. Approximately 330 psig of argon pressure was applied internally to the 700°C induction-heated capsule to cause the rupture.

Table 1. Summary of experimental operating conditions for Implant Tests 1 to 12[a]

	Implant test number											
	1	2	3	4	5	6	7	8	9	10	11	12
Mass Cs, mg	1.68	0.034	6.34	4.92	7.05	10.27	7.78	9.22	6.76	7.07	8.29	1.06
Mass I, mg	1.60	0.033	0.63	0.44	0.61	0.90	0.64	0.61	0.49	0.66	0.58	0.05
Mass Te, mg	0.0	0.0	1.68 ± 0.47	3.97	3.40	2.56	3.12	2.75	2.48	2.22	1.79	0.26
Av heatup rate, °C/sec	0.65	11.0	1.1	1.0	0.33	0.09	0.14	0.7	0.26	0.5	1.3	3.0
Heating method	b	b	b	b	b	c	c	b	c	c	b	b
Time-temp. before rupture, min-°C	(12-700)	(17.5-700)	(2.5-900)	d	(13-700)	e	e	(2.5-900)	f	e	3-900	2.1-900
Rupture pressure, psig	330.0	330.0	250.0	d	500.0[g]	e	e	425.0	f	e	h	250.0
Rupture size, mm^2	0.41[i]	0.22[i]	0.81	d	2.60	1.98[i]	1.98[i]	~24.0	7.92 → 88	1.98	~4	~84.0
Temp. after rupture, °C	700.0	700.0	900.0	900-1100	700.0	500.0	700.0	900-1100	500.0	700.0	900-1300	900.0
Time at temp., hr	1.0	1.5	2.0	0.20-0.80	2.0	20.0	5.0	0.04-0.96	20.0	5.0	0.25	2.0
Steam flow rate, cm^3 STP/min	277.0	305.0	311.0	330.0[j]	310.0	347.0	0	1454.0	0	339.0	1269.0	305.0
Argon flow rate, cm^3 STP/min	52.0	56.0	56.0	58.0[j]	59.0	59.0	k	274.0	ℓ	48.0	322.0	108.0
Furnace tube pressure, torr	750.0	735.0	745.0	781.0	750.0	750.0	755.0	750.0	740.0	740.0	750.0	750.0
Impactor pressure, torr	186.0	186.0	191.0	211.0	186.0	186.0	186.0	760.0	250.0	186.0	760.0	212.0
Cladding source, tube No.[m]	0001	0001	0001	0001	1223	1223	1223	1101	1101	1101	1101	0415

[a] The implanted UO_2 assembles were dried under vacuum for 30 min at 200°C, then maintained under 1 atm argon for 16 hr at 400°C.
[b] Induction heating.
[c] Resistance heating around the furnace tube.
[d] A leak due to overheating the inlet end cap prevented pressurizing to obtain a normal rupture.
[e] A hole was drilled through the Zircaloy cladding prior to testing.
[f] Four holes were drilled through the Zircaloy cladding prior to testing.
[g] A 5.1-cm length of wall was thinned on one side by grinding a curved surface to leave a thin "line" of 0.019 cm (0.0076 in.) in wall thickness.
[h] Not measured.
[i] The wall was thinned by grinding a flat spot 5.1 cm (2.0 in.) long; thinnest points, 0.023 cm (0.009 in.).
[j] Twenty minutes after reaching 900°C (8 min after reaching 1100°C), the orifice to the impactor region began to plug with particulate material. This required a reduction of the argon and steam flow rates to 38% of the rates cited.
[k] Dry air only (276 cm^3 STP/min).
[ℓ] Dry air only (412 cm^3 STP/min).
[m] For a description of tubing, see the following reference: R. H. Chapman, Characterization of Zircaloy-4 Tubing Procured for Fuel Cladding Research Programs, ORNL/NUREG/TM-29 (July 1976).

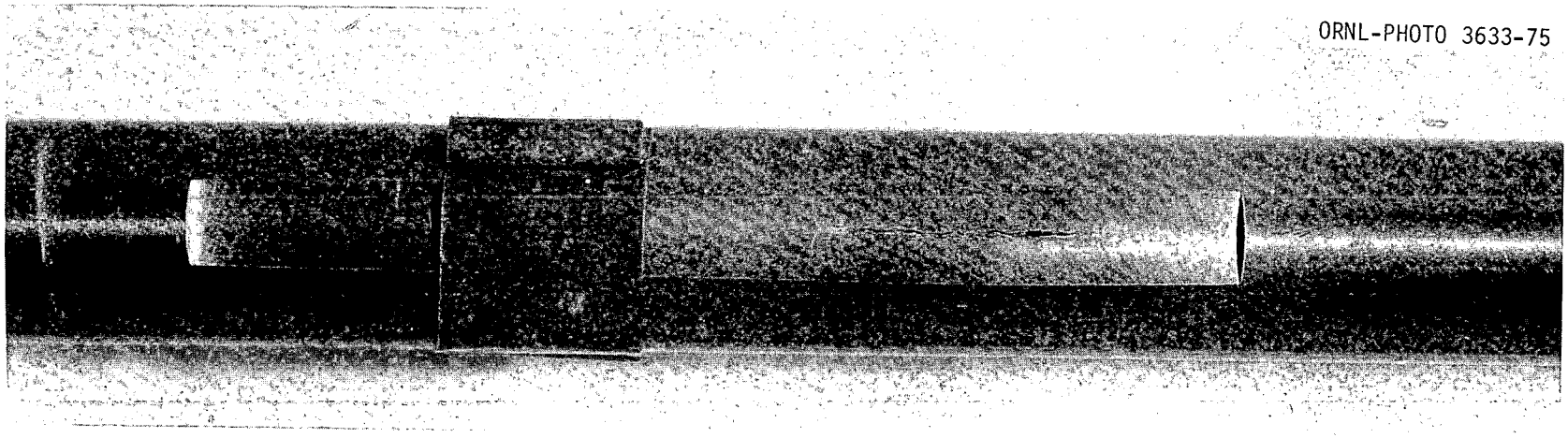

Fig. 4. Photograph showing the rupture opening in the fuel rod used in Implant Test 1.

Post-test distributions of the two tracer nuclides deposited on the apparatus components are presented in Table 2. These data indicate that 10.8% (181 μg) of the cesium and 22.5% (360 μg) of the iodine were released from the capsule. The disproportions of cesium and iodine at most locations shown in Table 2 demonstrate that chemical reactions occurred (decomposition of CsI) in the UO_2-Zircaloy-steam-quartz environment. The only locations with excess cesium are the UO_2 pellets and the first particulate filter paper. This suggests that CsI reacted with the fuel pellets to form a cesium uranate and elemental iodine. (Cesium uranates have low vapor pressures[3] compared to CsI at 700°C[4] and would tend to remain within the test capsule.)

The distributions of cesium and iodine within the fuel rod, as determined before and after the experiment, are presented graphically in Figs. 5 and 6. Release of material from the immediate vicinity of the rupture is unmistakable.

Most of the cesium and iodine that was released from the fuel rod deposited on the quartz furnace tube liner. In experiments utilizing induction heating, the furnace tube was heated only by heat radiation and convection from the heated fuel rod, except for the furnace tube inlet cap which was heated to ∿200°C with an auxiliary electric heater. Consequently, the cooler surfaces of the quartz furnace tube liner (≤500°C) probably permitted condensation of gaseous CsI that diffused from the rupture opening. Excess iodine was found in the furnace tube liner; previous experiments with elemental iodine in this same apparatus[1] indicated that a fraction of the I_2 was deposited on (sorbed or reacted with) the quartz liner in spite of its high volatility (bp, 183°C).

Data regarding the deposition of iodine species on the thermal gradient tube and on the impactor and filter assemblies during the test are presented graphically in Fig. 7. These data indicate that ∿30% of the iodine found in the thermal gradient tube was deposited immediately after the fuel rod was ruptured.

The concentration profile of cesium in the thermal gradient tube is shown in Fig. 8 along with those obtained for cesium and iodine in Control

Table 2. Distributions of cesium and iodine in Implant Test 1

Location	Temp. (°C)	Amount found in each location: Percent of total Cs	Percent of total I	μg Cs	μg I
Fuel rod, total	700	(89.2)	(77.5)		
UO_2 pellets		69.8	43.7	1173.0	699.0
Zircaloy cladding		19.4	33.8	326.0	541.0
Quartz furnace tube	∿200 to 500	9.4	19.7	158.0	315.0
Thermal gradient tube	720 to 160	1.04	1.25	17.5	20.0
Orifice assembly	145	0.02	0.14	0.34	2.2
Impactor assembly	145				
Impactor housing		0.117	1.21	1.97	19.4
First-stage paper		0.015	0.030	0.25	0.48
Second-stage paper		0.0085	0.013	0.14	0.21
Third-stage paper		0.0083	0.011	0.14	0.18
Fourth-stage paper		0.0071	0.0054	0.12	0.09
Fifth-stage paper		0.0308	0.037	0.52	0.59
Filter assembly	140				
Filter housing		0.0035	0.022	0.06	0.35
First filter paper		0.062	0.026	1.04	0.42
Second filter paper		0.0007	0.0019	0.01	0.030
Silver screen No. 1		0.0	0.152		2.43
Silver screen No. 2		0.0	0.013		0.21
Silver screen Nos. 3 to 12		0.0	0.024		0.38
Adsorber assembly	135				
Adsorber housing		0.0	0.0		
Charcoal No. 1		<0.001	0.021	<0.02	0.34
Charcoal No. 2		0.0	0.0003		0.005
Charcoal No. 3		0.0	0.0		
AgX		0.0	0.0		
Condenser assembly	0				
Condenser housing		<0.1	0.008	<2.0	0.13
Condensate		0.0	0.0002		0.003
Freeze trap	-78	0.0	0.0		
Cold charcoal trap	-78	0.0	0.0		

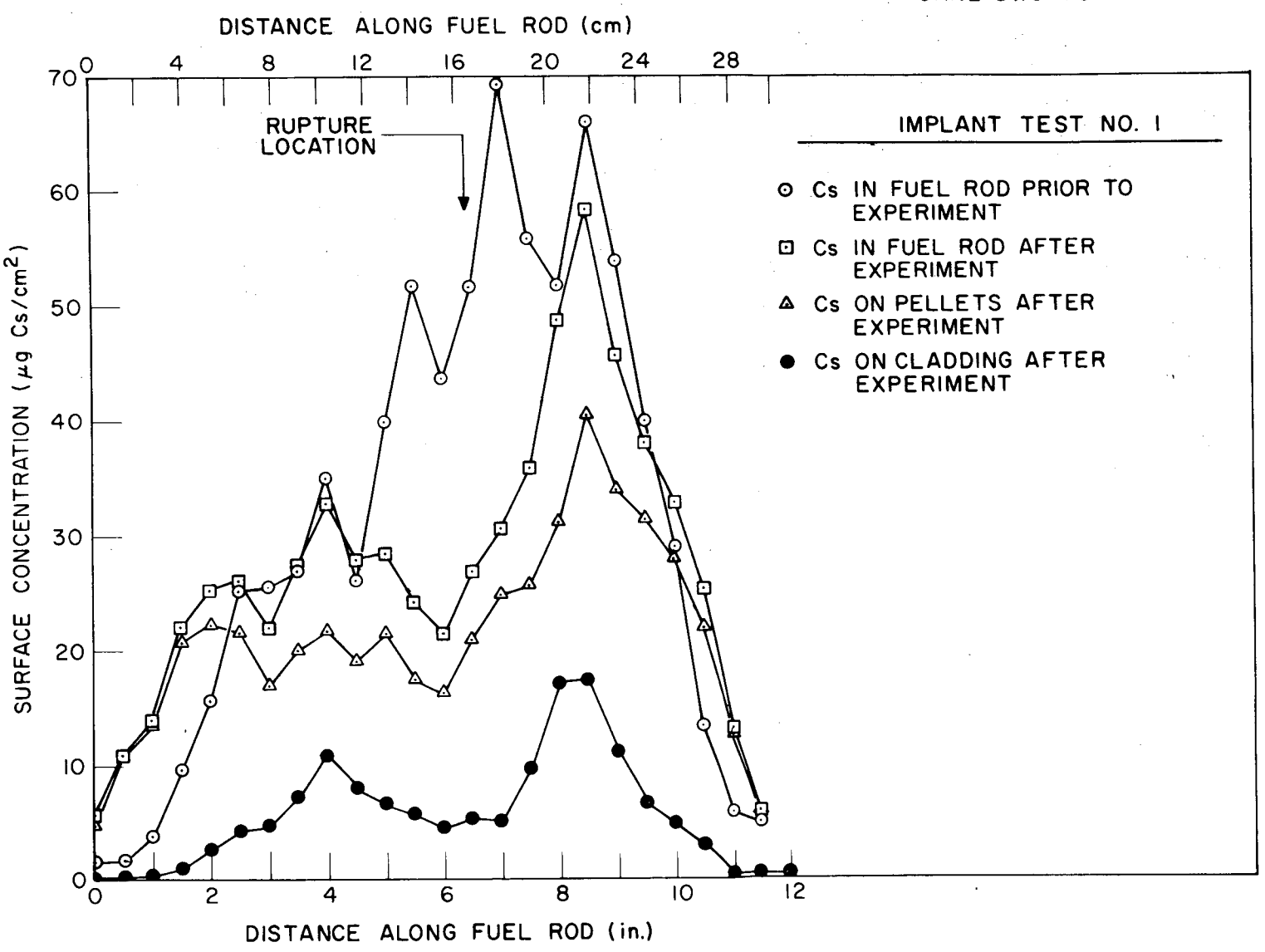

Fig. 5. Cesium distribution in the fuel rod of Implant Test No. 1.

ORNL DWG 76-149

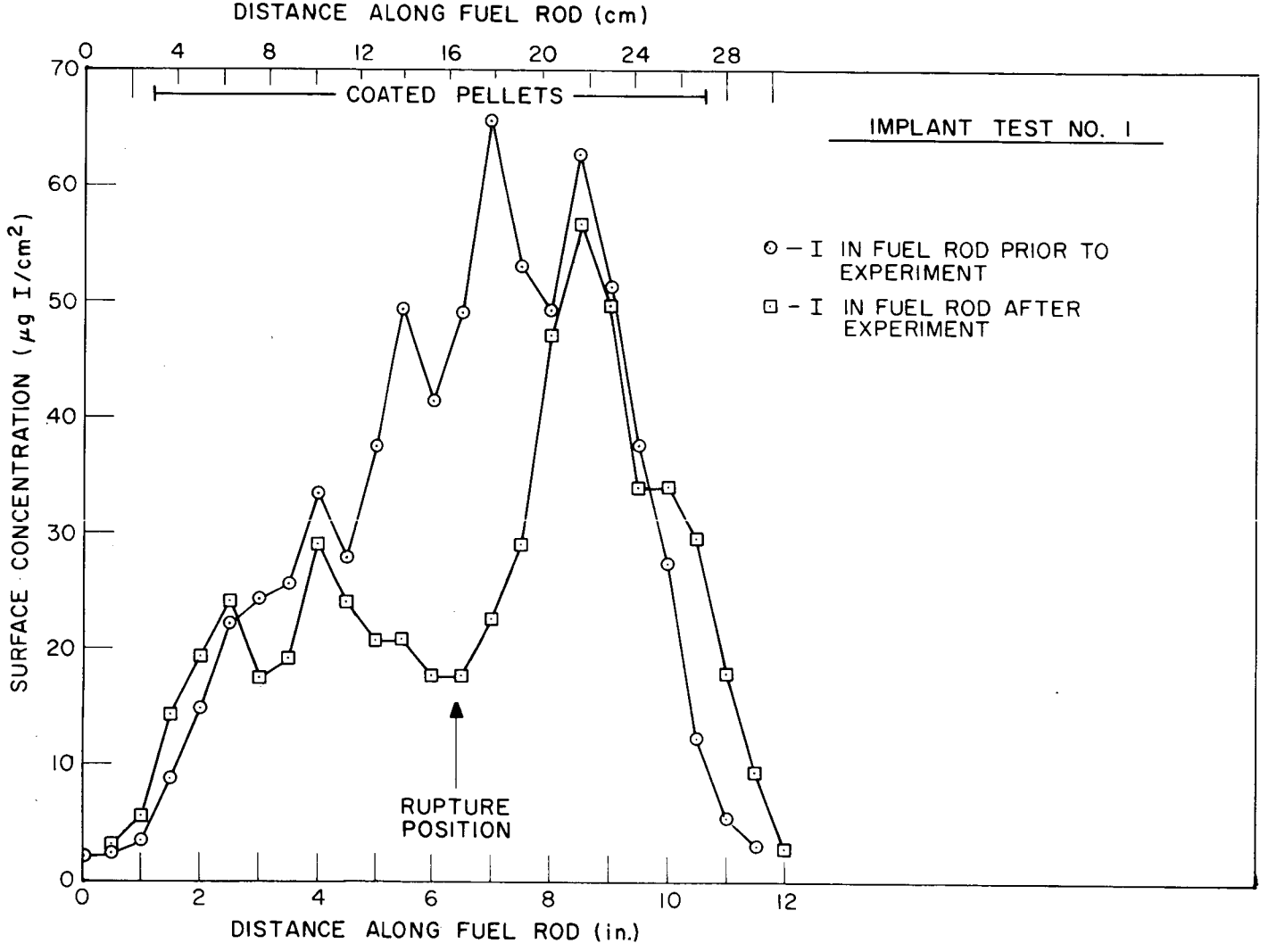

Fig. 6. Iodine distributions in the fuel rod of Implant Test No. 1.

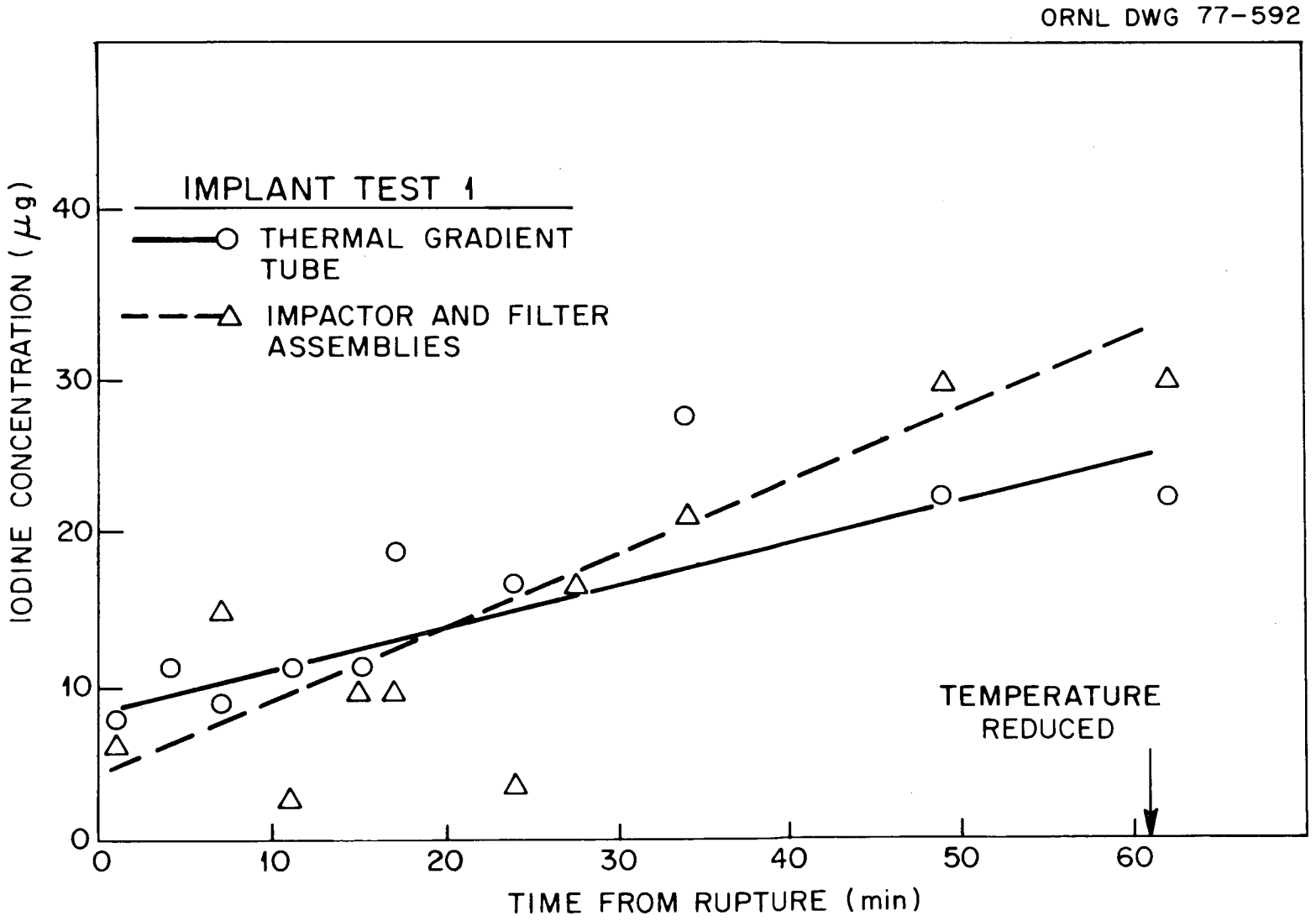

Fig. 7. Iodine deposition in the thermal gradient tube and impactor during Implant Test No. 1.

ORNL DWG 76-70

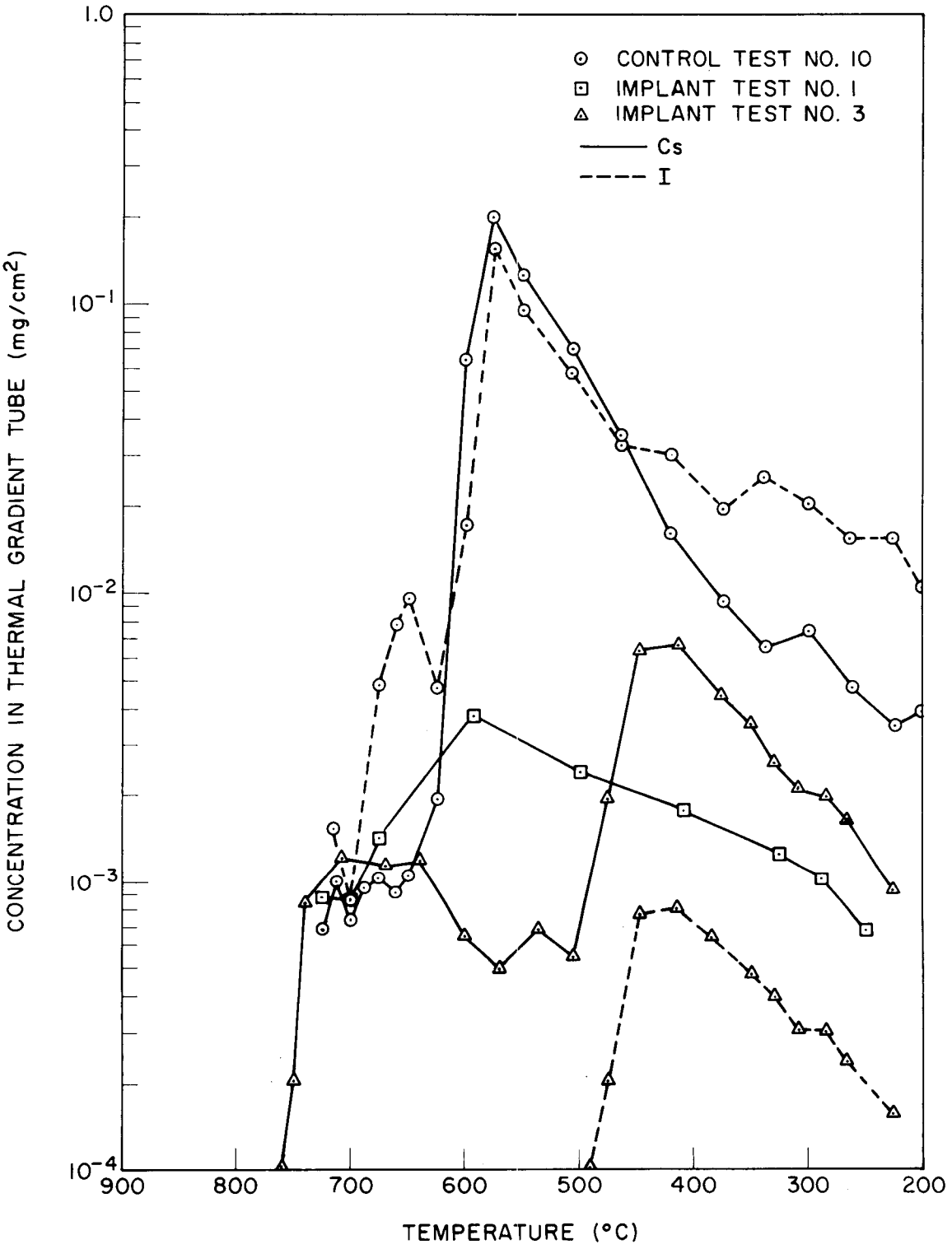

Fig. 8. Cesium and iodine profiles in the thermal gradient tube.

Test 10 (see ref. 1) and Implant Test 3. (Deposition in the thermal gradient tube in Control Test 10 was CsI; therefore, the profile is provided in the figure for comparison.) Nearly equal masses of cesium and iodine were found in the thermal gradient tube (Table 2); this suggests that the chemical form of the deposited cesium was CsI.

A sample of material that was obtained from the collector of the fifth impactor stage was examined by x-ray diffraction. No identifiable pattern was observed. Our sensitivity of detection was hampered by the hygroscopic nature of CsI and CsOH.

4.2 Cesium Iodide Behavior at Low Concentration at 700°C (Implant Test 2)

Implant Test 2 was identical to the preceding test, except that a 50-fold lesser concentration of CsI was employed, the rupture opening (0.22 mm^2) was about half the size, and the duration of the test was 30 min longer (cf. Table 1).

In this test, 7.3% of the implanted cesium and 16.5% of the implanted iodine were released from the fuel rod. The post-test distributions of cesium and iodine are presented in Table 3; and, from the disproportions of cesium and iodine, we calculate that a minimum of 21% of the CsI reacted in the UO_2-Zr-H_2O-SiO_2 environment to form separate cesium and iodine compounds. The only locations with an excess of cesium relative to iodine were the UO_2 pellets and the quartz furnace tube.

Cesium nuclide distributions in the fuel rod prior to and after experimentation are presented in Fig. 9. As in the previous test, these data indicate loss of material near the rupture point, 14.2 cm (5.6 in.) along the fuel rod.

The cesium that was deposited on the furnace tube walls was largely confined to an area near the location of the rupture of the capsule and was mainly in a form other than CsI. However, since CsI can react with quartz[1] to form less-volatile cesium silicates and elemental iodine, we are uncertain of the form in which the cesium was released from the fuel rod. Cesium hydroxide vapor would also react with the quartz to form the silicate.

Table 3. Distributions of cesium and iodine in Implant Test 2

Location	Temp. (°C)	Amount found in each location: Percent of total Cs	Percent of total I	μg Cs	μg I
Fuel rod, total	700	(92.7)	(83.5)		
UO_2 pellets		51.6	36.7	17.5	12.1
Zircaloy cladding		41.1	46.8	14.0	15.4
Quartz furnace tube	∿200 to 500	7.2	1.1	2.44	0.36
Thermal gradient tube	720 to 220	0.106	1.39	0.036	0.46
Orifice assembly	160	0.0049	1.16	0.0017	0.38
Impactor assembly	160				
Impactor housing		0.026	6.37	0.0088	2.10
First-stage paper		0.0020	0.047	0.00068	0.0155
Second-stage paper		0.0021	0.0027	0.00071	0.0009
Third-stage paper		0.0017	0.0064	0.00058	0.0021
Fourth-stage paper		0.0015	0.0062	0.00051	0.0020
Fifth-stage paper		0.00087	0.0022	0.00030	0.0007
Filter assembly	150				
Filter housing		0.00083	0.804	0.00028	0.265
First filter paper		0.00019	0.091	0.000065	0.030
Second filter paper		0.0[a]	0.085		0.028
Third filter paper		0.0	0.028		0.0092
Silver screen No. 1		0.0	3.84		1.27
Silver screen No. 2		0.0	0.24		0.079
Silver screen Nos. 3 to 8		0.0	0.61		0.020
Adsorber assembly	120				
Adsorber housing		0.0	0.007		0.002
Charcoal No. 1		0.0	0.834		0.275
Charcoal No. 2		0.0	0.015		0.0005
Charcoal No. 3		0.0	0.0022		0.0007
Charcoal Nos. 4 to 6		0.0	0.0040		0.0013
AgX (2)		0.0	0.0017		0.0006
Condenser assembly	0				
Condenser housing		<0.005	0.031	<0.0017	0.010
Condensate		0.0	0.0		
Freeze trap	-78	<0.005	0.0	<0.0017	
Cold charcoal trap	-78	<0.005	0.0	<0.0017	

[a]Amounts <0.0001% are indicated by 0.0.

ORNL DWG 76-163RI

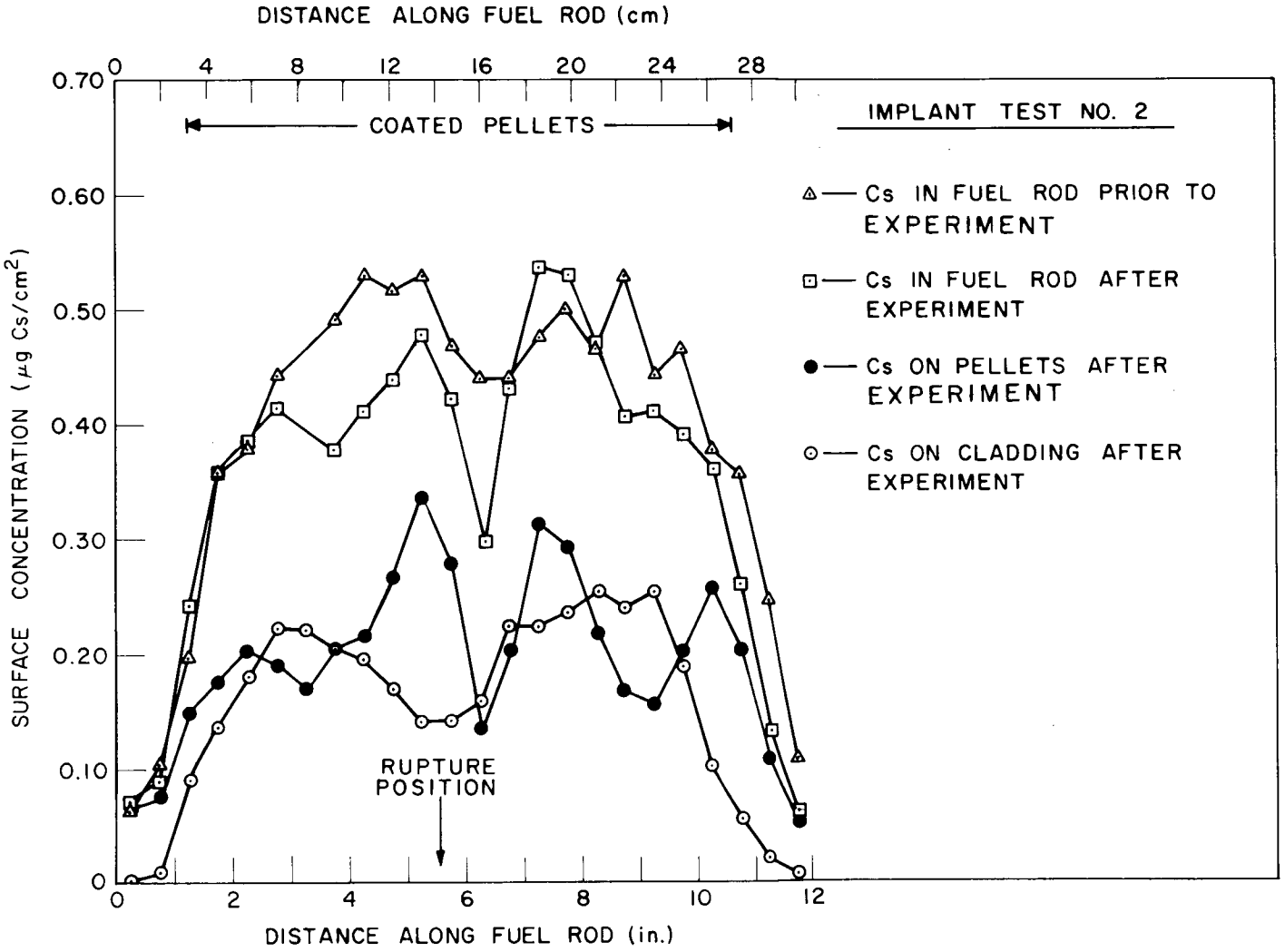

Fig. 9. Cesium distributions in the fuel rod of Implant Test No. 2.

Less than 0.04% of the original cesium and ∿13% of the original iodine were transported to the impactor, filter, and adsorber assemblies. The manner in which the iodine was accumulated by these components is displayed in Fig. 10. The data show some delay in the appearance of iodine in the filter pack assembly; this may be due to a holdup of iodine on the aluminum impactor housing. Most of the iodine was found on the surfaces of the housings and on the first silver screen; this is a strong indication of adsorbed and reacted (with silver) elemental iodine. We believe that all of the iodine was delayed temporarily in transit between the fuel rod and the impactor-filter assembly. According to the analysis detailed in Sect. 8, most of the released iodine and cesium escaped from the rod at the time of rupture.

The larger fractional formation and release of elemental iodine experienced in this test compared with Implant Test 1 can probably be attributed to the differences in initial concentration in the two tests. Similarly, a larger proportion of iodine appeared as organic iodides (i.e., collected on the sorbers beyond the silver screens) in this test as compared with the previous test, again probably for the same reason. Such concentration effects on the formation of organic iodide have been noted previously.[5]

4.3 Behavior of Fission Product Simulant Mixture at 900°C (Implant Test 3)

Implant Test 3 was the first test conducted in which three fission product simulants were employed. The experimental conditions are listed in Table 1, and the pertinent nuclide distributions at the conclusion of the tests are presented in Table 4. The rupture area (∿0.81 mm^2) of the cladding is depicted in Fig. 11.

Cesium concentration profiles in the fuel rod are displayed in Fig. 12; these data indicate some migration to the cooler ends and to the rupture area. (In the clad rupture region, the cladding distortion caused the induction-heated segment temperature to rise to ∿1000°C, whereas the remainder of the rod was maintained at 900°C--except for the cooler ends.)

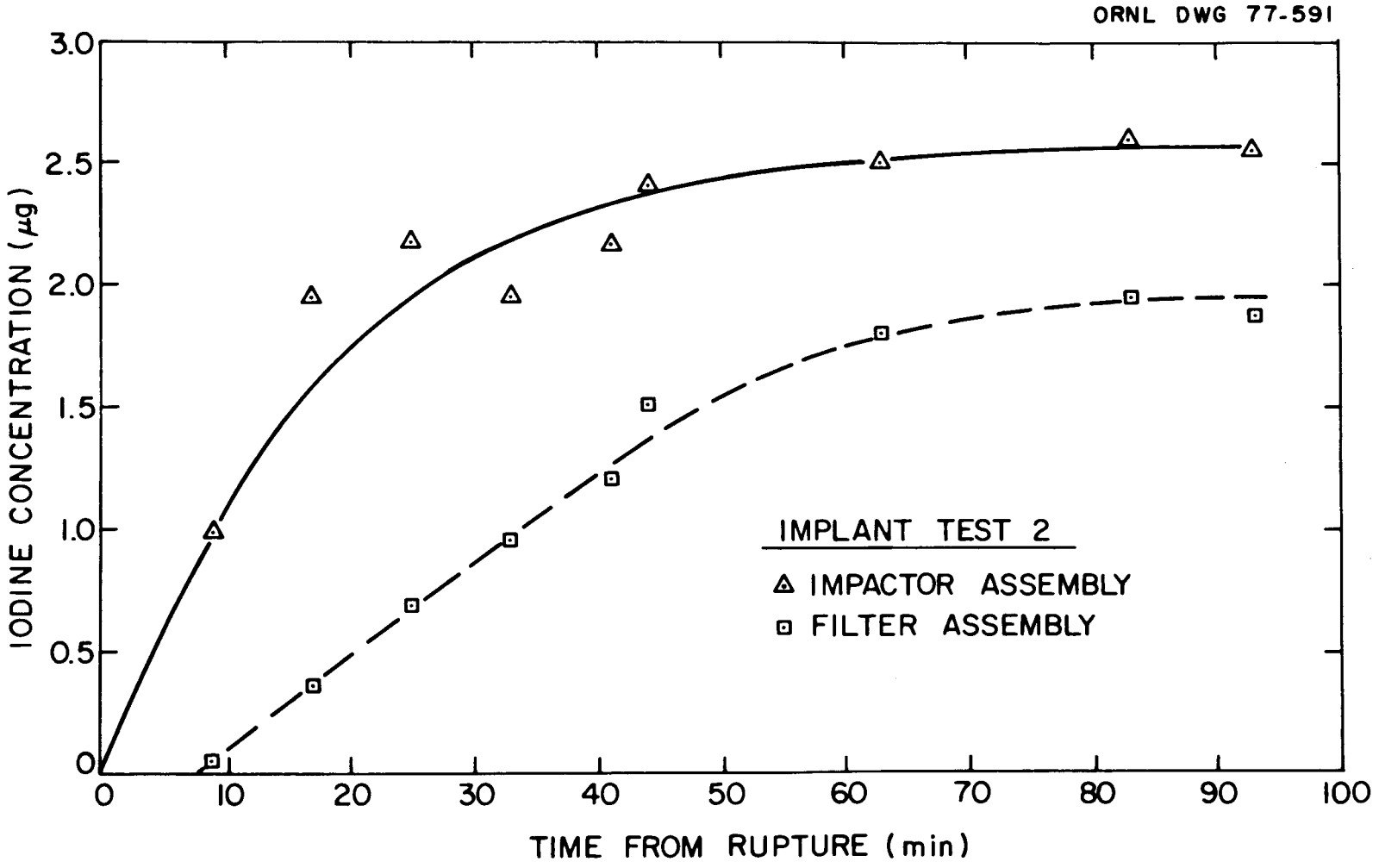

Fig. 10. Iodine deposition in the impactor and on the first silver screen during Implant Test No. 2.

Table 4. Distributions of cesium, iodine, and tellurium in Implant Test 3

Location	Temp. (°C)	Amount found in each location: Percent of total Cs	I	Te	μg Cs	I	Te
Fuel rod, total	900	(92.33)	(74.39)	(98.40)			
UO_2 pellets		61.58	54.59	3.6	3904.0	343.9	60.5
Zircaloy cladding		30.75	19.80	94.8	1950.0	124.7	1593.0
Quartz furnace tube	~200 to 700	6.46	23.80	1.6	410.0	149.9	26.9
Thermal gradient tube	750 to 150	1.08	0.86	0.0003	68.0	5.42	0.005
Orifice assembly	150	0.022	0.091	0.0005	1.39	0.57	0.008
Impactor assembly	145						
Impactor housing		0.051	0.61	0.01	3.23	3.84	
First-stage paper		0.0099	0.026	0.0	0.63	0.16	
Second-stage paper		0.0029	0.0014	0.0	0.18	0.009	
Third-stage paper		0.0024	0.0015	0.0	0.15	0.009	
Fourth-stage paper		0.0085	0.0104	0.0	0.54	0.066	
Fifth-stage paper		0.0051	0.043	0.0	1.20	0.27	
Filter assembly	140						
Filter housing		0.0018	0.050	0.001	0.11	0.32	0.02
First filter paper		0.0051	0.0046	0.0005	0.32	0.029	0.008
Second filter paper		0.0	0.0015	0.0		0.009	
Third filter paper		0.0	0.0007	0.0003		0.004	0.005
Silver screen No. 1		0.0	0.128	0.0		0.81	
Silver screen No. 2		0.0	0.0021	0.0		0.013	
Silver screen Nos. 3 to 8		0.0	0.0017	0.0		0.011	
Adsorber assembly	130						
Adsorber housing		<0.006	0.003	0.002	<0.38	0.02	0.03
Charcoal No. 1		0.0	0.007	0.0	0.0	0.04	
Charcoal No. 2		0.0	0.0	0.0	0.0		
Other adsorbers		0.001	0.0002	0.0	0.06	0.001	
Condenser assembly	0						
Condenser housing		<0.1	0.0	0.0	<5.0		
Condensate		0.002	0.0	0.0	0.13		
Freeze trap	-78	0.002	0.0	0.0	0.13		
Cold charcoal trap	-78		0.0	0.0			

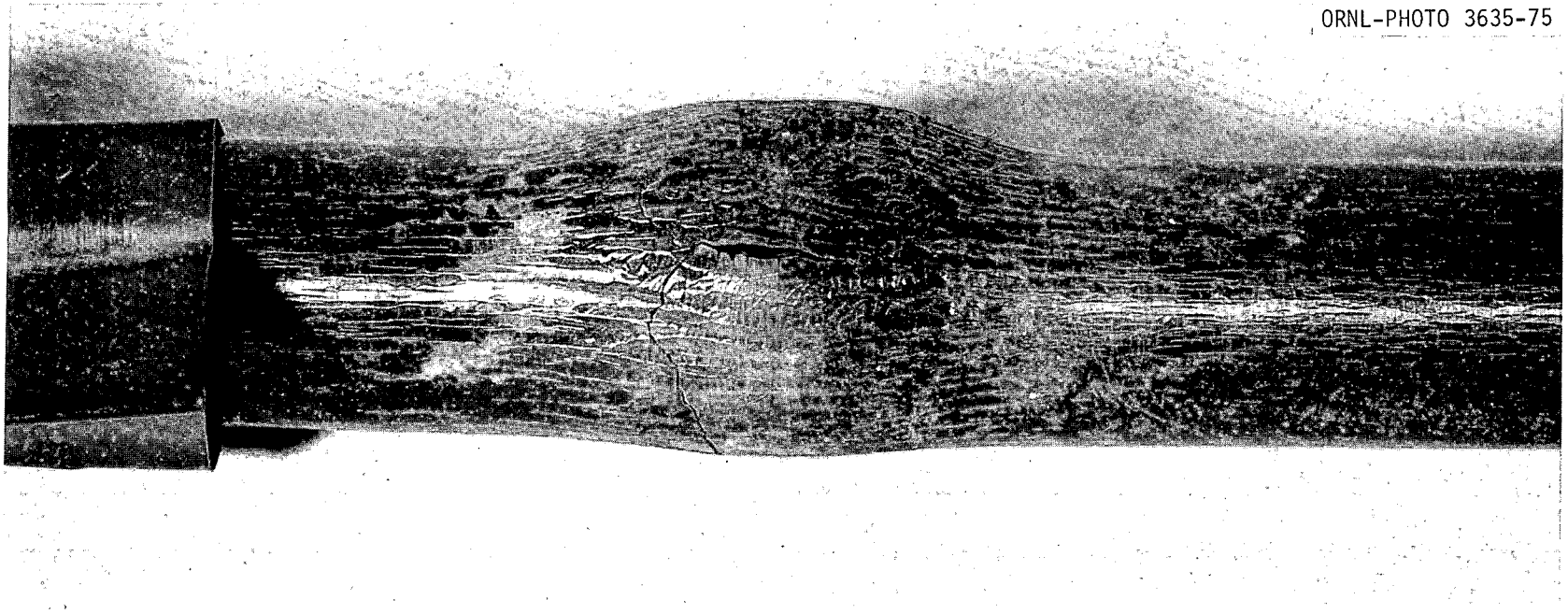

Fig. 11. Implant Test No. 3 cladding in the region of rupture.

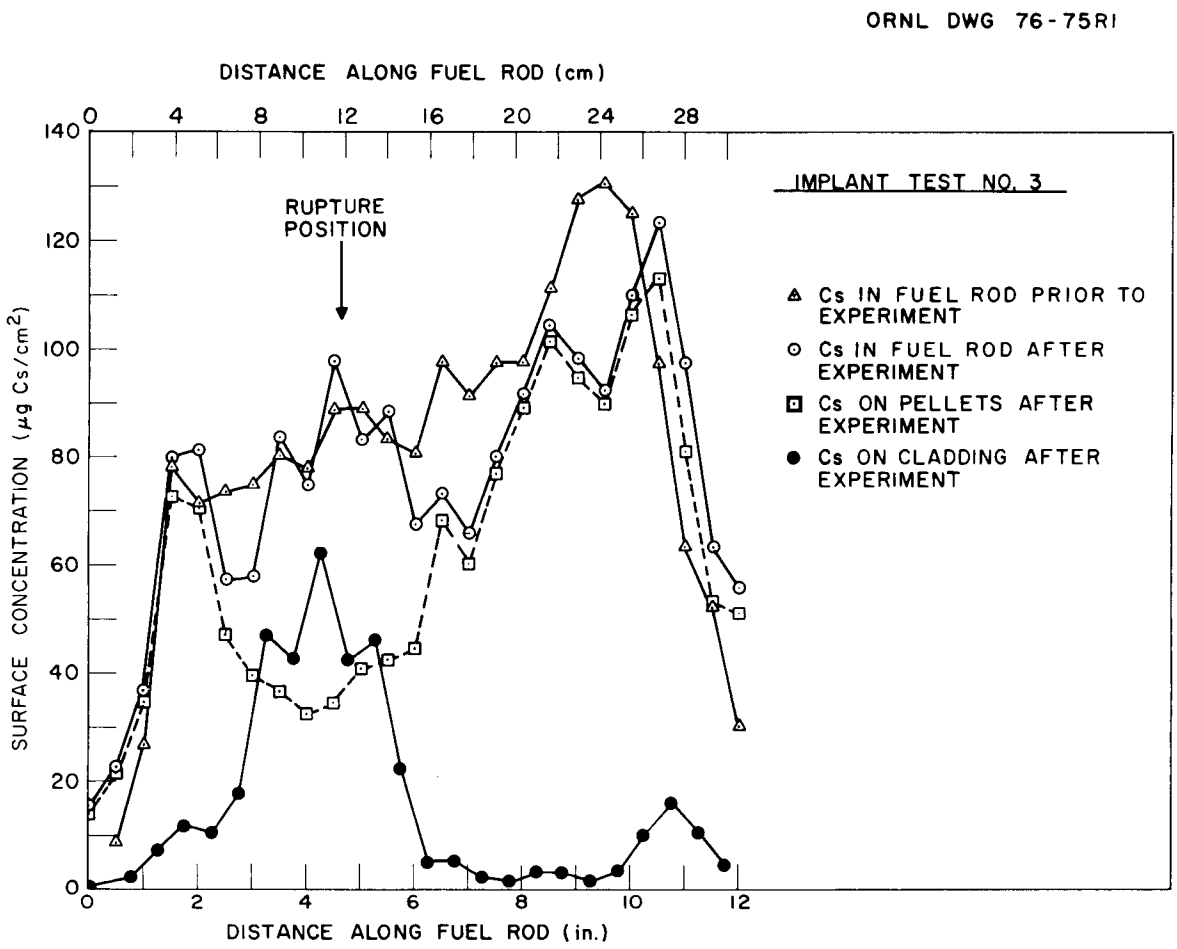

Fig. 12. Cesium distributions in the fuel rod of Implant Test No. 3.

Moreover, considerable relocation of cesium from the pellets to the cladding occurred within the rupture region. Axial migration of cesium toward the ends of the capsule was significantly less than that of iodine. Corresponding profiles for iodine are shown in Fig. 13. At temperatures of <950°C, CsOH is stabilized by uranate formation. For this reason, migration to the cooler ends of the rod occurred primarily as CsI. At 1000°C, we postulate sufficient decomposition of the uranate to permit transport of cesium to the cladding, as indicated by the profiles in Fig. 12. This postulated behavior does not appear to be at variance with Knudsen cell studies[3] of cesium partial pressures over UO_2.

Iodine activity as monitored at two points along the fuel rod during the experiment is displayed graphically in Fig. 14; these data indicate continuous transport of the iodine nuclide throughout the test. (Similar plots of iodine activity in the thermal gradient tube and the impactor assembly are presented in Fig. 15.)

Deposition of iodine in the thermal gradient tube probably occurred as CsI; this behavior is suggested by the correspondence of the cesium and iodine profiles in the thermal gradient tube as shown in Fig. 8. Moreover, about half of this material was collected within 5 min of the time of rupture. Less iodine was collected by the aluminum impactor housing at the time of rupture; it is believed to be elemental iodine.

During the test, 7.7% of the implanted cesium, 25.6% of the implanted iodine, and 1.6% of the implanted tellurium were released. From the data presented in Table 4, it was determined that 92.9% of the released iodine remained in the quartz furnace tube, probably as CsI. About 84% of the released cesium was found in the furnace tube, and an estimated 62% of this cesium was not associated with iodine. Most of the tellurium released was also deposited in the furnace tube.

About 95% of the implanted tellurium was found associated with the cladding, as is indicated in Table 4. Scans of tellurium activity that were made along a segment of the cladding revealed preferential deposition on the cladding at pellet interface locations. Since neither cesium nor iodine showed this behavior, it was decided to open the cladding and examine

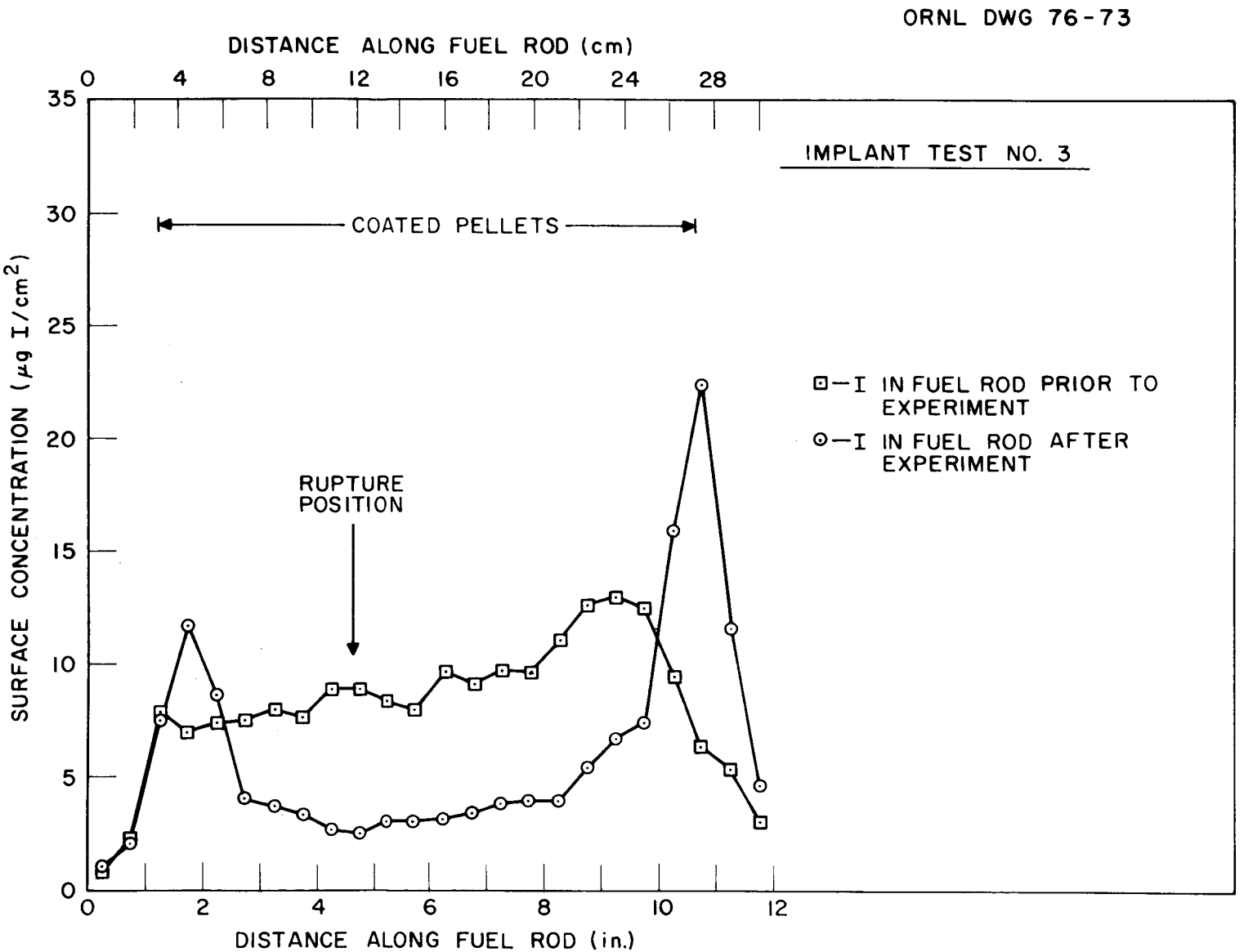

Fig. 13. Iodine distributions in the fuel rod of Implant Test No. 3.

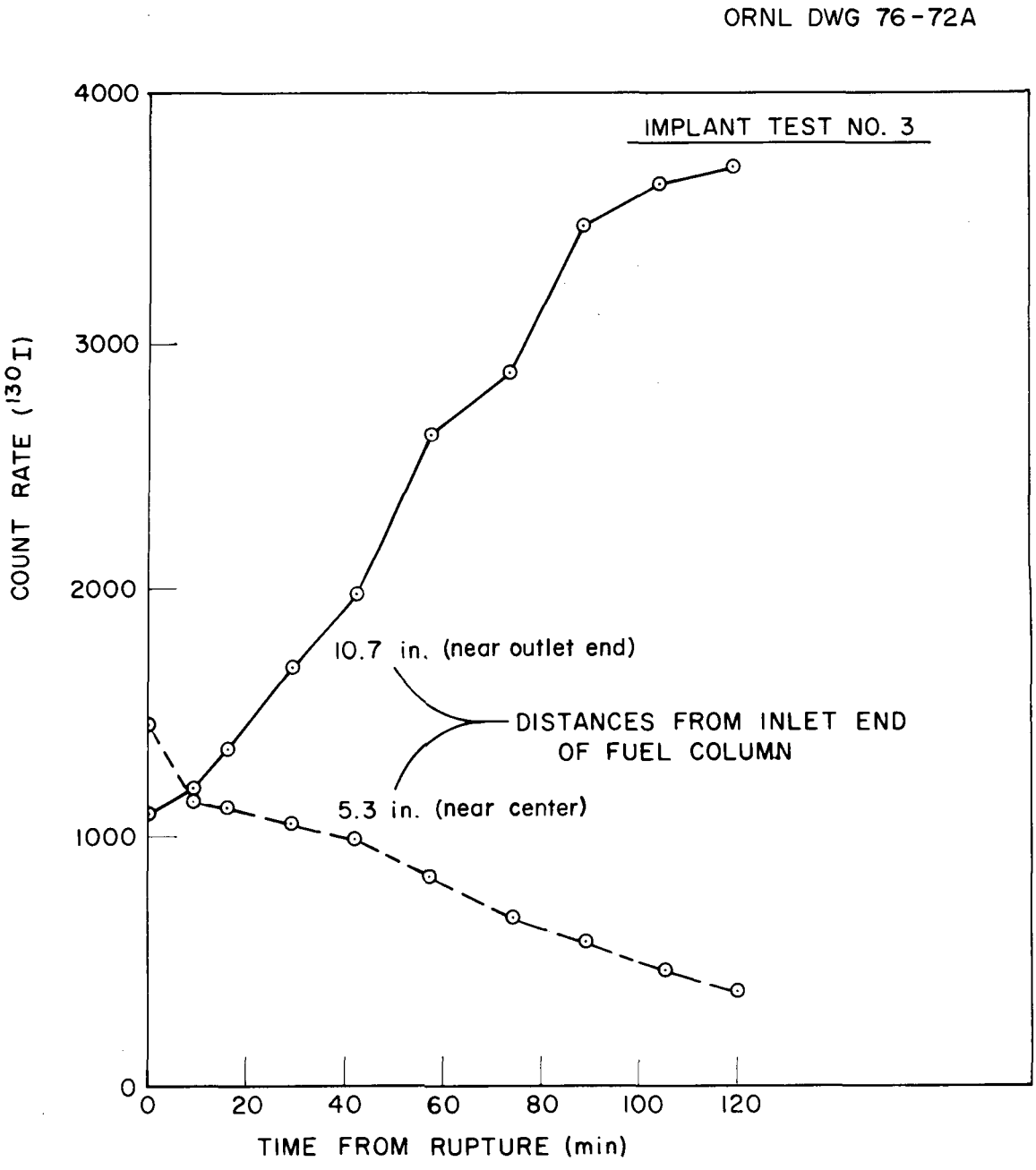

Fig. 14. Iodine-130 activity at selected points along the fuel rod during Implant Test No. 3 operation.

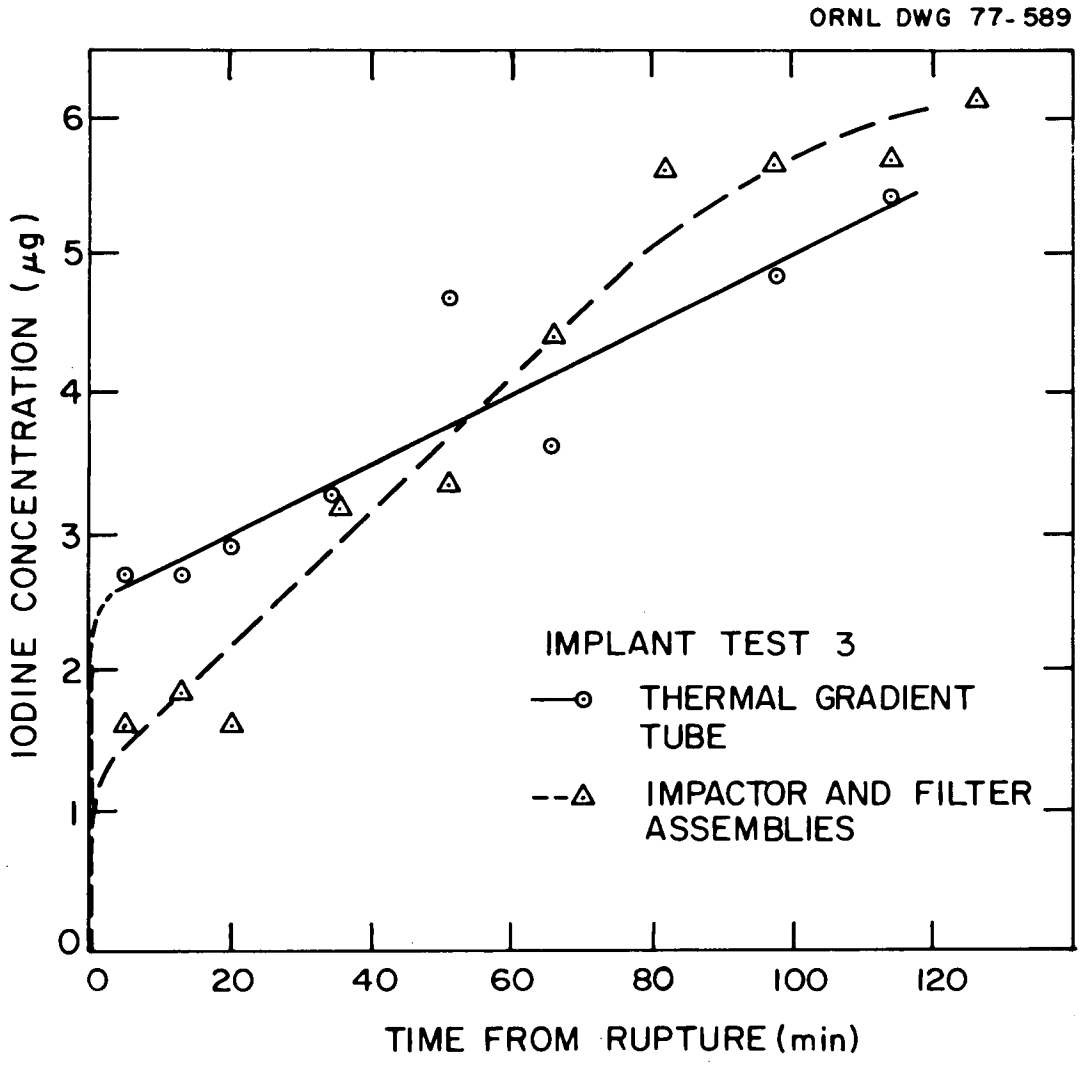

Fig. 15. Iodine deposition in the thermal gradient tube and impactor during Implant Test No. 3.

the internal surface. As can be readily seen from the photographs in Fig. 16, the activity scans accurately identified regions of preferential deposition; the tellurium species obviously did not distribute uniformly along the fuel rod. Samples of material removed from the regions of tellurium-clad interaction exhibited x-ray diffraction patterns that were identified as Te_3ZrO_5. As illustrated in Fig. 17(a), a longitudinal cut through one such reaction zone indicated that oxidation by steam was inhibited in this region. [The zone displayed in Fig. 17(a) was near the rupture opening; thus steam was available to form the thick oxide layer that is visible on the right side of the photomicrograph.] In Fig. 17(b), a thin layer of tin is present in the interface region between the oxidized (dark) and nonoxidized (light) layers of cladding. It was identified by x-ray analysis using a scanning electron microscope. (Zircaloy-4 cladding has between 1.2 and 1.7% tin.) Zirconium is readily oxidized by steam at high temperatures; however, tin, in the presence of the more active zirconium, is not. Consequently, the molten tin tends to agglomerate.

4.4 Behavior of Fission Product Simulant Mixture at 1100°C (Implant Test 4)

In Implant Test 4, the fuel rod was maintained at 900°C for 12 min and at 1100°C for 48 min in a flowing-steam-argon atmosphere. In an attempt to minimize an axial temperature gradient along the fuel rod, a lengthened induction coil was utilized. However, this caused the stainless steel ferrule fitting at the inlet end of the rod to become overheated; this resulted in the leakage of the argon pressurizing gas, so that rupture of the rod could not be effected. Nonetheless, ∿25.2% of the cesium (1240 μg), 32.9% of the iodine (145 μg), and 0.1% of the tellurium (4 μg) were released. Most of the iodine that was released deposited on the quartz liner of the furnace tube near the entrance to the thermal gradient tube (Fig. 18). Approximately 24% of the original cesium deposited on the quartz liner of the furnace tube and ∿1.2% of the original cesium deposited in the thermal gradient tube. X-ray diffraction analysis also revealed the presence of $CsOH \cdot H_2O$ in the material collected on the fifth collector stage of the cascade impactor (Fig. 19).

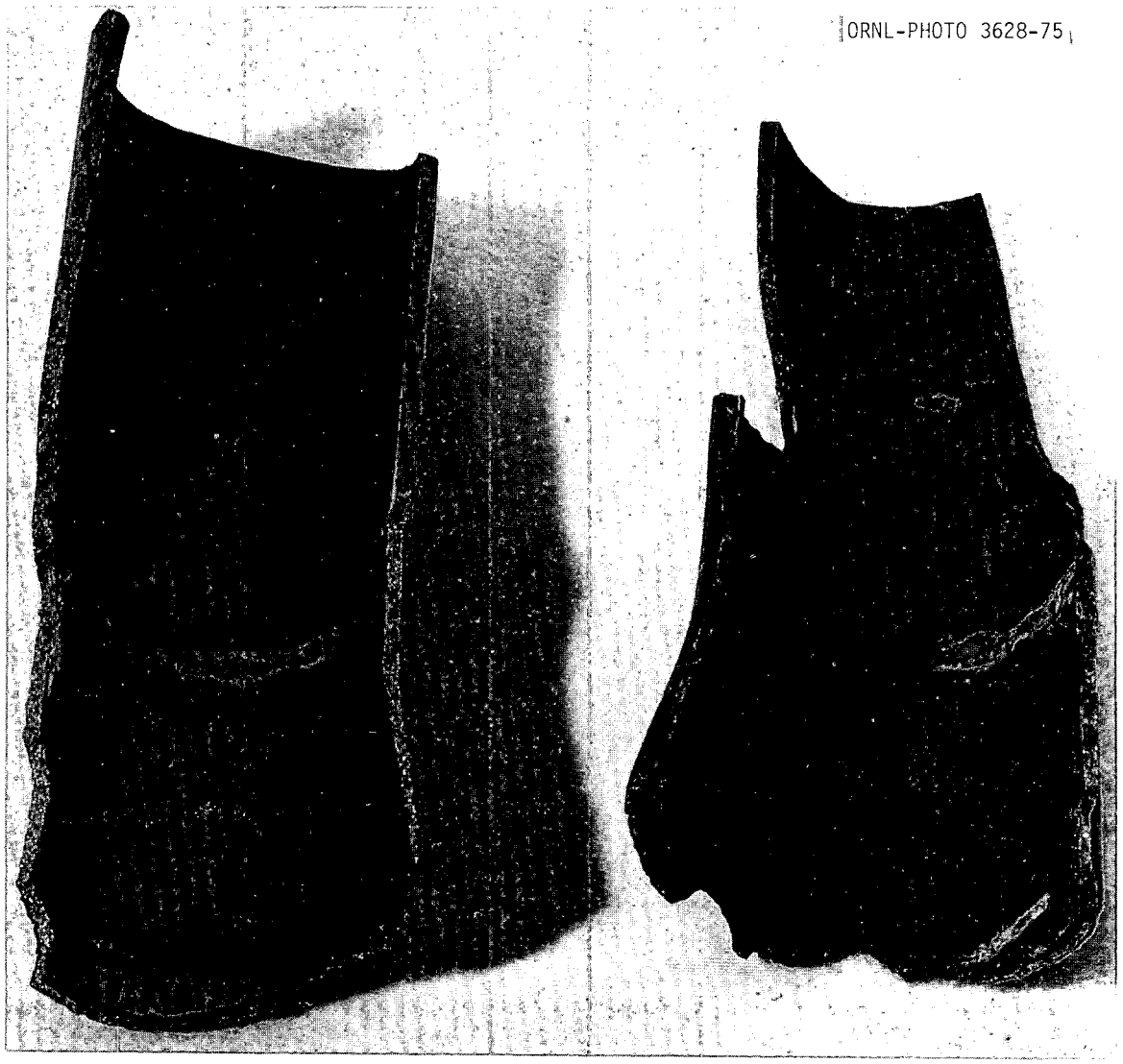

Fig. 16. View of the cladding inner surface of Implant Test No. 3 showing tellurium deposition rings.

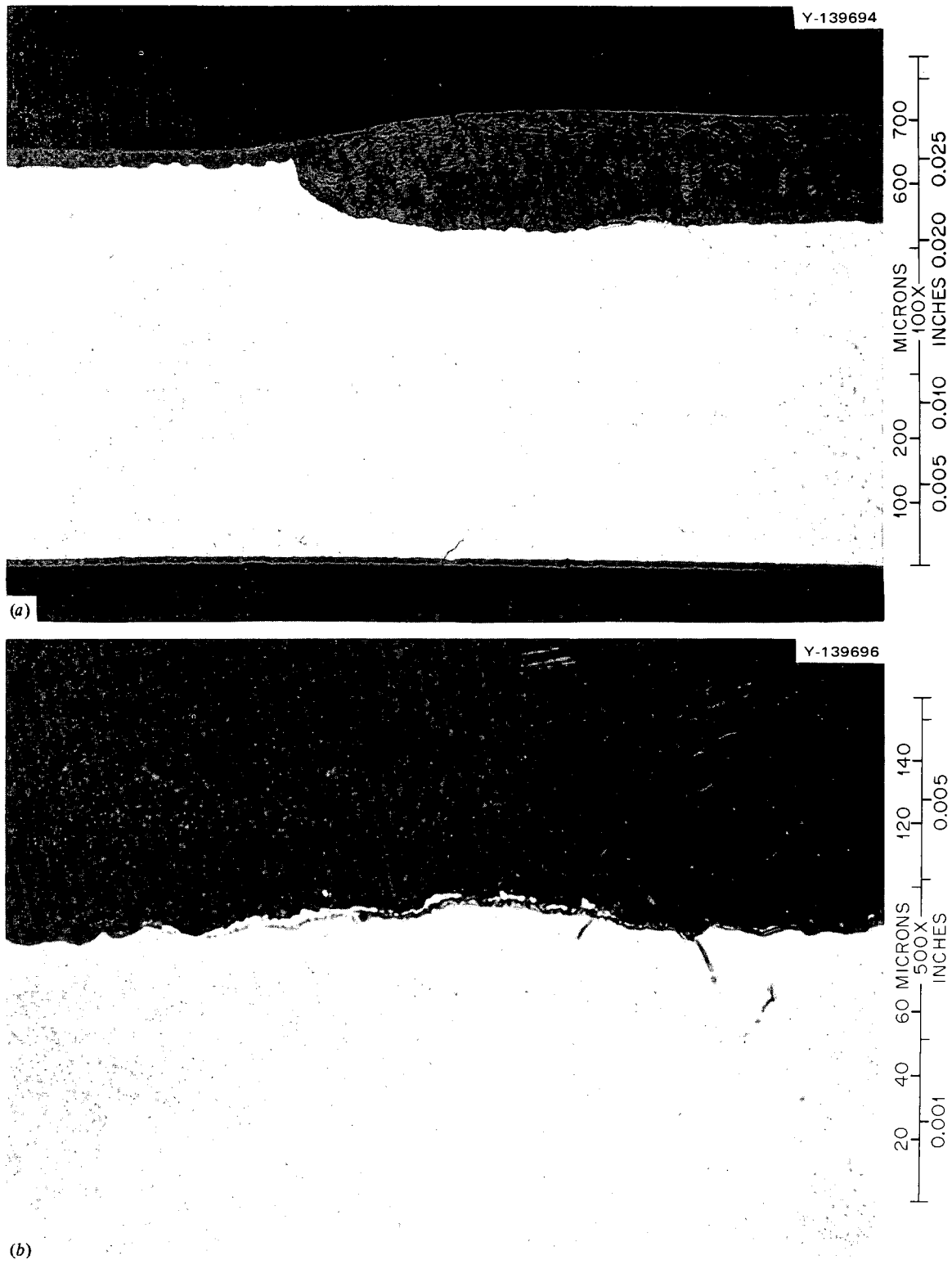

Fig. 17. (a) Photomicrographic view of tellurium reaction zone (upper left) and steam-oxidized cladding (upper right) of the inner surface of the fuel rod of Implant Test No. 3. (b) Enlarged view showing a tin layer in the interface region between the oxidized and nonoxidized layers.

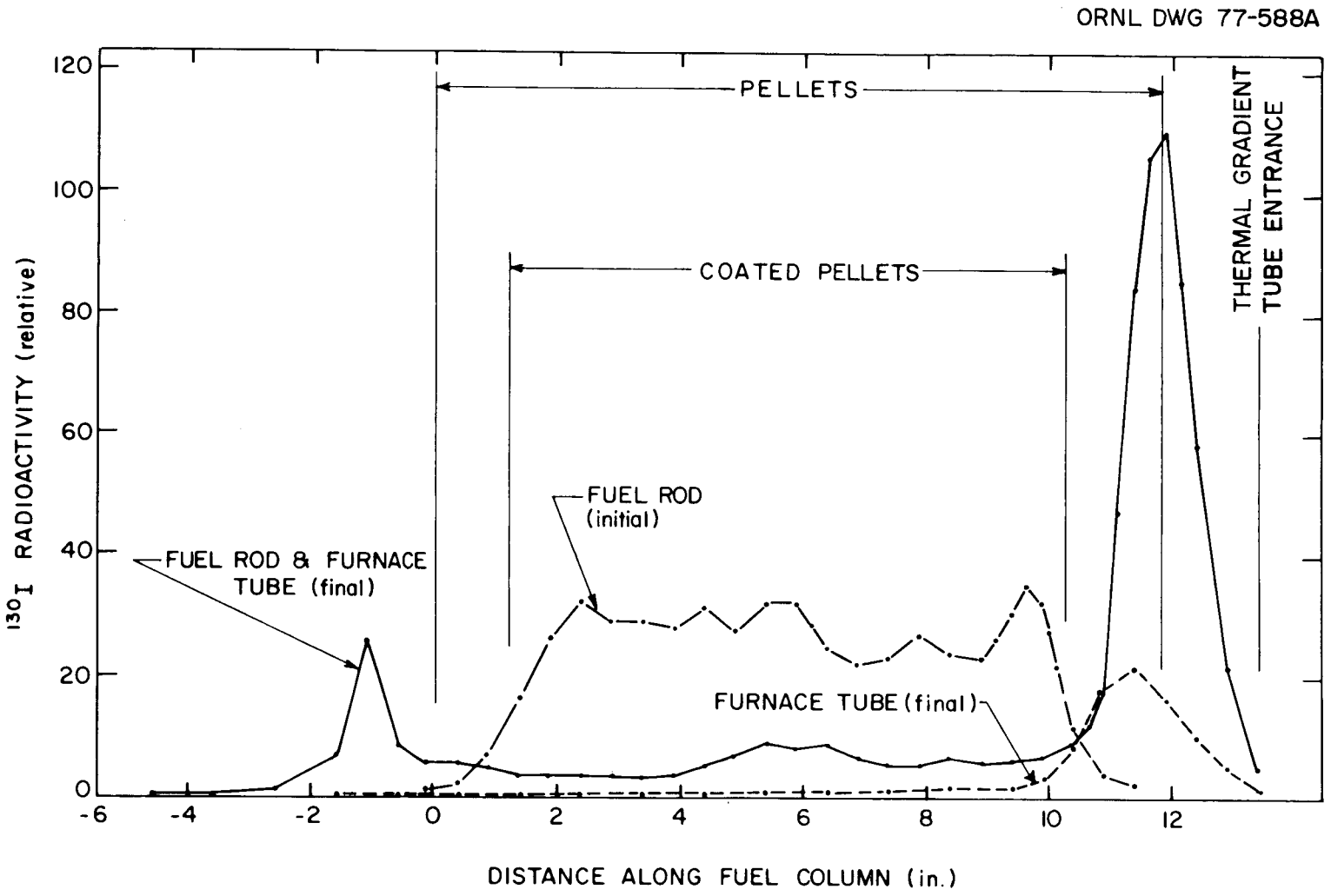

Fig. 18. Iodine-130 distribution in the fuel rod and furnace tube in Implant Test No. 4.

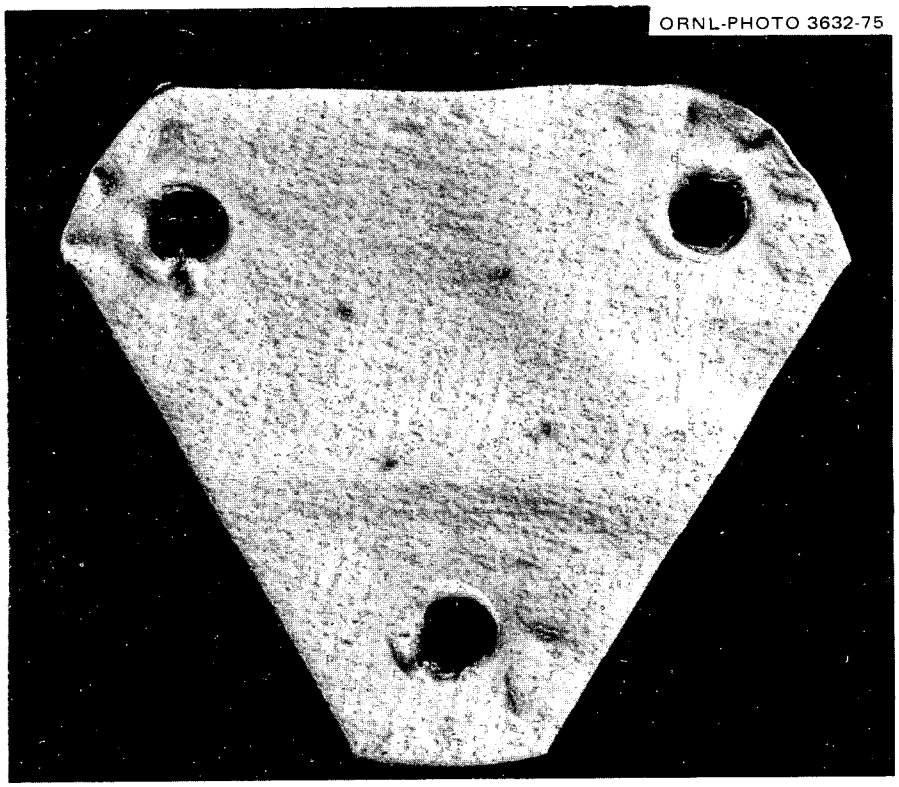

Fig. 19. Fifth collector stage from the cascade impactor showing material collected during Implant Test No. 4. Some of this material has been identified as $CsOH \cdot H_2O$.

Because the size and darkness of the material deposited on the impactor collection plates usually do not correlate with the amount of associated radioactivity, the existence of independent aerosol sources is indicated. Detailed distributions of the implanted species are presented in Table 5.

Concentration profiles of the cesium and iodine in the thermal gradient tube are presented in Fig. 20. The iodine peak at the 500°C location is likely CsI. Large particles, probably of cladding material, were found deposited along the entire length of the thermal gradient tube. These particulates most likely contained cesium and are probably responsible for the lack of structure in the cesium profile.

Oxidation of the Zircaloy cladding at 1100°C produced smoke-like deposits of ZrO_2 on the furnace tube liner, which ranged in color from black to white. After 20 min of experimentation, these ZrO_2 particulates began to accumulate at the orifice at the entrance to the cascade impactor; this necessitated a reduction of the steam-argon flow. As a result, a hydrogen-rich atmosphere developed in the furnace tube.

A sample of the cladding near the center of the rod was found to have a hydrogen content of 0.27%. Post-test examination of the cladding revealed it to be very brittle, and the surface flaky. Because some of the pellets were fused to the cladding, and because the cladding was too brittle, not all of the pellets could be removed from the cladding. This prevented the determination of separate nuclide concentration profiles for the cladding and pellets. Only the iodine profiles for the fuel rod before and after the test were determined; most of the iodine migrated to the cool ends (especially the outlet end) during the test. From a few segments of fuel rod where the pellets could be cleanly removed, it was found that the tellurium that had been placed on the pellets had been transferred almost completely by vaporization to the cladding, where it reacted to form a less-volatile compound. The reaction rings observed on the inner cladding surface in Implant 3 were not evident in this test, although the cladding was just as effective in preventing tellurium from being released from the rod.

Table 5. Distributions of cesium, iodine, and tellurium in Implant Test 4

Location	Temp. (°C)	Amount found in each location: Percent of total Cs	Percent of total I	Percent of total Te	μg Cs	μg I	μg Te
Fuel rod, total	900 to 1100	(74.78)	(67.14)	(99.90)			
UO_2 pellets		~47.13	~35.49	~6.0	2319.0	156.0	238.0
Zircaloy cladding		~27.65	~31.65	~93.9	1360.0	139.0	3728.0
Quartz furnace tube	~200 to 900	23.93	29.10	0.1	1177.0	128.0	4.0
Thermal gradient tube	750 to 190	1.21	1.43	0.0	59.5	6.3	
Orifice assembly	190	0.010	0.33	0.0	0.49	1.5	
Impactor assembly	145						
Impactor housing		0.002	1.29	<0.001	0.10	5.68	<0.04
First-stage paper		0.0	0.008	0.0		0.04	
Second-stage paper		0.001	0.004	0.0	0.05	0.02	
Third-stage paper		0.0	0.0	0.0			
Fourth-stage paper		0.0	0.001	0.0		0.004	
Fifth-stage paper		0.001	0.0	0.0	0.05		
Filter assembly	145						
Filter housing		0.001	0.37	<0.001	0.05	1.63	<0.04
First filter paper		0.0	0.010	0.0		0.04	
Second filter paper		0.0	0.010	0.0		0.04	
Third filter paper		0.0	0.003	0.0		0.01	
Silver screen No. 1		0.0	0.25	0.0		1.10	
Silver screen No. 2		0.0	0.006	0.0		0.03	
Silver screen Nos. 3 to 8		0.0	0.018	0.0		0.08	
Adsorber assembly	145						
Adsorber housing		<0.04	0.005	0.0	<2.0	0.02	
Charcoal No. 1		0.0	0.015	0.0		0.07	
Charcoal No. 2		0.0	0.0	0.0			
Charcoal No. 3		0.0	0.0	0.0			
AgX		0.0	0.0	<0.001			<0.04
Condenser assembly	0						
Condenser housing		0.0	0.0	0.0			
Condensate		0.0	0.0	0.0			
Freeze trap	-78	<0.004	0.0	0.0	<0.2		
Cold charcoal trap	-78	0.0	0.0	0.0			

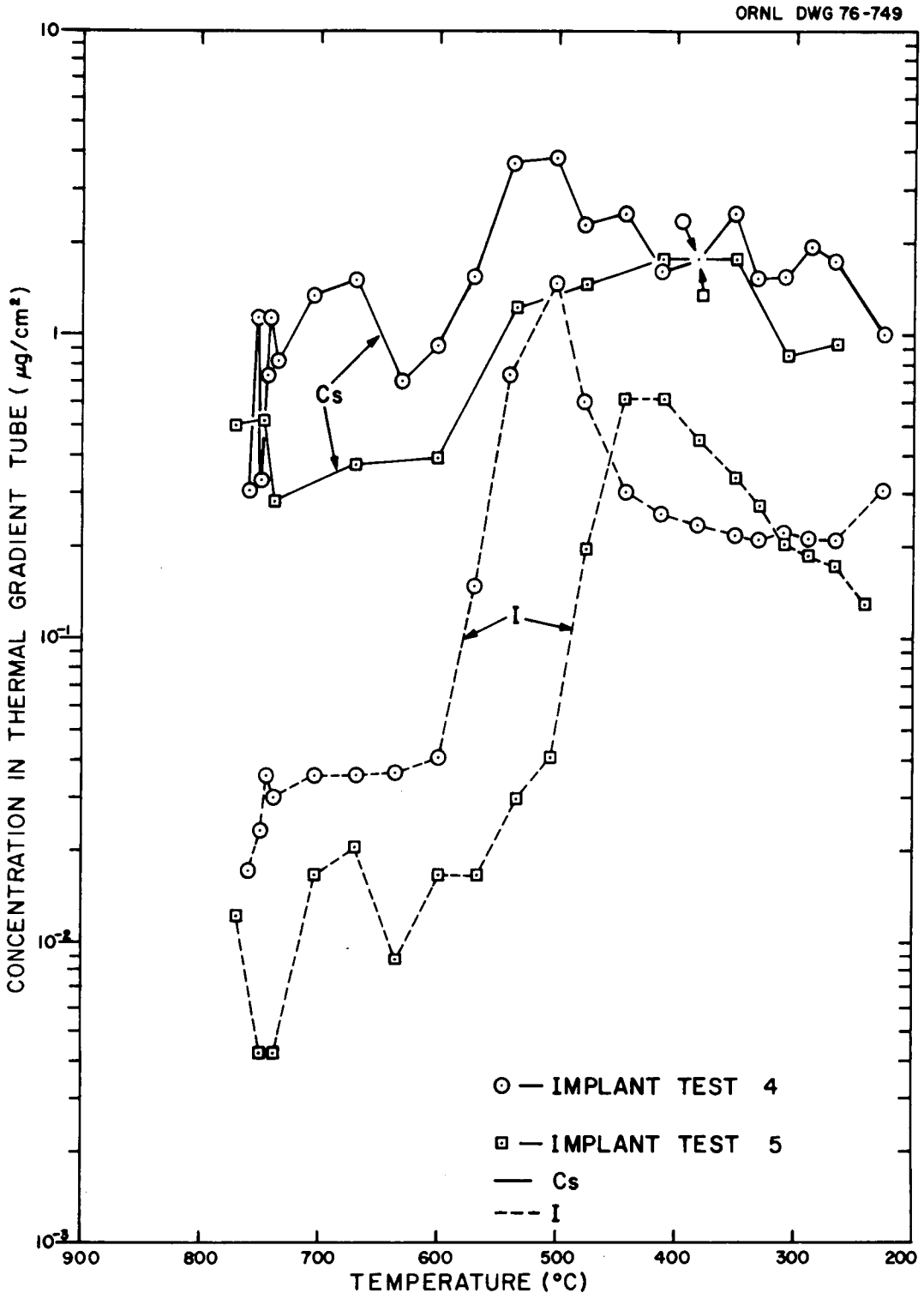

Fig. 20. Iodine and cesium concentration profiles in the thermal gradient tubes used in Implant Tests 4 and 5.

4.5 Behavior of Fission Product Simulant Mixtures at 700°C (Implant Test 5)

This test, which was conducted over a 2-hr period, utilized a Zircaloy rod which was thinned in one region to effect tube rupture at a burst pressure which would not be detrimental to the quartz furnace tube. The method of thinning the rod, which involved grinding part of the surface circumferentially to effect a uniform reduction in cladding thickness, resulted in a more energetic rupture than had been experienced in previous tests. Approximately 500-psi argon pressure was required to burst the rod, compared with a 330-psi burst pressure that was required in Implant Tests 1 and 2 (at 700°C), and 250 psi in Implant Test 3 (at 900°C). The resulting slit-like rupture in the thinned region of the rod is displayed in Fig. 21. As in all of the previous implant tests, the fuel rod was induction-heated, but the standard length induction coil was used to avoid overheating the stainless steel fittings at the ends of the rod. Detailed distributions of the implanted species are listed in Table 6.

Cesium concentration profiles in the fuel rod prior to testing and in the fuel rod components after testing are presented graphically in Fig. 22; corresponding profiles for iodine activity are given in Fig. 23. Axial migration of the iodine to the cooler ends of the rod was not evident. However, iodine buildup did occur at the 7-1/2-in. location; most of this buildup was associated with the cladding. A similar buildup of cesium on the cladding also occurred at the same location.

The percentages obtained for iodine on the pellets (48.9%) and on the cladding (33.2%) were very similar to those obtained for iodine on the pellets (43.7%) and cladding (33.8%) in Implant Test 1. Although the extent of CsI dissociation cannot be determined, as was done in Implant Test 1 (about 40%), it is likely that CsI was similarly dissociated. [The presence of the CsOH simulant (also ^{134}Cs traced) complicates the situation.] Both this test and Implant Test 1 were conducted under similar experimental conditions, except in this test the capsule was kept at 700°C for 2 hr.

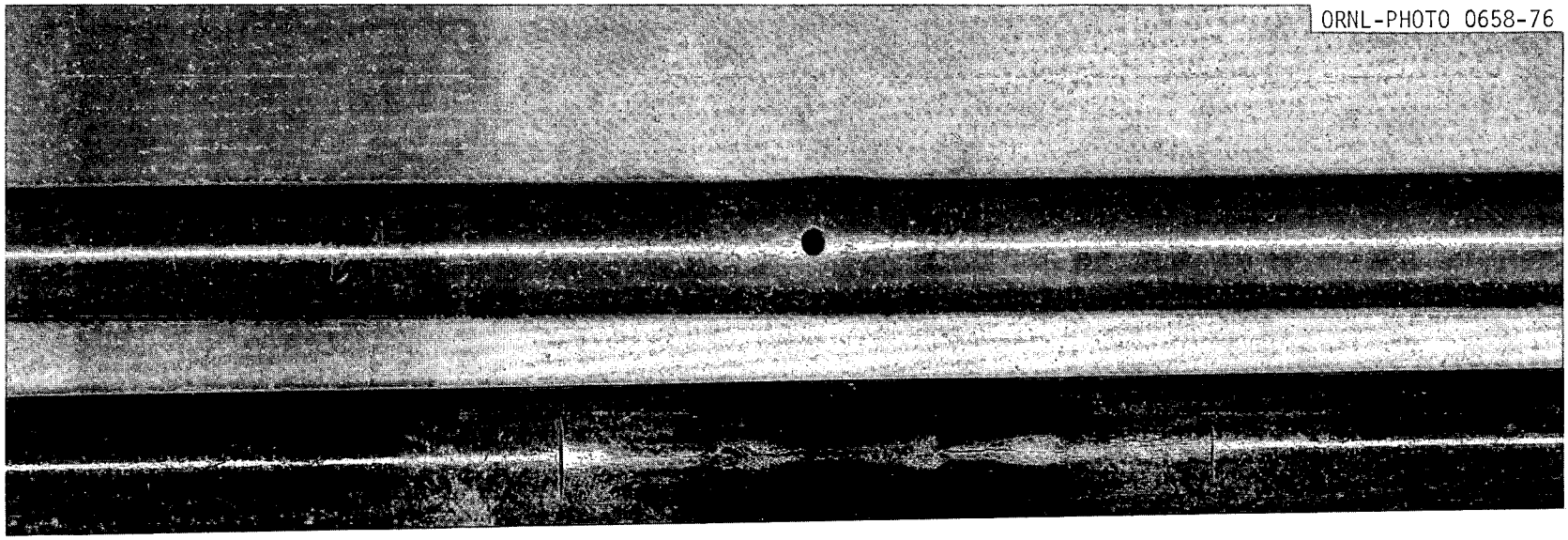

Fig. 21. Photograph of the fuel rods from Implant Test 5 (lower rod) and Implant Test 7 (upper rod).

Table 6. Distributions of cesium, iodine, and tellurium in Implant Test 5

Location	Temp. (°C)	Amount found in each location: Percent of total Cs	Percent of total I	Percent of total Te	μg Cs	μg I	μg Te
Fuel rod, total	700	(94.54)	(82.17)	93.50)			
UO_2 pellets		59.29	48.94	50.4	4178.0	298.5	1714.0
Zircaloy cladding		35.25	33.23	43.1	2485.0	202.7	1465.0
Quartz furnace tube	~200 to 500	4.97	16.20	6.3	350.0	98.8	214.0
Thermal gradient tube	770 to 200	0.32	0.65	0.0	22.56	3.97	0.01
Orifice assembly	160	0.0078	0.074	0.01	0.55	0.45	0.34
Impactor assembly	140						
Impactor housing		0.062	0.68	0.015	4.37	4.15	0.51
First-stage paper		0.0112	0.0625	0.025	0.79	0.38	0.85
Second-stage paper		0.0067	0.0087	0.016	0.47	0.053	0.54
Third-stage paper		0.0074	0.012	0.025	0.52	0.07	0.85
Fourth-stage paper		0.0088	0.021	0.025	0.62	0.13	0.85
Fifth-stage paper		0.0020	0.0053	0.0035	0.14	0.032	0.10
Filter assembly	120						
Filter housing		0.0007	0.025	0.0	0.05	0.15	0.0
First filter paper		0.0027	0.0050	0.001	0.19	0.030	0.34
Second filter paper		0.0004	0.0028	0.0	0.03	0.017	
Third filter paper		0.0	0.0031	0.0		0.019	
Silver screen No. 1		0.0006	0.064	0.0	0.04	0.39	
Silver screen No. 2		0.0	0.003	0.0		0.02	
Silver screen Nos. 3 to 8		0.0004	0.010	0.0	0.03	0.06	
Adsorber assembly	120						
Adsorber housing		0.009	0.0	0.0	0.63		
Charcoal No. 1		0.0003	0.006	0.0	0.02	0.04	
Charcoal No. 2		0.0005	0.0	0.0	0.04		
Charcoal No. 3		0.0004	0.0	0.0	0.03		
AgX		0.0023	0.0	0.0	0.16		
Condenser assembly	0						
Condenser housing		0.0	0.0	0.0			
Condensate		0.0	0.0	0.0			
Freeze trap	-78	0.0	0.0	0.0			
Cold charcoal trap	-78	0.0	0.0	0.0			

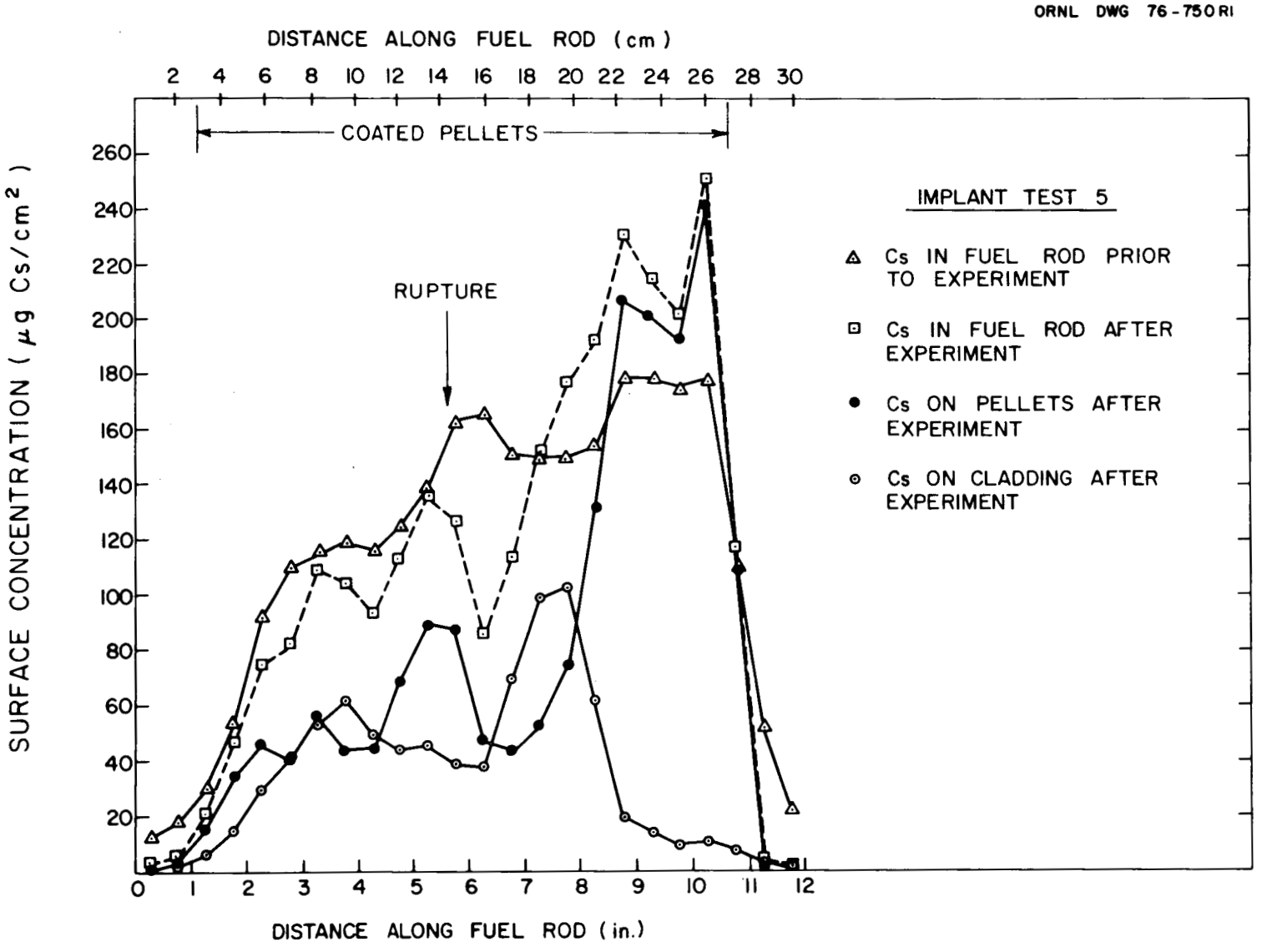

Fig. 22. Cesium distributions in the fuel rod of Implant Test No. 5.

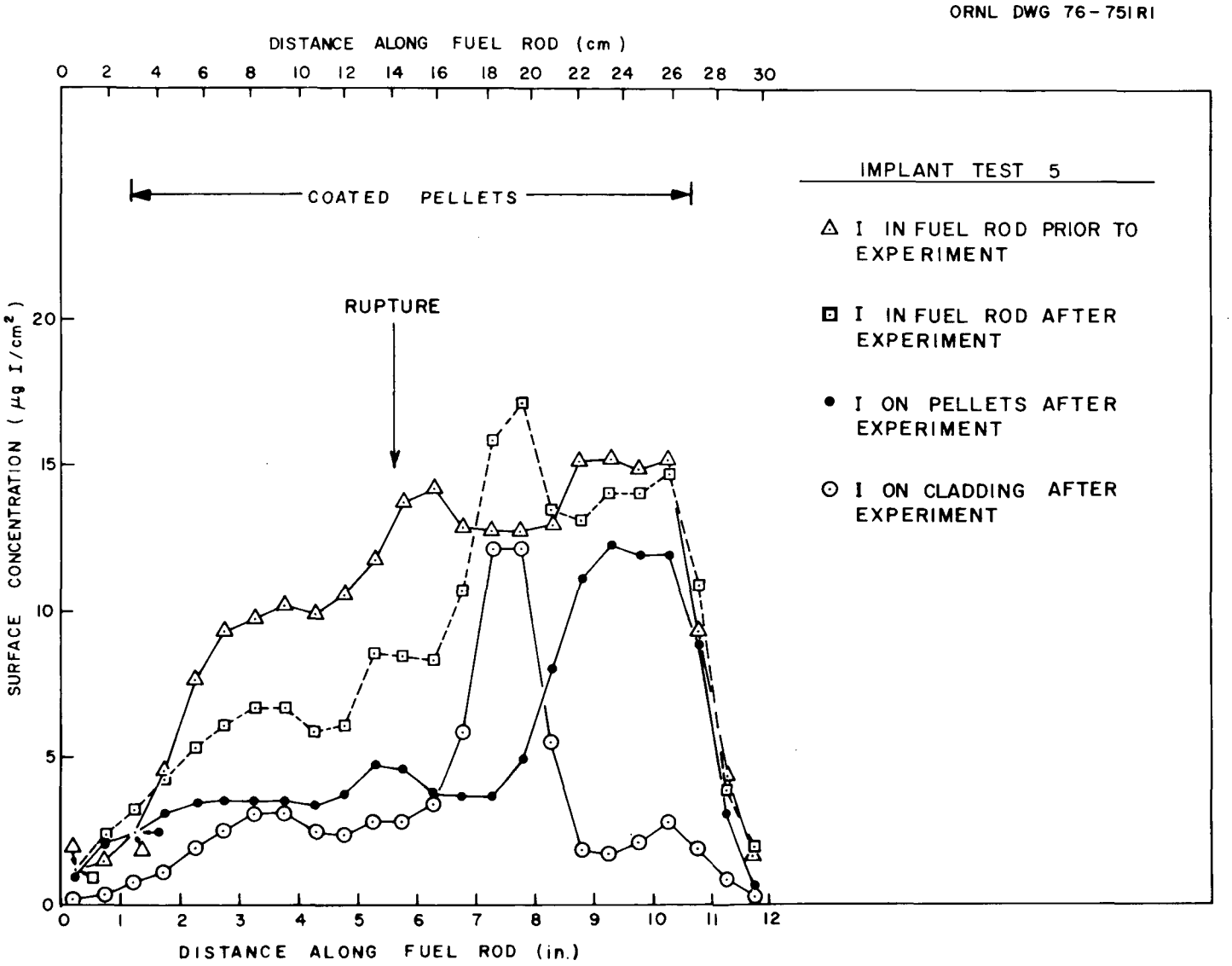

Fig. 23. Iodine distributions in the fuel rod of Implant Test No. 5.

As is readily evident from an examination of the data presented in Table 6, ∿5.5% of the cesium (385 μg), 17.8% of the iodine (109 μg), and 6.5% of the tellurium (221 μg) had been released from the burst rod. Because of the manner in which the rupture occurred, the tellurium release was larger than the releases obtained in the other nine implant tests that contained tellurium.

Continuous scanning of the collection system indicated that most of the iodine release occurred within 6 min of the time of rupture. This is readily seen from the results presented in Fig. 24; ∿70% of the iodine that had been deposited in the impactor and filter assembly did so shortly after rod rupture. Note that only ∿0.7% of the original iodine appeared to be released in elemental form (i.e., collected beyond the thermal gradient tube).

A dark deposit of smoke-like material was observed on the quartz liner of the furnace tube opposite the rod rupture. This material was found to contain $CsOH \cdot H_2O$, U_4O_9, and ZrO_2. Moreover, considerable iodine activity (probably CsI and zirconium iodide) was also detected at that location.

As in Implant Test 4, the cesium profile in the thermal gradient tube does not show much structure (Fig. 20), except to suggest that the iodine peak around 450°C is probably due to CsI.

4.6 Behavior of Fission Product Simulant Mixture at 500°C (Implant Test 6)

Implant Test 6 was conducted at 500°C over a 20-hr period. Unlike the previous tests, the operating temperature was maintained with an electric resistance heater. Because of difficulties that were encountered with a tension spring located at the furnace inlet end of the fuel rod, it was necessary to employ only two uncoated pellets (rather than three) at the furnace outlet end of the rod. Consequently, 29 rather than 30 pellets were used in the assembly. Moreover, a 1.6-mm-diam hole was drilled through the cladding at the center of the rod prior to insertion into the apparatus. (This size opening provides an area that is approximately equivalent to that obtained by rupturing the rods by internal pressurization. This method

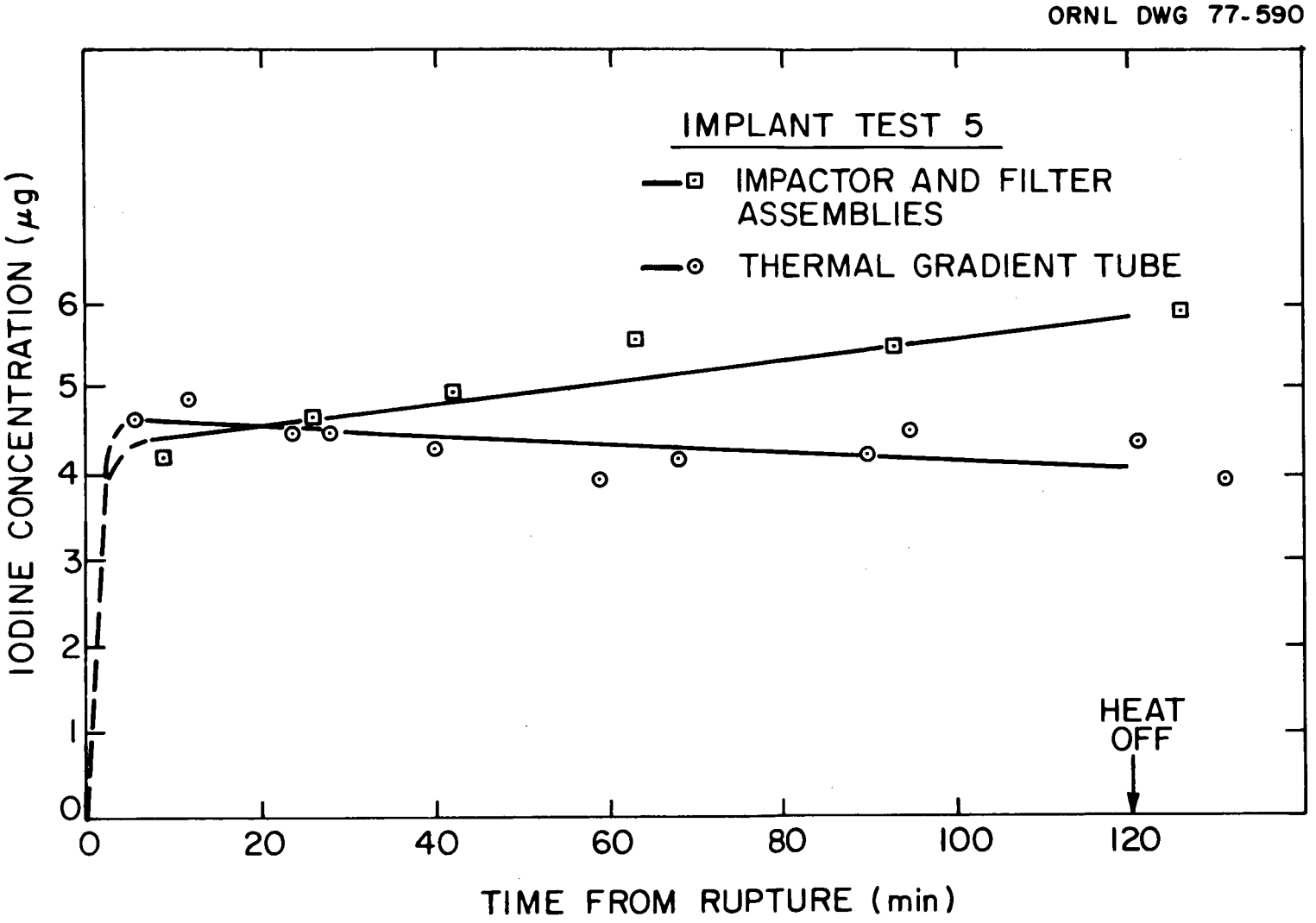

Fig. 24. Iodine deposition in the thermal gradient tube and the impactor-filter assembly during release from Implant Test No. 5.

of rupture simulation permits a more controlled study of the release of vapor species from the rod.)

Releases from the rod over the entire test period were quite small [0.5% tellurium (∿14 μg), ≤0.42% cesium (∿43 μg), and 0.65% iodine (5.8 μg)], as is apparent from the distributions which are listed in Table 7. Most of the iodine was deposited in elemental form, and ∿0.09% was sorbed by the first charcoal cartridge. This component, which penetrated the silver screens, is probably an organic iodide compound.

Release of the iodine, as deduced from measurements of activity in the impactor-silver screen filter assembly, appeared to be virtually linear with time over the 20-hr test period (Fig. 25). Redistribution of iodine in the axial direction was not observed (Fig. 26); similarly, no significant axial migration of cesium within the rod was detected (Fig. 27). This behavior was not unexpected in view of the low operating temperature. Approximately 44% of the implanted iodine, 33% of the implanted cesium, and 45% of the implanted tellurium deposited on the cladding.

The small amounts of material which were deposited along the thermal gradient tube were insufficient for concentration profile determinations.

4.7 Behavior of Fission Product Simulant Mixture in Dry Air at 700°C (Implant Test 7)

Implant Test 7 was the first experiment in this series to be conducted in a dry-air stream in simulation of SFTA conditions. As in the case with Implant Test 6, the cladding was perforated prior to the experiment by drilling a 1.6-mm-diam hole at about the midpoint location, and the rod was brought to temperature by a resistance heater. The distributions of iodine and cesium which were determined at the conclusion of the test are summarized in Table 8.

A notable difference in this test was the appearance of a copper-to-pink coloration on the exterior surface of the cladding. Unlike the finely cracked, black ZrO_2 surfaces which were observed in the previous implant tests, this surface had a smooth, unbroken texture. (The contrast is demonstrated photographically in Fig. 21.) Furthermore, as can be seen

Table 7. Distributions of cesium, iodine, and tellurium in Implant Test 6

Location	Temp. (°C)	Amount found in each location: Percent of total Cs	Percent of total I	Percent of total Te	µg Cs	µg I	µg Te
Fuel rod, total	500	(99.58)	(99.35)	(99.50)			
UO_2 pellets		66.54	55.22	54.8	6834.0	497.0	1403.0
Zircaloy cladding		33.04	44.13	44.7	3393.0	397.0	1144.0
Quartz furnace tube	500	<0.05	0.0	0.3	<5.14		7.7
Thermal gradient tube	750 to 150	<0.40	0.15	0.15	<41.08	1.35	3.8
Orifice assembly	150	0.001	0.009	0.03	0.10	0.08	0.77
Impactor assembly	130						
Impactor housing		0.012	0.069	0.066	1.23	0.62	1.69
First-stage paper		0.0	0.0	0.011			0.28
Second-stage paper		0.0	0.0	0.0			
Third-stage paper		0.0	0.0	0.0			
Fourth-stage paper		0.0	0.0	0.0			
Fifth-stage paper		0.0	0.0	0.0			
Filter assembly	130						
Filter housing		<0.001	0.02	0.0	<0.10	0.18	
First filter paper		0.0	0.002	0.0		0.02	
Second filter paper		0.0	0.001	0.0			
Third filter paper		0.0	0.0	0.0			
Silver screen No. 1		0.0	0.100	0.0		0.90	
Silver screen No. 2		0.0	0.04	0.0		0.36	
Silver screen Nos. 3 to 8		0.0	0.14	0.0		1.26	
Adsorber assembly	130						
Adsorber housing		0.0	0.003	0.0		0.03	
Charcoal No. 1		0.0	0.094	0.0		0.85	
Charcoal No. 2		0.0	0.0	0.0			
Charcoal No. 3		0.0	0.0	0.0			
AgX		0.0	0.003	0.0		0.03	
Condenser assembly	0						
Condenser housing		0.0	0.0	0.0			
Condensate		0.0	0.0	0.0			
Freeze trap	-78	0.0	0.009	0.0		0.08	
Cold charcoal trap	-78	0.0	0.0	0.0			

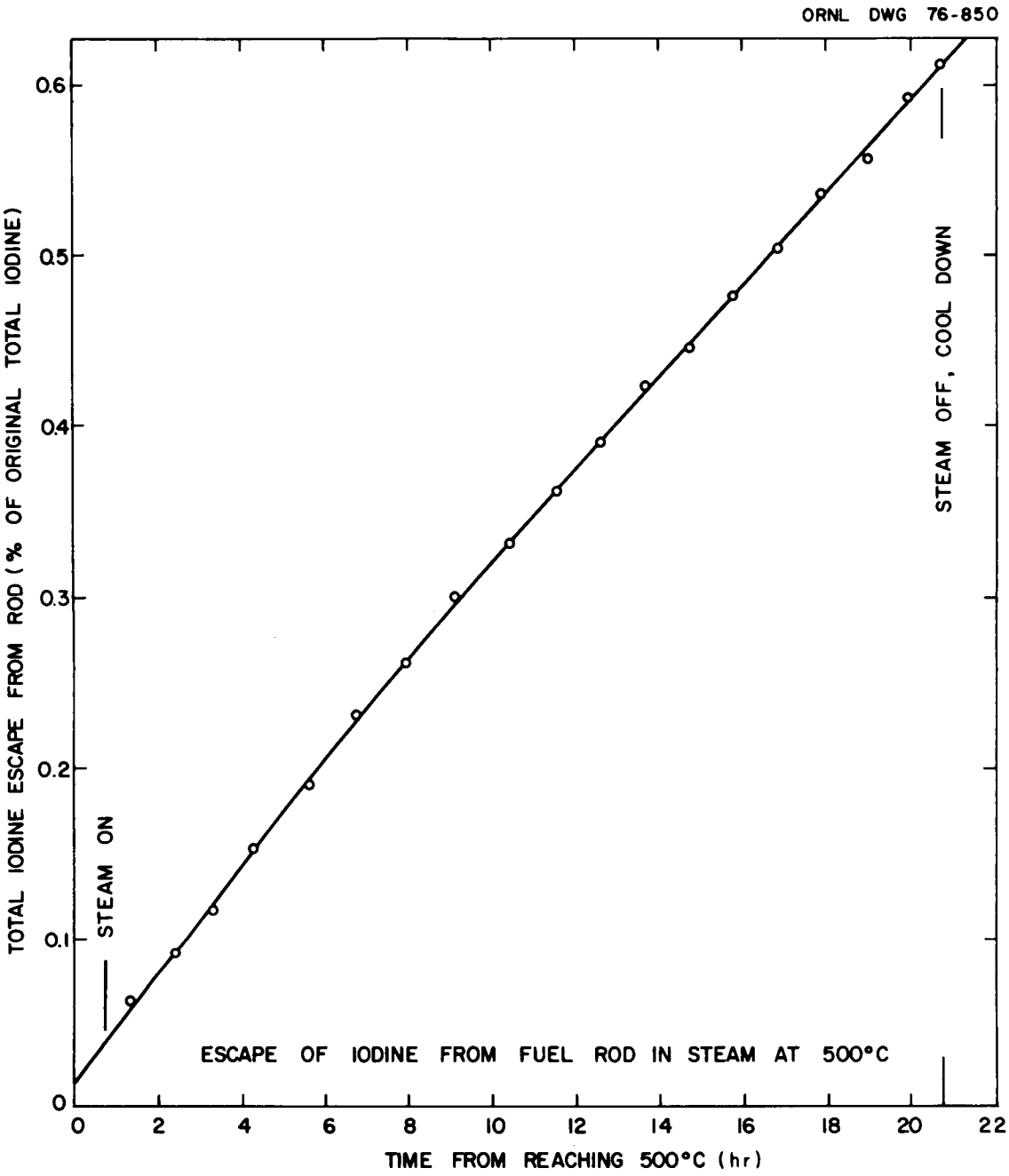

Fig. 25. Iodine release from a perforated fuel rod at 500°C in a flowing steam-argon atmosphere.

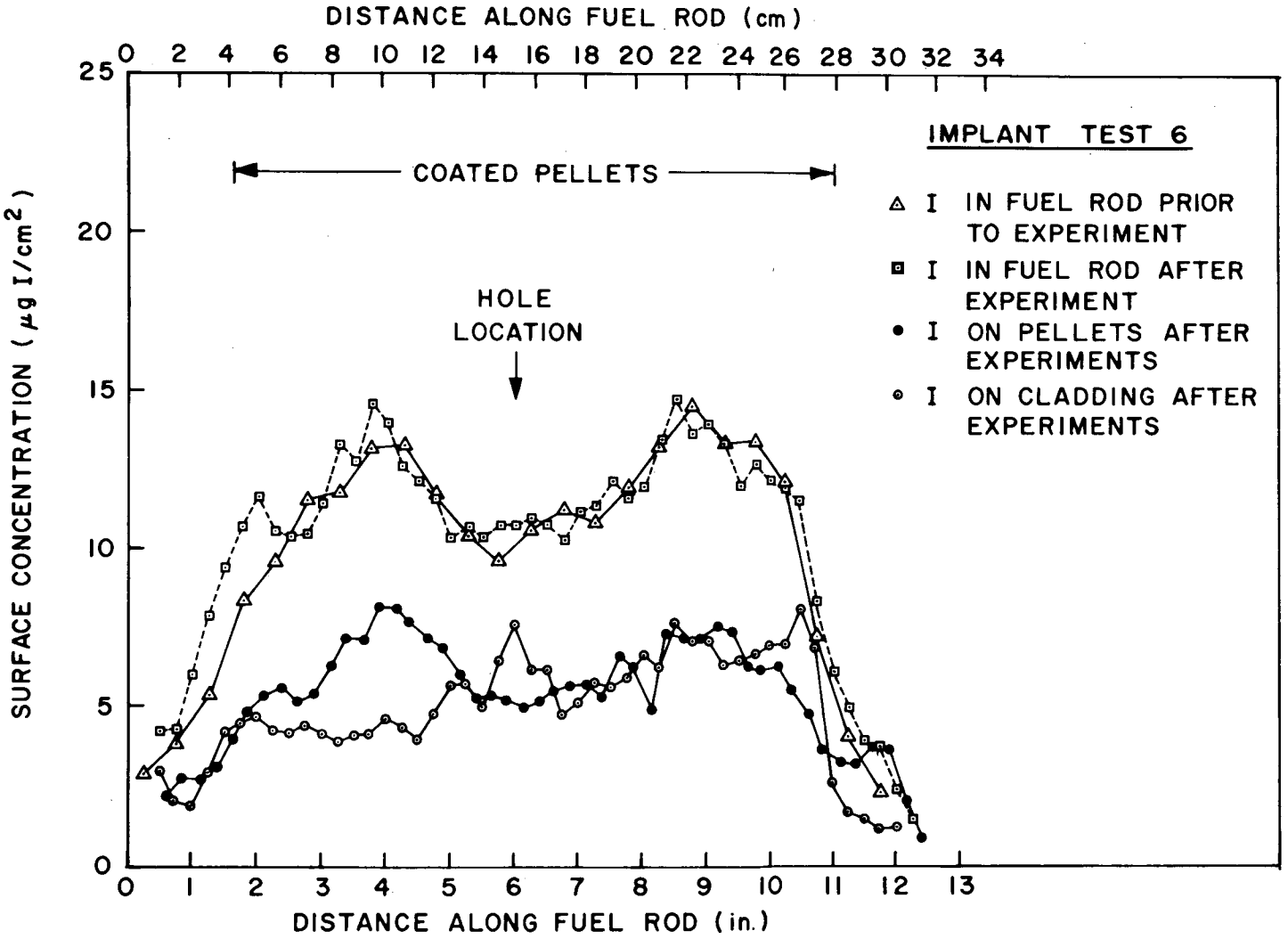

Fig. 26. Iodine distributions in the fuel rod employed in Implant Test No. 6.

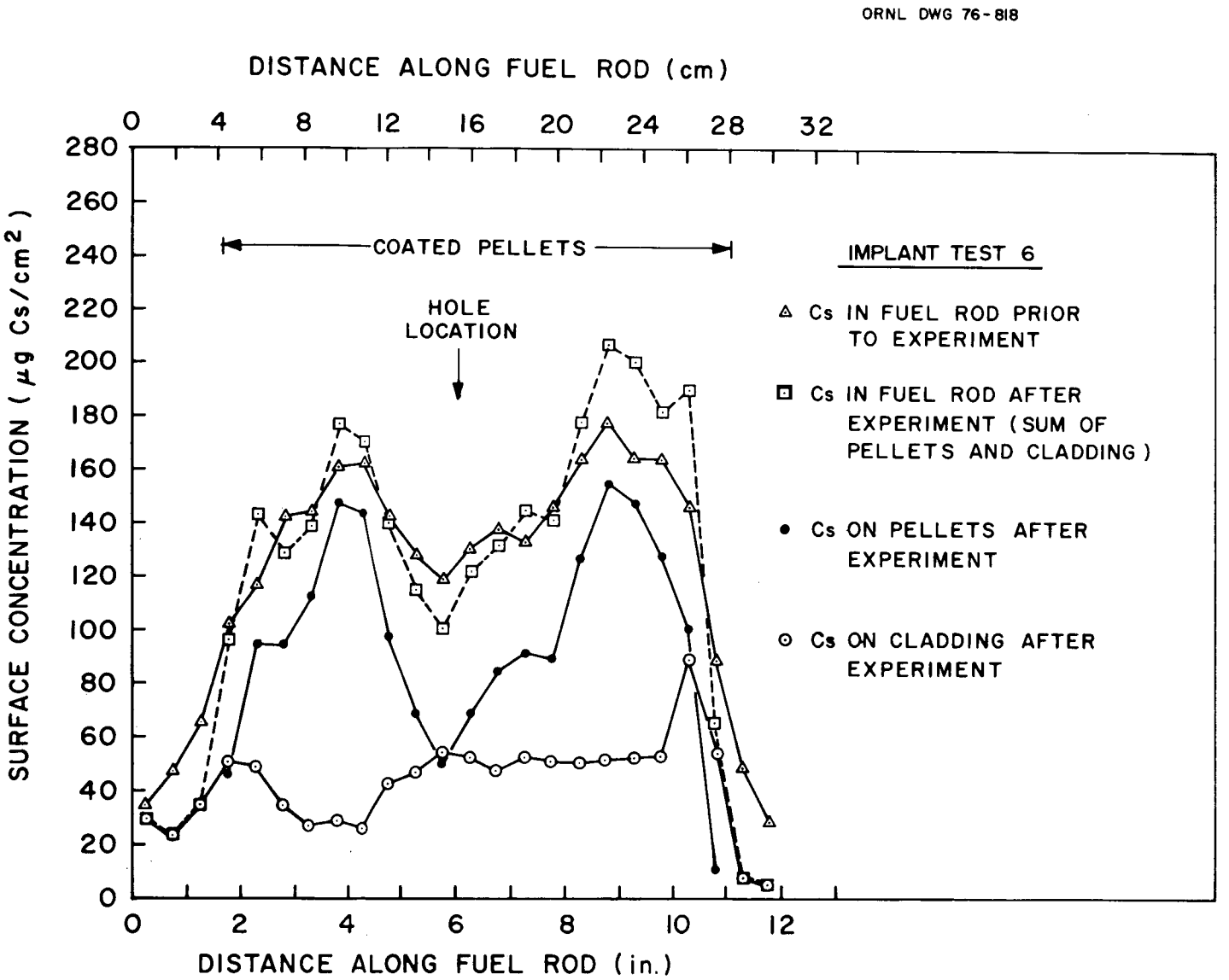

Fig. 27. Cesium distributions in the fuel rod employed in Implant Test No. 6.

Table 8. Distributions of cesium, iodine, and tellurium in Implant Test 7

Location	Temp. (°C)	Amount found in each location: Percent of total Cs	Percent of total I	Percent of total Te	µg Cs	µg I	µg Te
Fuel rod (total)	700	(98.88)	(88.42)	(99.99)			
UO_2 pellets		62.30	41.03		4847.0	262.6	3119.38
Zircaloy cladding		36.58	47.39		2846.0	303.3	
Quartz furnace tube	700	0.66	0.017	0.0	51.4	0.11	
Thermal gradient tube	750 to 165	0.44	0.322	<0.013	34.2	2.06	<0.41
Orifice assembly	165	0.0	0.008	<0.0003		0.05	<0.01
Impactor assembly	130						
Impactor housing		0.0057	0.183	<0.0006	0.44	1.17	<0.02
First-stage paper		0.0	0.008	0.0		0.05	
Second-stage paper		0.0	0.0	0.0			
Third-stage paper		0.0006	0.0	0.0	0.05		
Fourth-stage paper		0.0006	0.0	0.0	0.05		
Fifth-stage paper		0.0	0.004	0.0		0.03	
Filter assembly	130						
Filter housing		0.0020	0.238	0.0	0.16	1.52	
First filter paper		0.0020	0.066	0.0	0.16	0.42	
Second filter paper		0.0012	0.031	0.0	0.09	0.20	
Third filter paper		0.0014	0.051	0.0	0.11	0.33	
Silver screen No. 1		0.0009	10.47	0.0	0.07	67.0	
Silver screen No. 2		0.0014	0.053	0.0	0.11	0.34	
Silver screen Nos. 3 to 8		0.0005	0.015	0.0	0.04	0.10	
Adsorber assembly	125						
Adsorber housing		0.010	0.001		0.78	0.006	
Charcoal No. 1		0.0006	0.097	<0.0003	0.05	0.62	0.01
Charcoal No. 2		0.0	0.007	0.0		0.04	
Charcoal No. 3		0.0	0.0	0.0			
AgX		0.0013	0.0	0.0	0.10		
Condenser assembly	0						
Condenser housing		0.0	0.0	0.0			
Condensate		0.0	0.0	0.0			
Freeze trap	-78	0.0	0.0	0.0			
Cold charcoal trap	-78	0.0	0.0	0.0			

in Fig. 28, the surface features extended to part of the interior surface near the perforation. An x-ray diffraction pattern indicated the material to be identical to the black ZrO_2 identified from the previous tests but probably was comprised of smaller-sized crystallites.

A slight swelling of the cladding in the vicinity of the hole is readily seen in Fig. 21; this corresponds to a maximum circumferential change of ∿3 mm. The ends of the two pellets nearest the perforation and in the expanded region of the cladding were observed to be pulverized, whereas the opposite ends of these pellets were wedged tightly against the cladding. This behavior is unquestionably due to oxidation of the UO_2, which is quite rapid in air at temperatures >400°C.

The distribution of cesium in the rod prior to and after testing are presented graphically in Fig. 29; those for iodine are given in Fig. 30. The initial distributions of both species were somewhat less uniform than desirable. A larger percentage of iodine was found on the cladding in this test (44%) than in Implant Test 1 (34%) and 5 (33%), which were also conducted at 700°C (with steam-argon mixtures rather than air). The high oxygen atmosphere in conjunction with hyperstoichiometric fuel, which had an oxygen-to-metal ratio (O/M) of 2.0004, provided improved conditions for increased reactivity between the CsI and the fuel; this liberated additional elemental iodine which was subsequently available for reaction with the cladding or release from the capsule. [CsI has been shown to be thermally and chemically stable in hypostoichiometric fuel (O/M <2.0) and transports as CsI without interacting with the fuel or blanket material.[6]] About 37% of the cesium was found on the cladding and ∿62% on the pellets. In contrast, ∿96% of the implanted tellurium appeared on the cladding (the vapor pressure[7] of TeO_2 at 700°C is 4×10^{-2} torr); once again, the tellurium deposited on the cladding in the immediate vicinity of the pellet interfaces on which it had been implanted.

Less than 0.015% (0.4 μg) of the tellurium inventory was released in this test, whereas 1.1% of the cesium (87 μg) and 11.6% of the iodine (74 μg) were released. The iodine deposition characteristics indicate that virtually all of the iodine found was of the elemental form; as

Fig. 28. View of the interior of the cladding used in Implant Test No. 7.

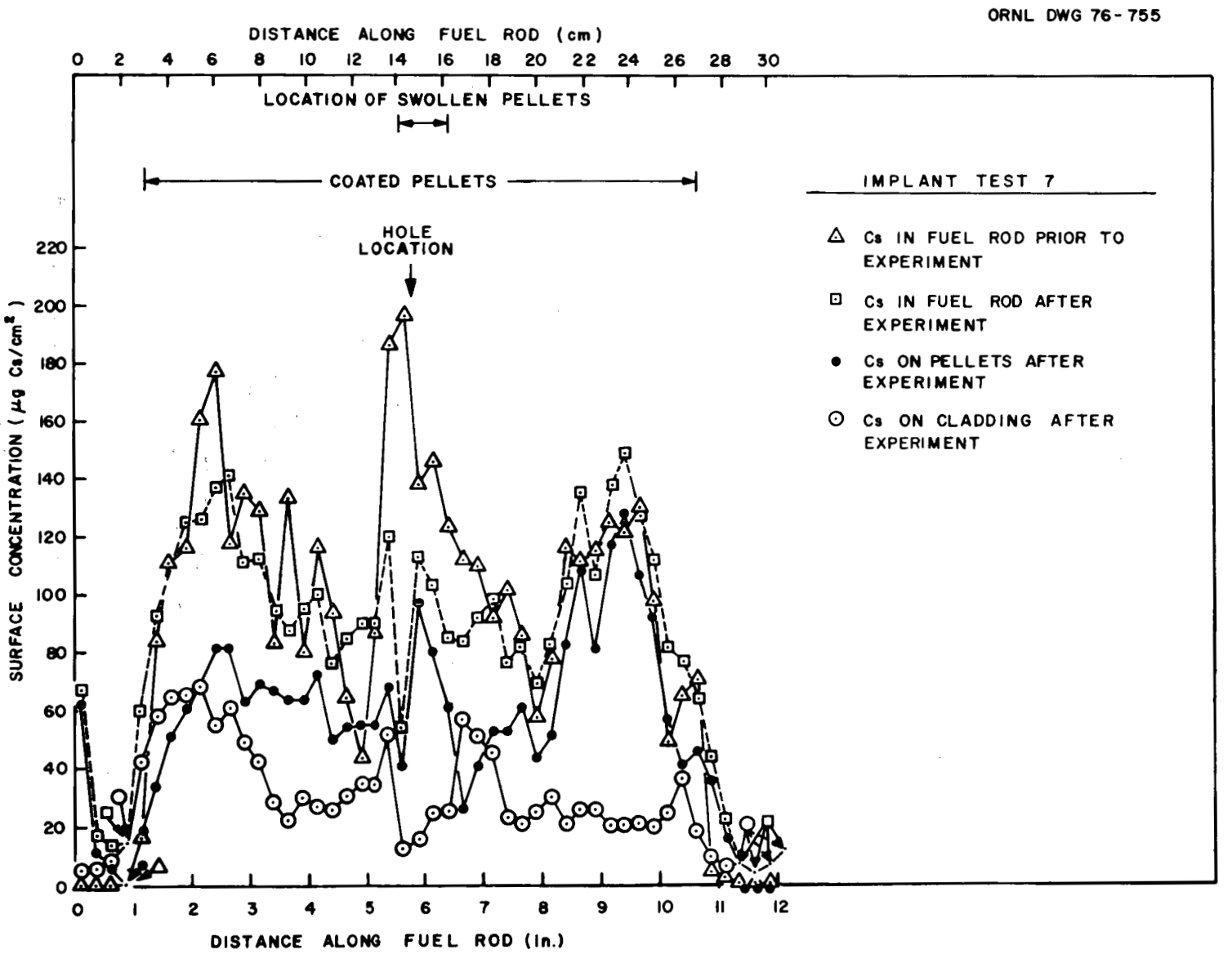

Fig. 29. Cesium distributions in the fuel rod of Implant Test No. 7.

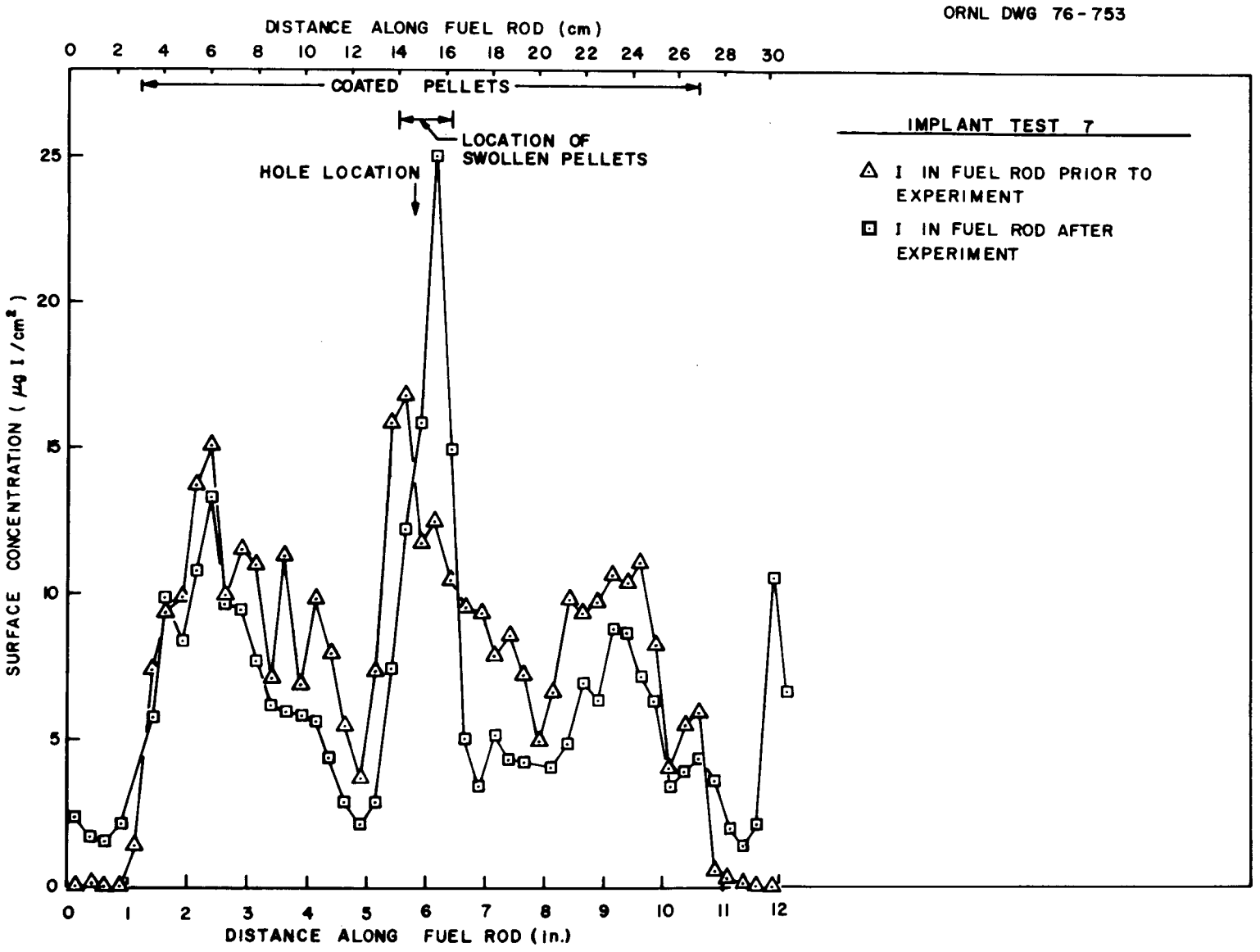

Fig. 30. Iodine distributions in the fuel rod of Implant Test No. 7.

seen in Table 8, ∿10.0% of the initial inventory was collected on the silver screen. The elemental iodine probably resulted as a product of CsI reaction with the fuel and/or the quartz furnace tube. The effect of the dry-air atmosphere as related to the deposition of cesium and iodine compounds in the thermal gradient tube (Fig. 31) is not fully understood. More than half of the cesium species which was deposited in the thermal gradient tube appeared in the high-temperature region (∿650°C). This suggests a less-volatile species of cesium. (Deposits of more-volatile CsOH and CsI are normally found in the region of 300 to 600°C.)

The rate of release of iodine from the rod, as determined by monitoring iodine activity in the impactor-filter assembly, is presented graphically in Fig. 32.

4.8 Behavior of Fission Product Simulant Mixture at 1100°C (Implant Test 8)

Implant Test 8 was performed at 1100°C over a 1-hr period. The orifice plate in the collection system was not used, and the steam flow rate was increased by a factor of 4 over normal in order to ensure a steam-rich atmosphere. (The reaction of steam with Zircaloy to form ZrO_2 and H_2 is very rapid at 1100°C.) The induction-heated fuel rod was ruptured at 900°C upon application of 425 psig internal argon pressure; this caused a rupture opening of about 24 mm^2. The rod temperature was subsequently raised to 1100°C. A photograph showing the post-test appearance of the fuel rod is presented in Fig. 33. The maximum circumferential change about the rupture area was ∿7.5 mm.

The distributions of cesium in the rod prior to and after testing are presented graphically in Fig. 34; those for iodine are given in Fig. 35. It can be seen that there was considerable axial migration of both cesium and iodine to the cool ends of the fuel rod. Figure 36 shows that most of the iodine migrated to the cool ends of the fuel rod in the first 8 min following the rupture. (It took 4 min to raise the temperature of the fuel rod from 900 to 1100°C after rupture.) The increase in cesium concentration at the rupture location of the fuel rod, as can be seen from the data

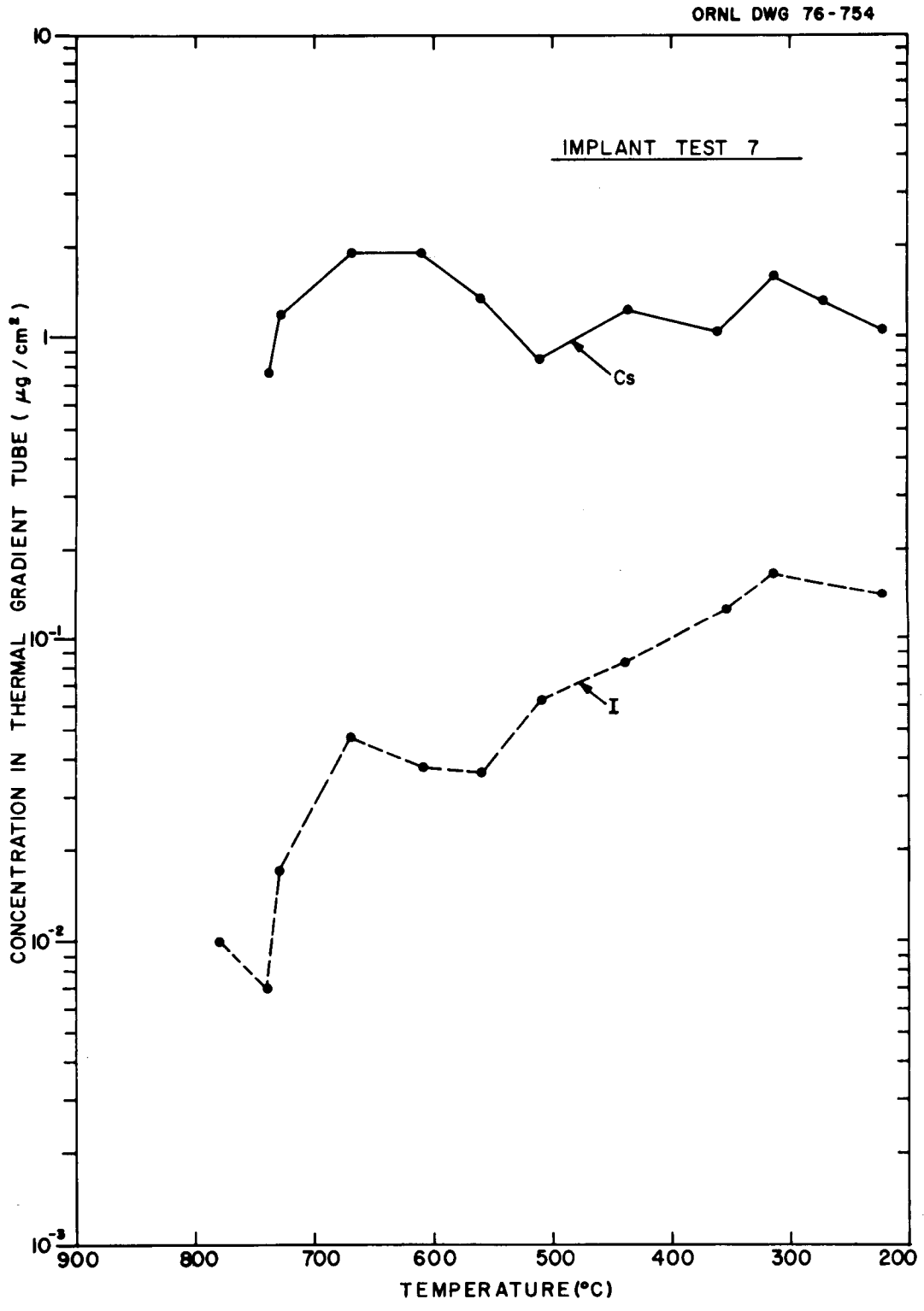

Fig. 31. Cesium and iodine concentration profiles in the thermal gradient tube from Implant Test No. 7.

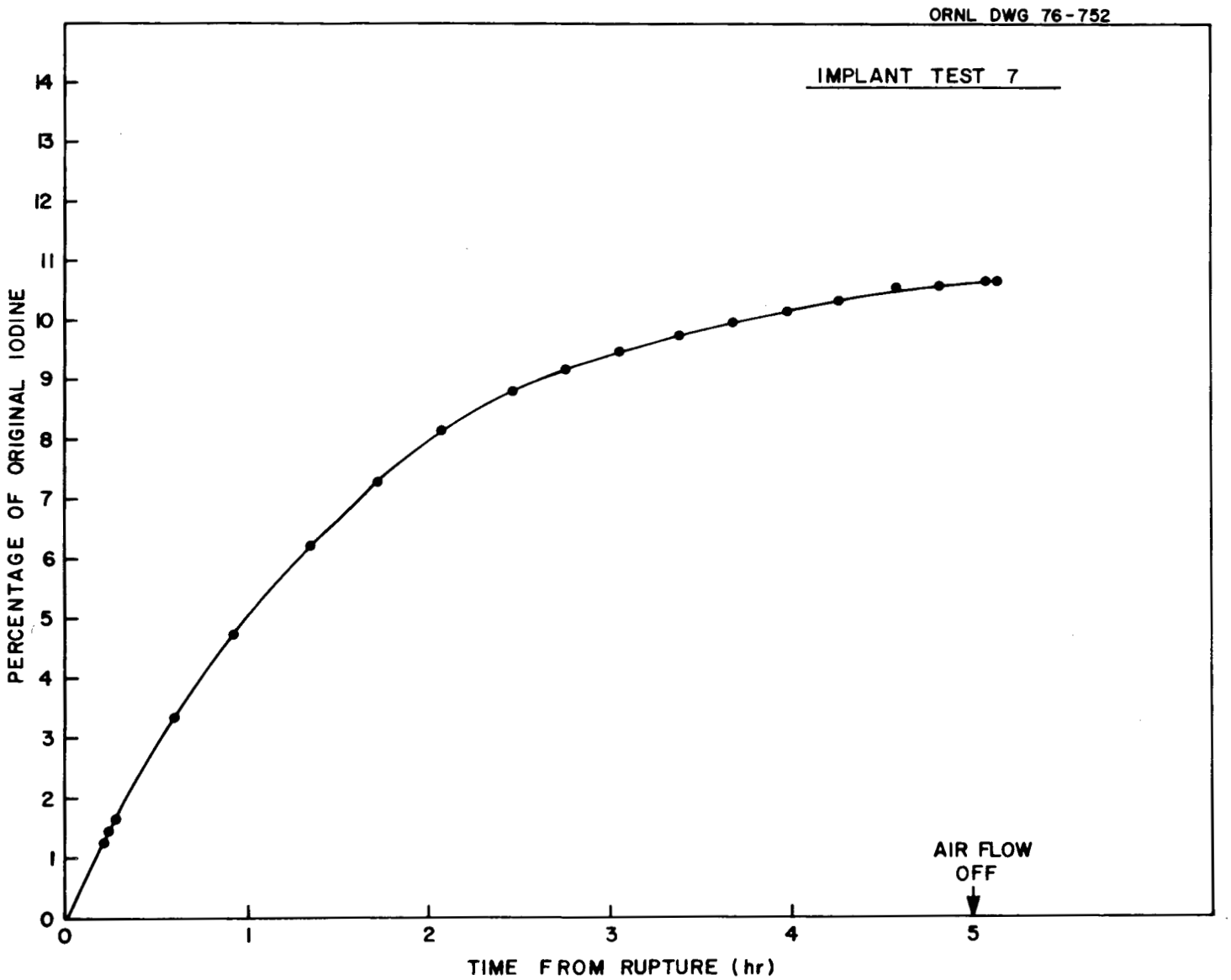

Fig. 32. Iodine deposition in the impactor-filter assembly during Implant Test No. 7.

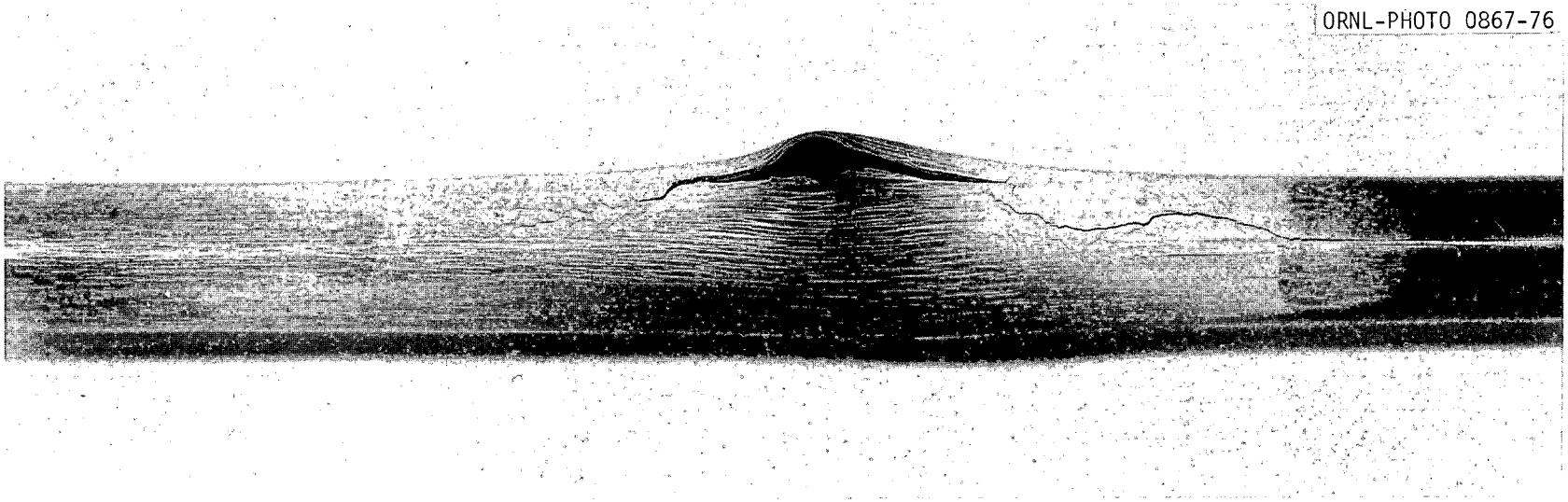

Fig. 33. Photograph of the fuel rod used in Implant Test No. 8.

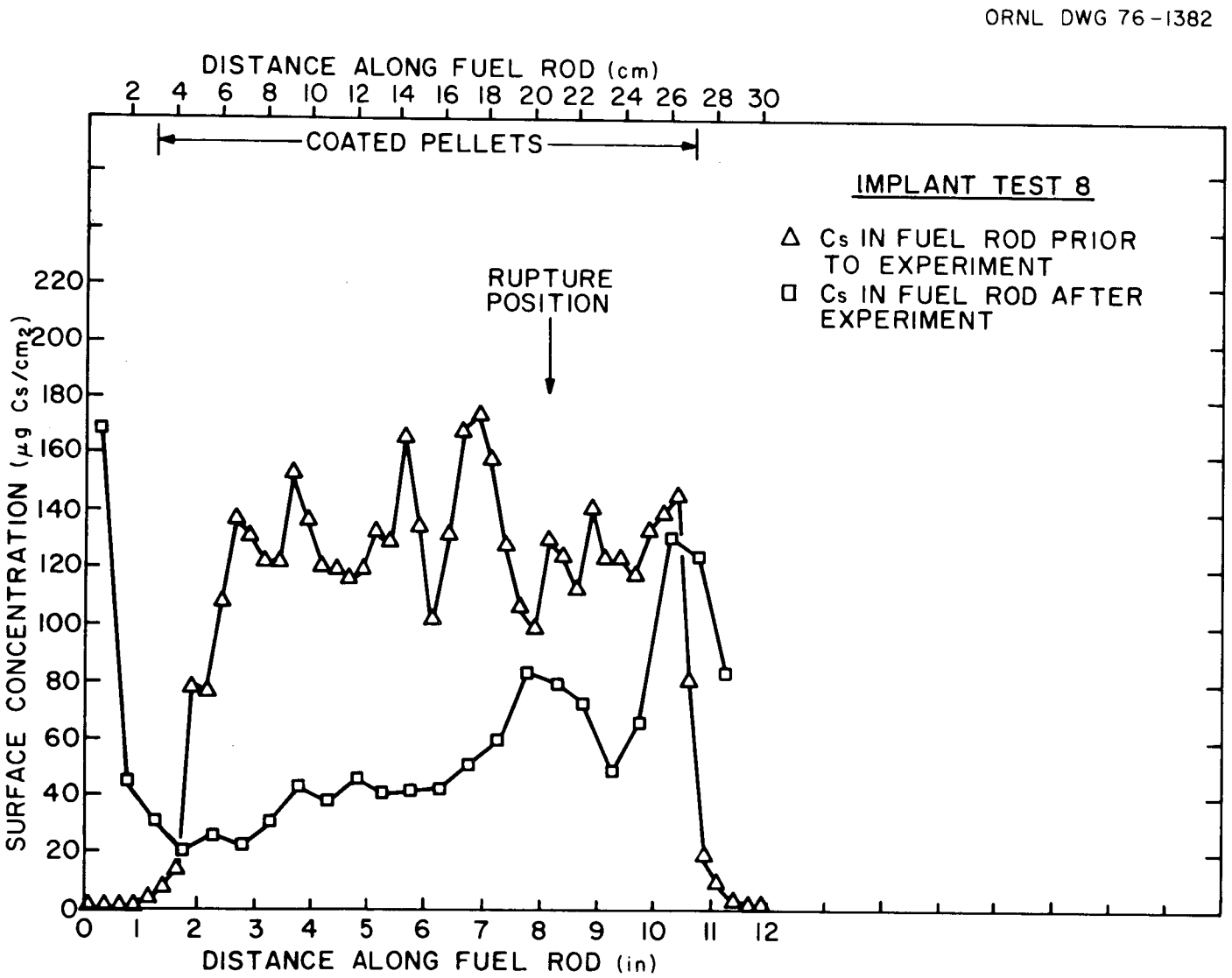

Fig. 34. Cesium distributions in the fuel rod of Implant Test No. 8.

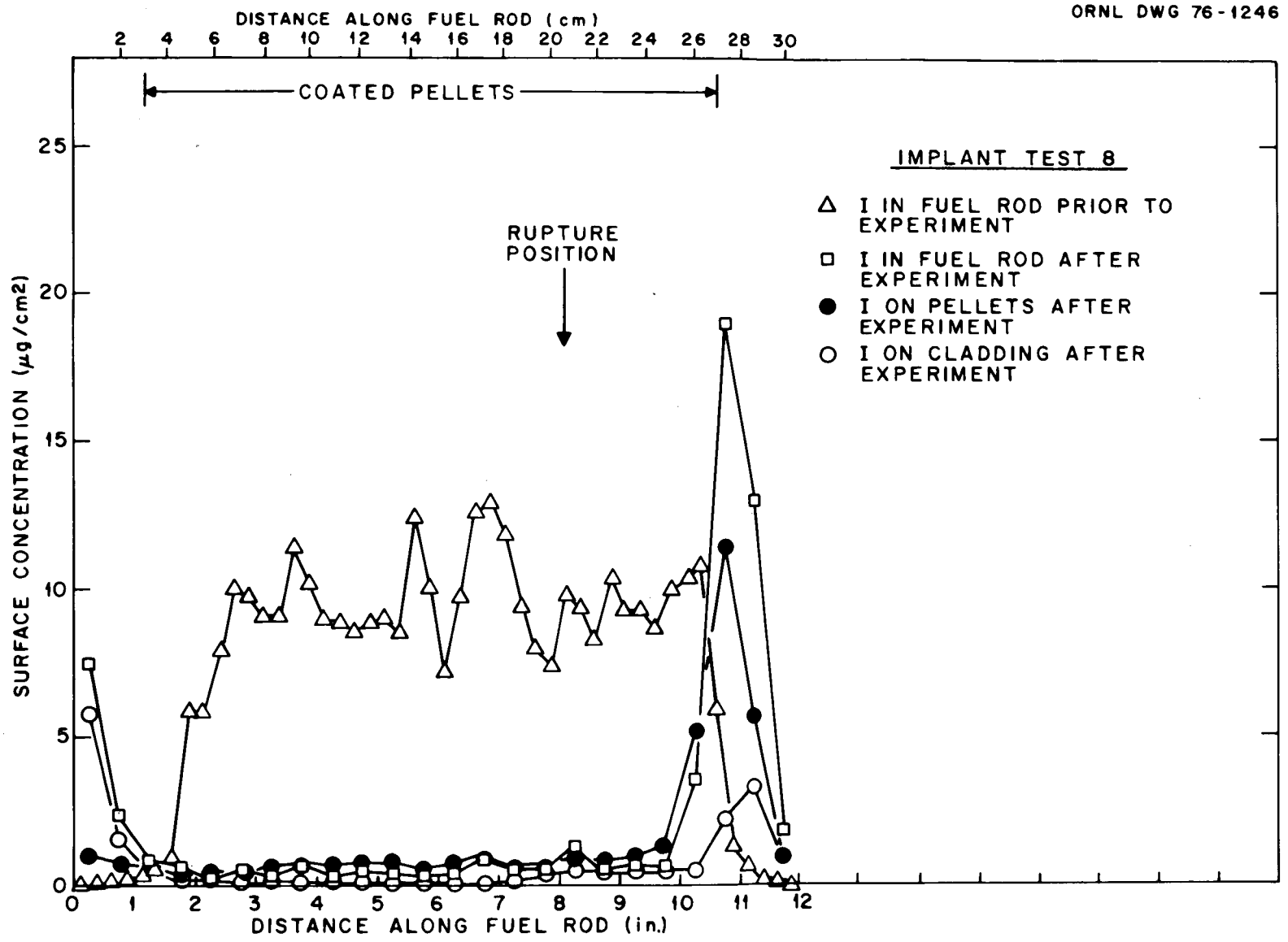

Fig. 35. Iodine distributions in the fuel rod of Implant Test No. 8.

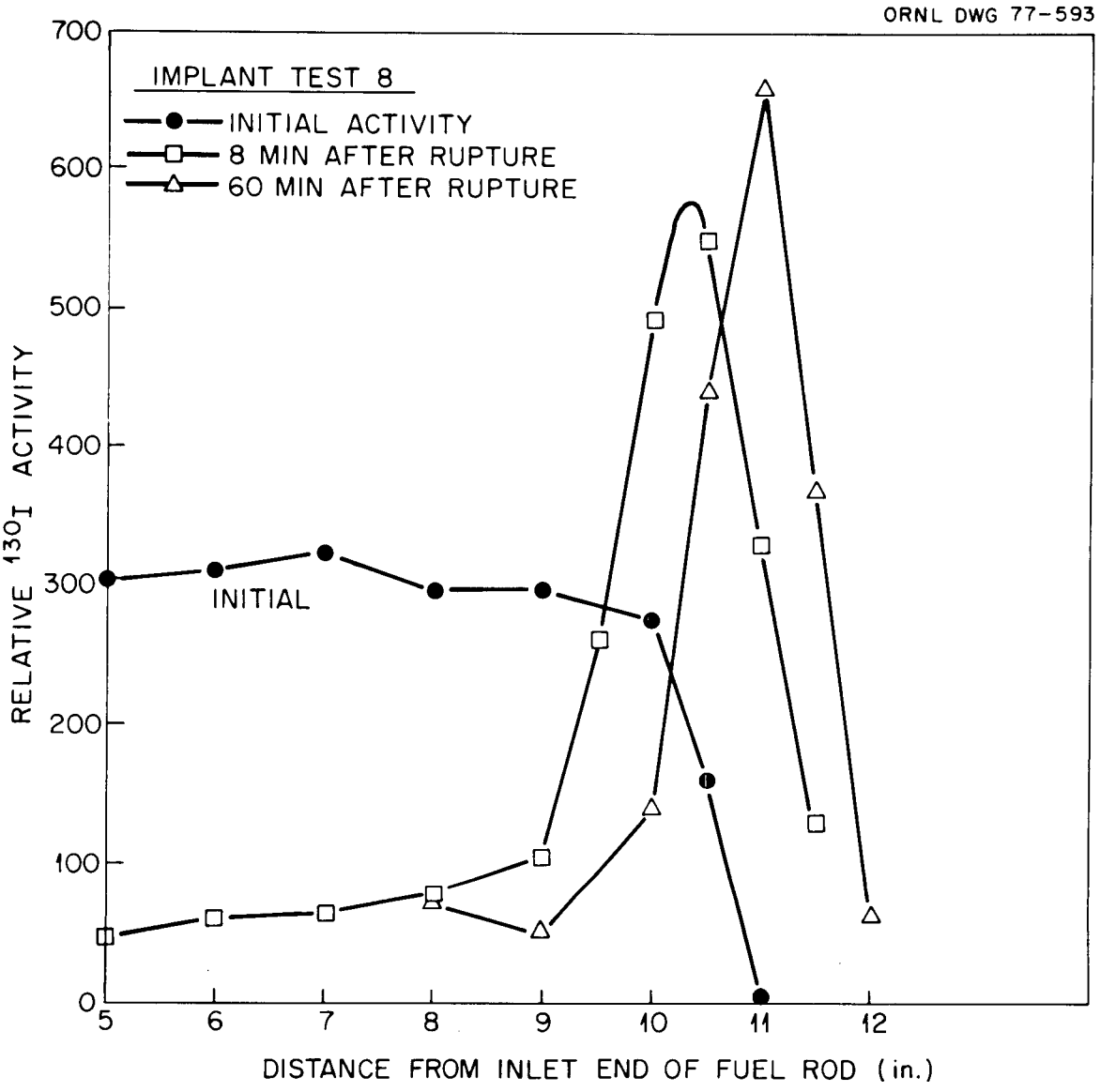

Fig. 36. Rate of axial migration of iodine to the cooler outlet end of the fuel rod in Implant Test No. 8.

displayed in Fig. 34, was probably caused by that area being at a lower temperature than the rest of the rod (excluding the cool ends). After the fuel rod ruptured, the rupture location darkened (in contrast with the rest of the glowing-red rod), and the darkened area slowly expanded during the test. Obviously, the darkened area was at a lower temperature than the adjacent regions. (An axial split, or oxidation of the Zircaloy, would result in reduced electromagnetic coupling with the induction heating coil.)

The data presented in Table 9 indicated that 35.9% of the cesium (3312 μg), 65.8% of the iodine (401 μg), and 3.3% of the tellurium (91 μg) inventories were released from the fuel rod. In addition to the high fuel-rod temperature (1100°C), the large rupture opening undoubtedly contributed to the considerable release of iodine and cesium. In the experiments that were conducted at lower temperatures, release of cesium was apparently restricted by reaction of the CsOH simulant with the fuel and cladding. Such was not the case in this experiment, however. On the other hand, reaction of the tellurium with the cladding again limited the release of this species. About 91% of the original tellurium was deposited on the cladding in the immediate vicinity of the pellet interfaces on which it had been implanted. Approximately 24% of the original cesium was deposited on the quartz liner of the furnace tube. Post-test scans of the furnace tube (Fig. 37) revealed that the iodine was located in the cooler section of the furnace tube, between the end of the induction coil and the entrance to the thermal gradient tube; most of the cesium was located adjacent to the rupture opening. A tellurium peak was also found opposite the rupture.

As shown by the data presented in Fig. 38, ∿70% of the iodine in the thermal gradient tube and 77% of the iodine in the impactor and filter assembly deposited within 10 min following rupture. Concentration profiles of cesium and iodine in the thermal gradient tube are shown in Fig. 39. The peaks of iodine and cesium at the 380°C location probably represent condensed CsI and CsOH. (The presence of $CsOH \cdot H_2O$ was determined by x-ray diffraction.) Only ∿20% of the cesium in the thermal gradient tube was cesium iodide, based on the amount of iodine present.

Table 9. Distributions of cesium, iodine, and tellurium in Implant Test 8

Location	Temp. (°C)	Amount found in each location: Percent of total Cs	Percent of total I	Percent of total Te	µg Cs	µg I	µg Te
Fuel rod, total	1100	(64.08)	(34.25)	(96.68)			
UO_2 pellets		44.57	22.46	6.07	4109.0	137.0	166.9
Zircaloy cladding		19.51	11.79	90.61	1799.0	71.9	2492.0
Quartz furnace tube	~200 to 800	24.19	15.86	0.87	2230.0	96.7	23.9
Thermal gradient tube	750 to 180	6.80	22.32	0.0	627.0	136.2	0.0
Orifice assembly	155	0.050	0.26	0.04	4.61	1.59	1.10
Impactor assembly	155						
Impactor housing		2.04	8.43	1.31	188.0	51.4	36.0
First-stage paper		0.49	2.49	0.51	45.0	15.19	14.0
Second-stage paper		0.20	0.49	0.06	18.0	2.99	1.65
Third-stage paper		0.18	0.68	0.04	17.0	4.15	1.10
Fourth-stage paper		0.29	0.91	0.07	27.0	5.55	1.93
Fifth-stage paper		0.21	2.66	0.19	19.0	16.23	5.23
Filter assembly	155						
Filter housing		0.12	1.15	0.03	11.0	7.02	0.83
First filter paper		1.07	3.14	0.04	99.0	19.15	1.10
Second filter paper		0.031	0.17	0.02	2.9	1.04	0.55
Third filter paper		0.034	0.17	0.02	3.1	1.04	0.55
Silver screen No. 1		0.0068	5.52	0.10	0.63	33.7	2.75
Silver screen No. 2		0.0084	0.23	0.003	0.77	1.40	0.08
Silver screen Nos. 3 to 8		0.060	0.41	0.006	5.5	2.50	0.17
Adsorber assembly	115						
Adsorber housing		0.062	0.33	0.01	5.7	2.01	0.28
Charcoal No. 1a		0.0064	0.105	0.0015	0.59	0.64	0.04
Charcoal No. 1b		0.0027	0.025	0.0006	0.25	0.15	0.02
Charcoal No. 1c		0.0032	0.019	0.0008	0.30	0.12	0.02
Charcoal No. 1d		0.0043	0.022	0.0006	0.40	0.13	0.02
Charcoal No. 2		0.0157	0.081	0.003	1.45	0.49	0.08
Charcoal No. 3		0.0092	0.051	0.001	0.85	0.31	0.03
AgX		0.0066	0.038	0.001	0.61	0.23	0.03
Condenser assembly	0						
Condenser housing		0.003	0.002	0.0	0.3	0.01	0.0
Condensate		0.018	0.18	0.0	1.66	1.10	0.0
Freeze trap	-78	0.0	0.0	0.0	0.0	0.0	0.0
Cold charcoal trap	-78	<0.04	0.0	0.0	<3.7	0.0	0.0

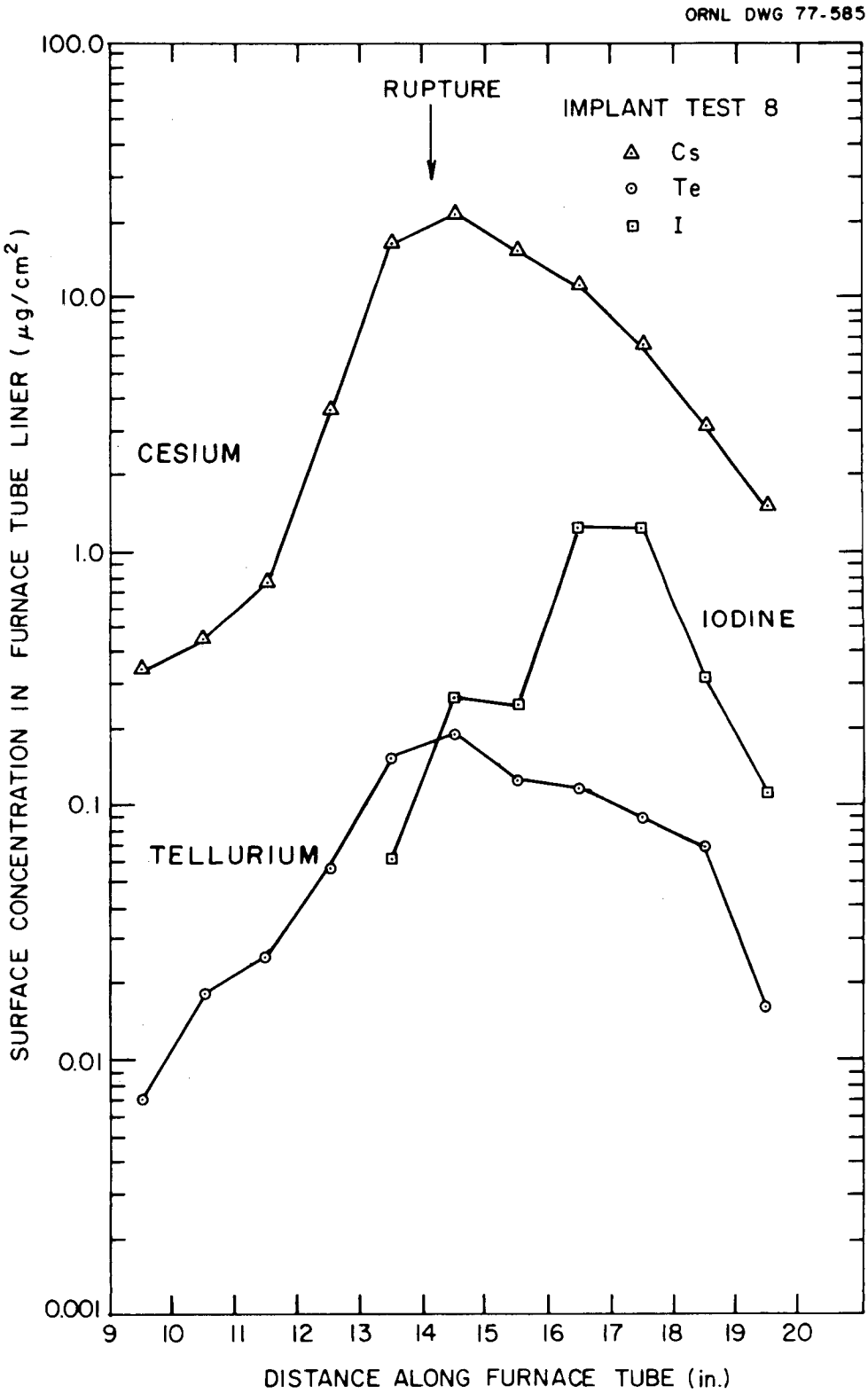

Fig. 37. Distribution of radionuclides along the quartz furnace tube liner in Implant Test No. 8.

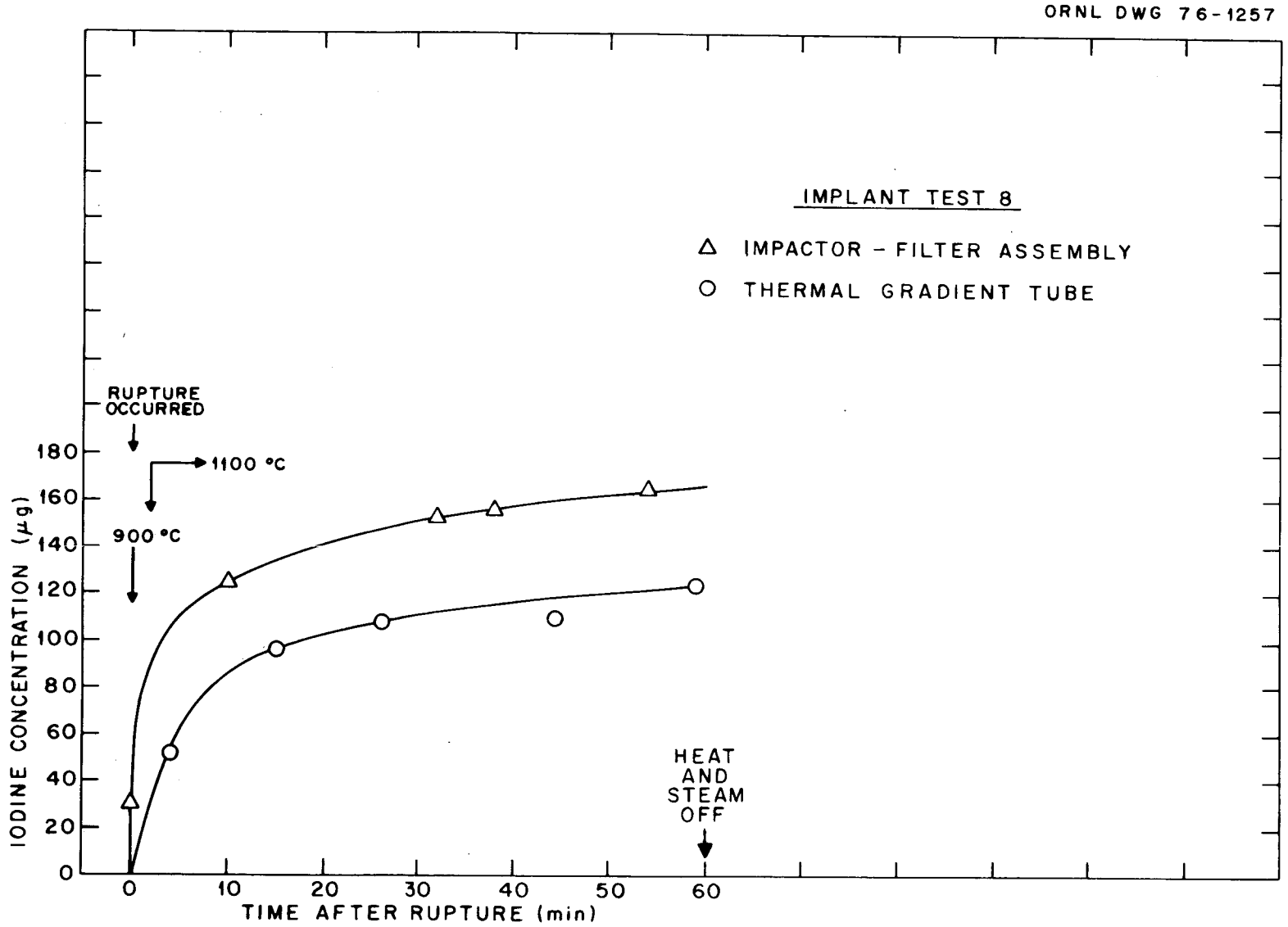

Fig. 38. Iodine deposition in the thermal gradient tube and the impactor-filter assembly during Implant Test No. 8.

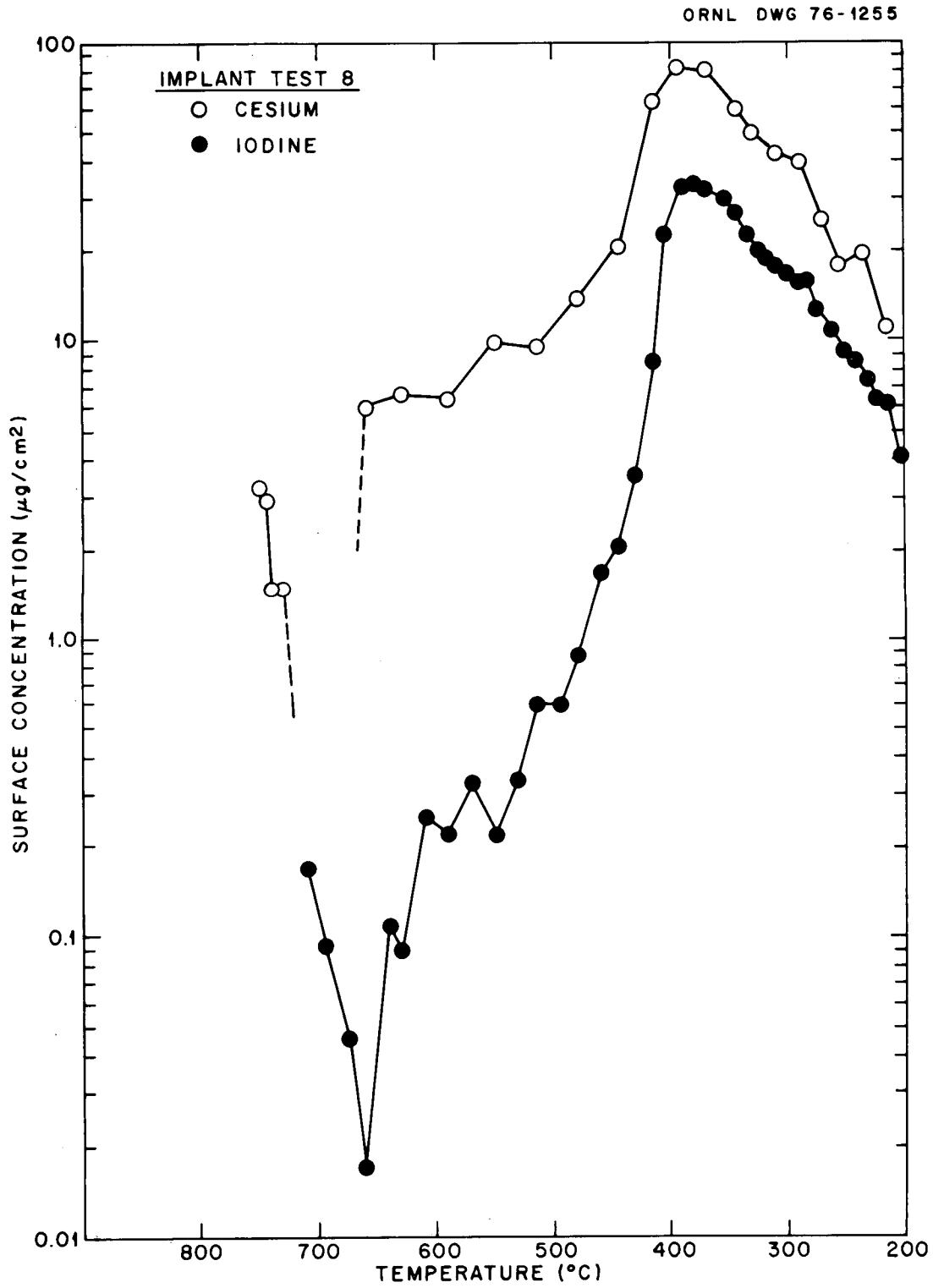

Fig. 39. Cesium and iodine concentration profiles in the thermal gradient tube of Implant Test No. 8.

An unusually heavy particulate deposition was observed on the impactor filter papers; this is readily visible in Fig. 40. The presence of $CsOH \cdot H_2O$ on the first-stage paper and of CsI on the fifth-stage paper was confirmed by x-ray diffraction. Notice the lack of correlation between the amount of dark material collected on each stage and the amounts of radioactive material (cf. Table 9). This lack of correlation between visible and radioactive deposits occurred with many implant tests.

Approximately 12% of the original iodine inventory deposited as reactive iodine (I_2 and/or HI) on the silver screens in the filter assembly and on the metal surfaces of the impactor and filter assembly. Corona arcing in the furnace tube around the fuel rod for a few seconds after rupture (when the atmosphere was richer in argon) may have caused some dissociation of CsI, thus contributing to some of the elemental iodine. Also, CsI in contact with hot quartz at temperatures >620°C likewise tends to dissociate.[1,8] Thus it is difficult to ascertain accurately the fraction of iodine that exited the fuel rod in elemental form.

In an effort to better define the penetrability of iodine forms such as CH_3I through the charcoal collection beds, the first charcoal cartridge was sectioned into four equal units using stainless steel screens (Table 9). Note also that some of the iodine penetrated the adsorbers and dissolved in the condensate; this behavior is not understood.

4.9 Behavior of Fission Product Simulant Mixture in Dry Air at 500°C (Implant Test 9)

Implant Test 9 was the second experiment in this series to be conducted in dry air, in simulation of possible SFTA conditions. The cladding was perforated prior to the experiment by drilling four 1.6-mm-diam holes at the midpoint of the rod. The rod was heated by means of a resistance heater that surrounded the furnace tube. In order to obtain meaningful release data from this experiment, the test was performed over a 20-hr period. The distributions of the nuclides that were determined at the conclusion of the test are summarized in Table 10.

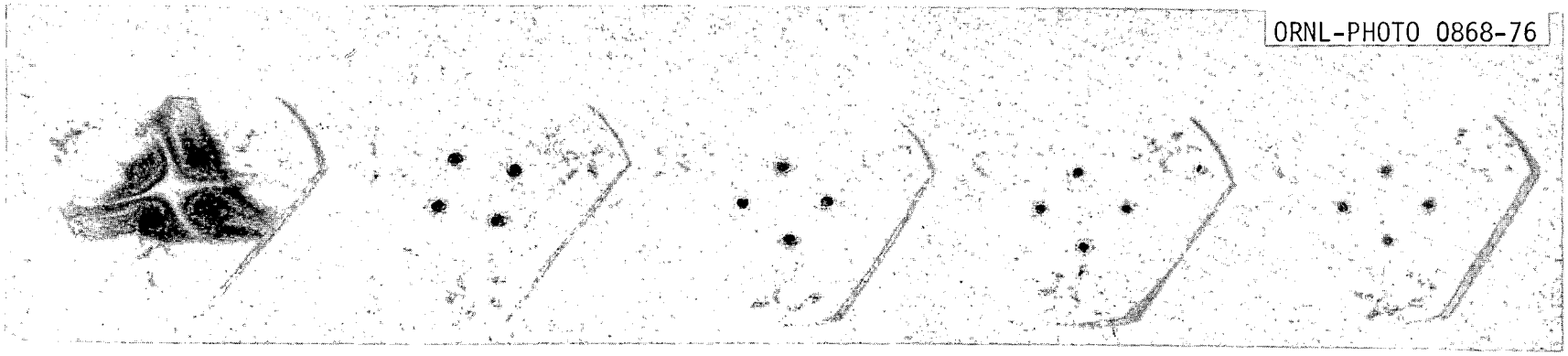

Fig. 40. Photograph of the collection stages from the cascade impactor of Implant Test No. 8 showing the particulate material collected.

Table 10. Distributions of cesium, iodine, and tellurium in Implant Test 9

Location	Temp. (°C)	Amount found in each location: Percent of total Cs	Percent of total I	Percent of total Te	μg Cs	μg I	μg Te
Fuel rod, total	500	99.70	91.43	99.997	6740.0	448.0	2480.0
UO_2 pellets							
Zircaloy cladding							
Quartz furnace tube	500	0.02	0.11	0.0	1.35	0.54	
Thermal gradient tube	700 to 200	0.27	0.31	0.0	18.3	1.52	
Orifice assembly	120	0.0	0.01	0.0004	0.0	0.05	0.01
Impactor assembly	120						
Impactor housing		0.0006	0.05	0.0004	0.04	0.25	0.01
First-stage paper		0.0004	0.0008	0.0	0.03	0.004	
Second-stage paper		0.0	0.0	0.0	0.0		
Third-stage paper		0.0005	0.0004	0.0	0.03	0.002	
Fourth-stage paper		0.0	0.0	0.0	0.0		
Fifth-stage paper		0.0004	0.0002	0.0	0.03	0.001	
Filter assembly	120						
Filter housing		0.0	0.70	0.001		3.43	0.03
First filter paper		0.0	0.106	0.0		0.52	
Second filter paper		0.0	0.095	0.0		0.47	
Third filter paper		0.0	0.033			0.16	
Silver screen No. 1		0.0	6.75			33.1	
Silver screen No. 2		0.0	0.30			1.47	
Silver screen Nos. 3 to 8		0.0	0.07	0.0		0.34	
Adsorber assembly	125						
Adsorber housing		≤0.004	0.0	0.0	≤0.27	0.0	
Charcoal No. 1a		0.0	0.034	0.0		0.17	
Charcoal No. 1b		0.0	0.001	0.0		0.005	
Charcoal No. 1c		0.0	0.0	0.0			
Charcoal No. 1d		0.0	0.002	0.0		0.01	
Charcoal No. 2		0.0	0.0	0.001			0.03
Charcoal No. 3		0.0	0.0004	0.0		0.002	
AgX		0.0007	0.0008	0.0	0.05	0.004	
Condenser assembly	0						
Condenser housing		0.0	0.0	0.0			
Condensate		0.0	0.0	0.0			
Freeze trap	-78	0.0	0.006	0.0		0.03	
Cold charcoal trap	-78	0.0	0.0	0.0			

As can be seen in Fig. 41, extensive swelling occurred in the perforation area due to oxidation of the UO_2. The cladding between the four perforations was torn apart, creating an opening of about 77 mm^2. The constrictions in the swollen area are located at the pellet interfaces. (The rate of oxidation of sintered UO_2 pellets in air has been found to be maximal near 500°C.)[9]

In Fig. 42, the metallographic transverse (a) and longitudinal (b) sections from the swollen region at midcapsule reveal extensive oxidation. The transverse cross section was taken at the defect opening, and the 1-in. longitudinal section was taken on the downstream side of the transverse cut. The longitudinal section shows the axial pattern of oxidation. The cracks and channels in the fuel which are formed during the oxidation provide avenues for air to reach unoxidized fuel. Only ZrO_2 was identified by x-ray diffraction to be present in the pitted areas along the inner cladding surface seen in the transverse cross section in Fig. 42a and also in the photomicrographic view in Fig. 43.

Pre- and post-test concentration profiles of cesium and iodine in the fuel rod are presented in Figs. 44 and 45 respectively. Little movement of these nuclides within the rod was noted. The iodine that was released appears to have come from the swollen area in the central section of the rod.

Approximately 8.6% (42 μg) of the original iodine was released in the course of the experiment; only 0.3% (20 μg) of the cesium and 0.003% of the tellurium were released. This suggests that at least half of the iodine was released in elemental form. However, virtually all of the iodine found in the collection system (∿8% of the original) was collected as elemental iodine. Since the quartz furnace tube was maintained at 500°C, and since CsI has little tendency to react with Quartz below its melting point[1] (621°C), it is likely that most of the iodine had actually been released in the elemental form. The majority of the cesium released was found to deposit in the thermal gradient tube.

Concentration profiles of cesium and iodine along the thermal gradient tube are presented in Fig. 46. Ten times more cesium was found deposited

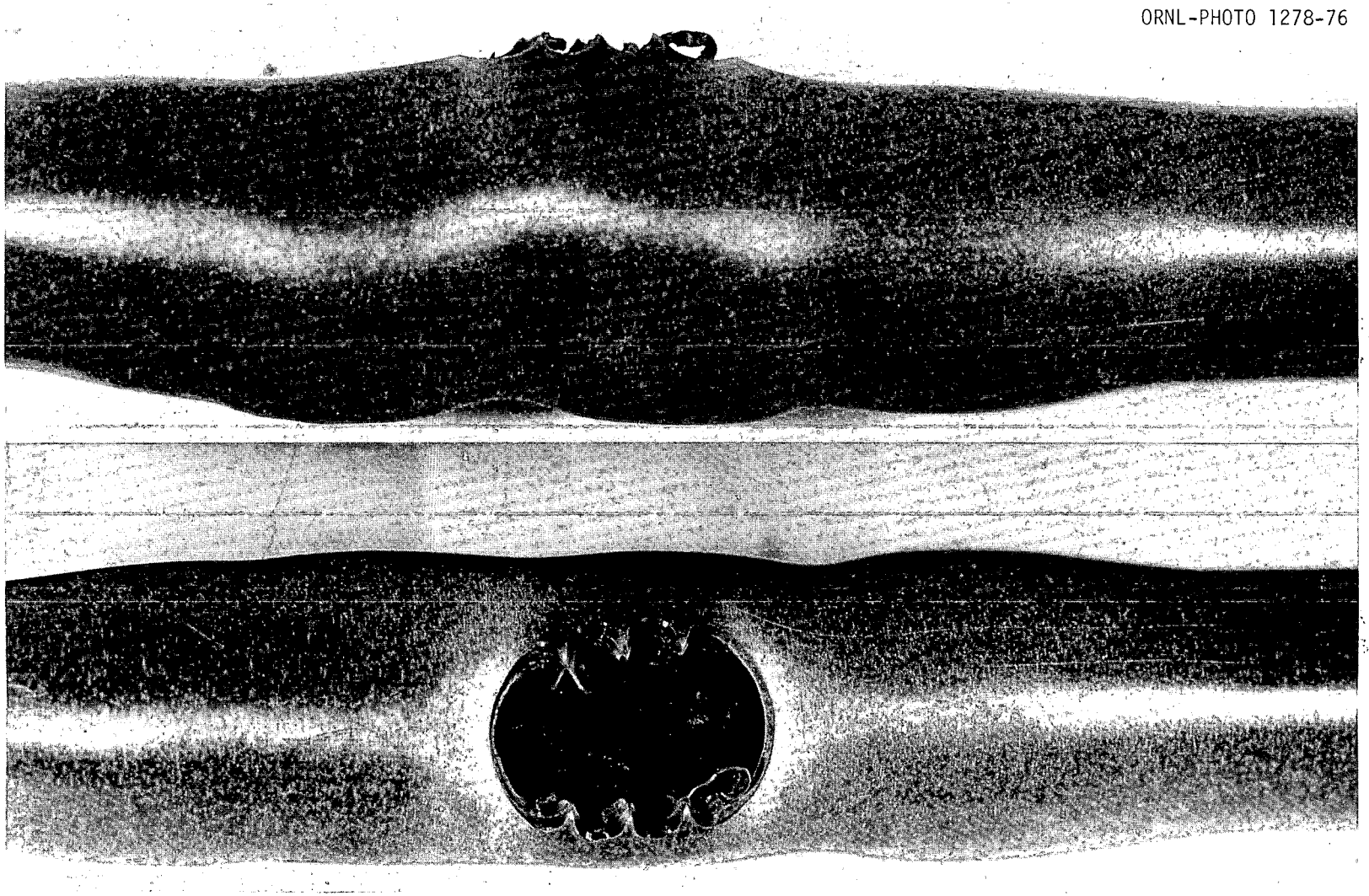

Fig. 41. Photograph showing two views of the swollen portions of the fuel rod of Implant Test No. 9.

Fig. 42. Metallographic transverse (a) and longitudinal (b) sections from the swollen region of the Implant Test No. 9 fuel rod.

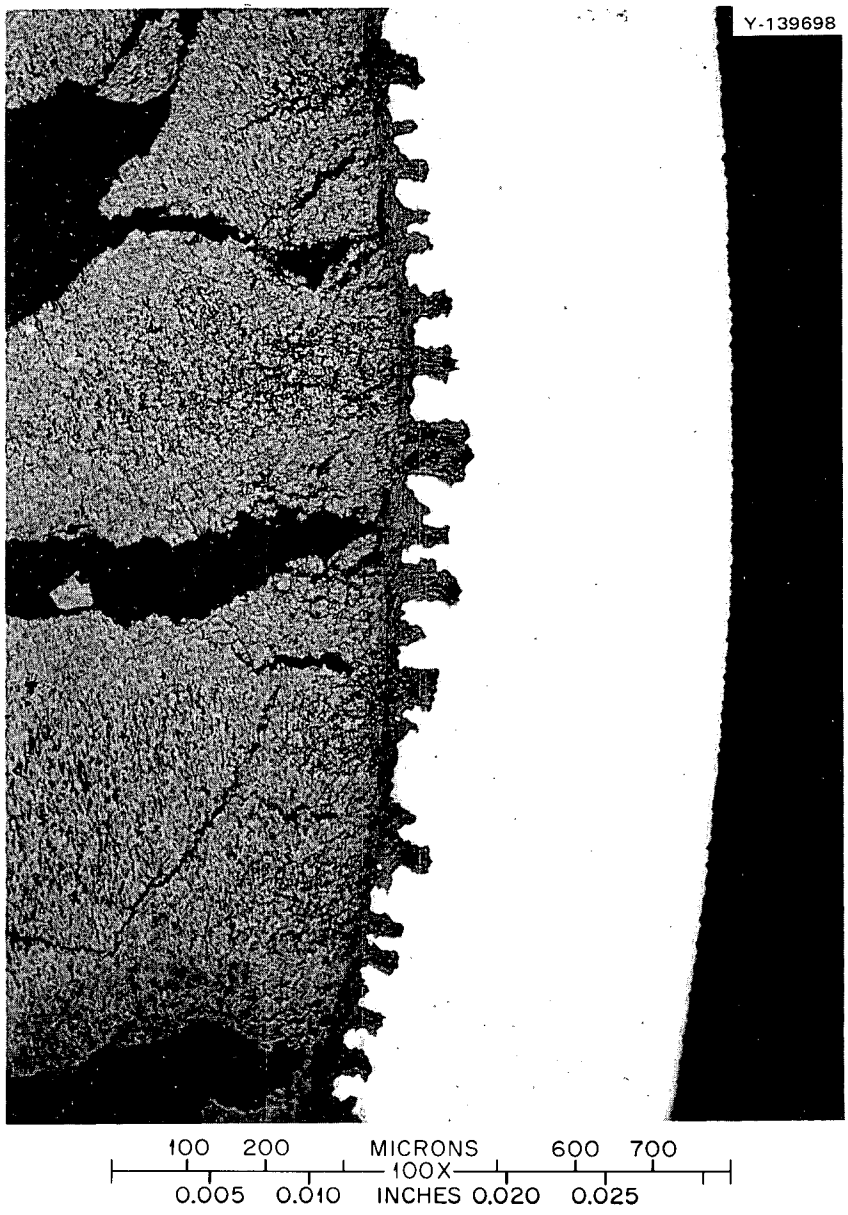

Fig. 43. A high-magnification view of the pitted areas along the inner cladding surface seen in the transverse cross section in Fig. 42(a).

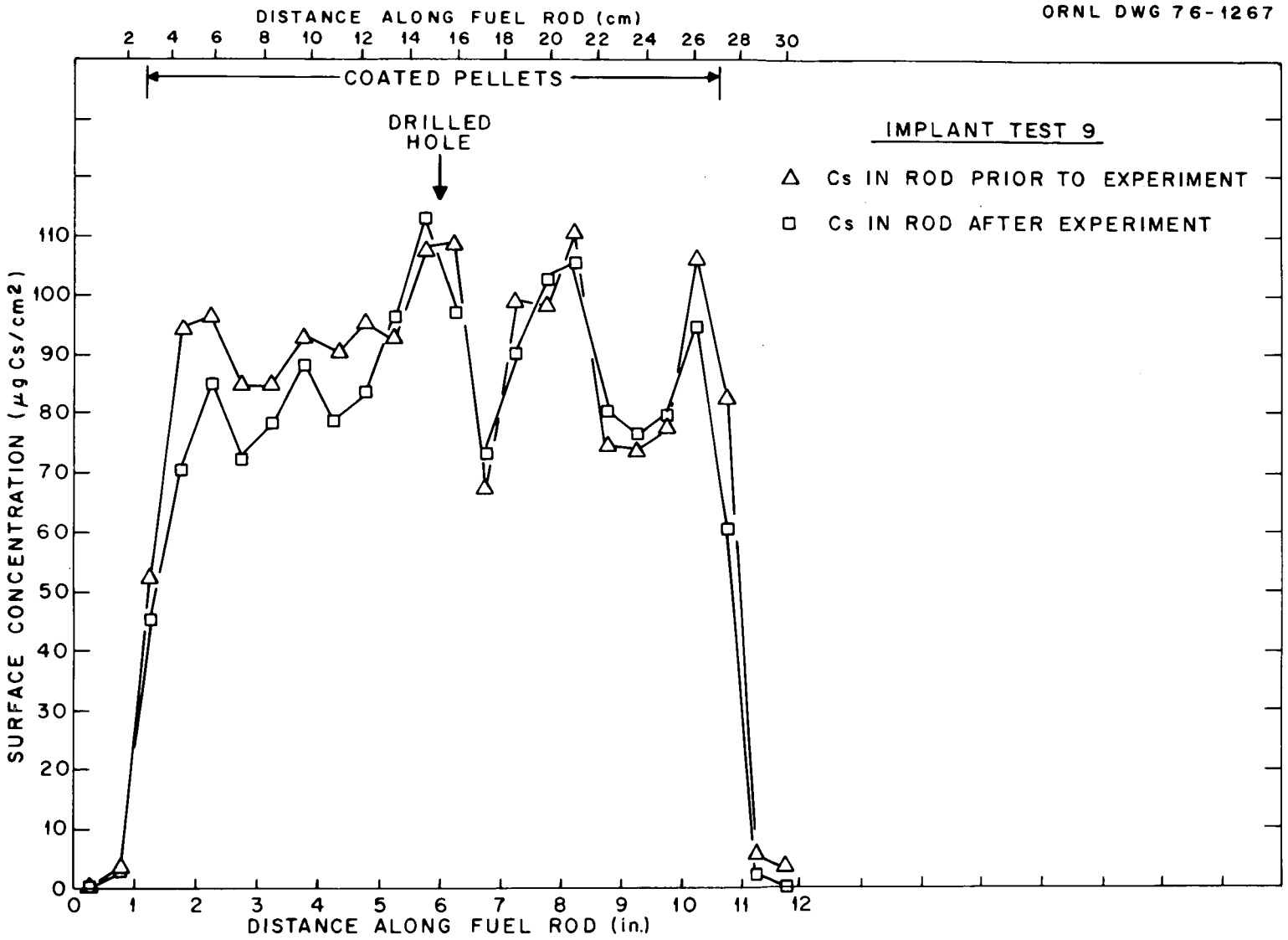

Fig. 44. Cesium distributions in the fuel rod of Implant Test No. 9.

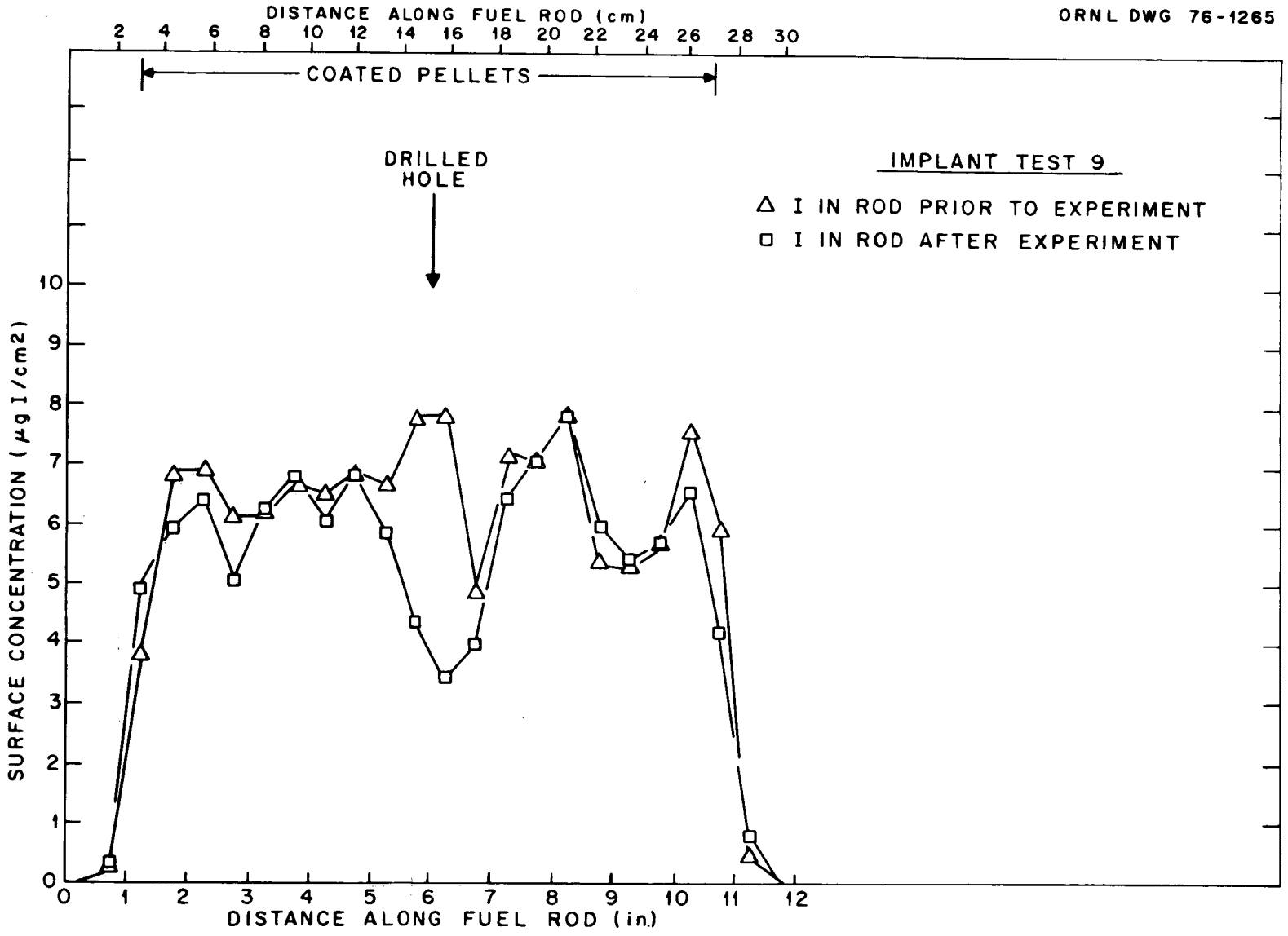

Fig. 45. Iodine distributions in the fuel rod of Implant Test No. 9.

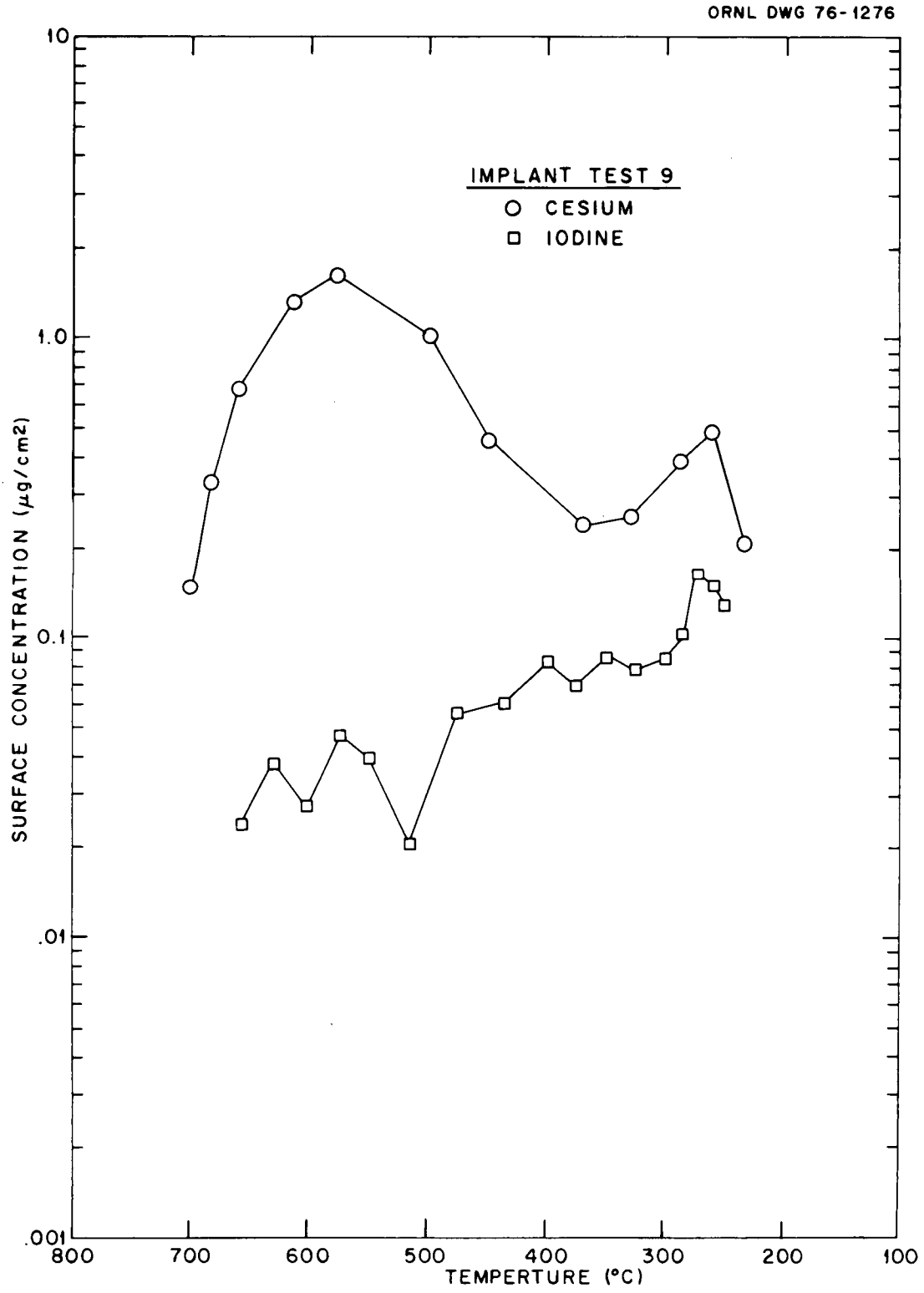

Fig. 46. Cesium and iodine concentration profiles in the thermal gradient tube of Implant Test No. 9.

along the thermal gradient tube than iodine. As with Implant 7, the other dry-air experiment, much of the cesium was deposited in the higher-temperature region. Continuous monitoring of the thermal gradient tube, as is graphically displayed in Fig. 47, indicated that most of the iodine was deposited there in the first hour of the experiment; little change in concentration was noted at later time intervals.

Deposition of elemental iodine, as deduced from measurements of activity in the impactor-silver screen filter assembly, appeared to be sensibly linear with time over the 20-hr test period (Fig. 48). Since ∿93% of the iodine that was released from the fuel rod was deposited in the impactor-silver screen filter assembly, the data presented in Fig. 48 also provides a good representation of the rate of release of this species from the fuel rod.

4.10 Behavior of Fission Product Simulant Mixture at 700°C (Implant Test 10)

The operating conditions of this test were similar to those used in Implant Test 7 which was conducted over a 5-hr period at 700°C; unlike Implant Test 7, however, this test was made in a steam-argon atmosphere rather than dry air. A summary of the operating conditions is provided in Table 1; the distributions of the pertinent nuclides are listed in Table 11.

The exterior coloration of the cladding was copper-to-pink; moreover, the surface texture was smooth and unbroken. This appearance was similar to that seen in Implant Test 7. In previous tests, the cladding surfaces were black and finely cracked.

Concentration profiles of cesium and iodine in the fuel rod prior to and after testing, and in the fuel rod components after testing, are presented graphically in Figs. 49 and 50. The concentration of cesium and iodine at the 3-3/4-in. location may not have been caused by axial temperature gradients. Implant Tests 6 and 9 (500°C) and 7 and 10 (700°C) were conducted with the same resistance-heated furnace, so that axial temperature gradients should have been small and essentially identical. Depletion

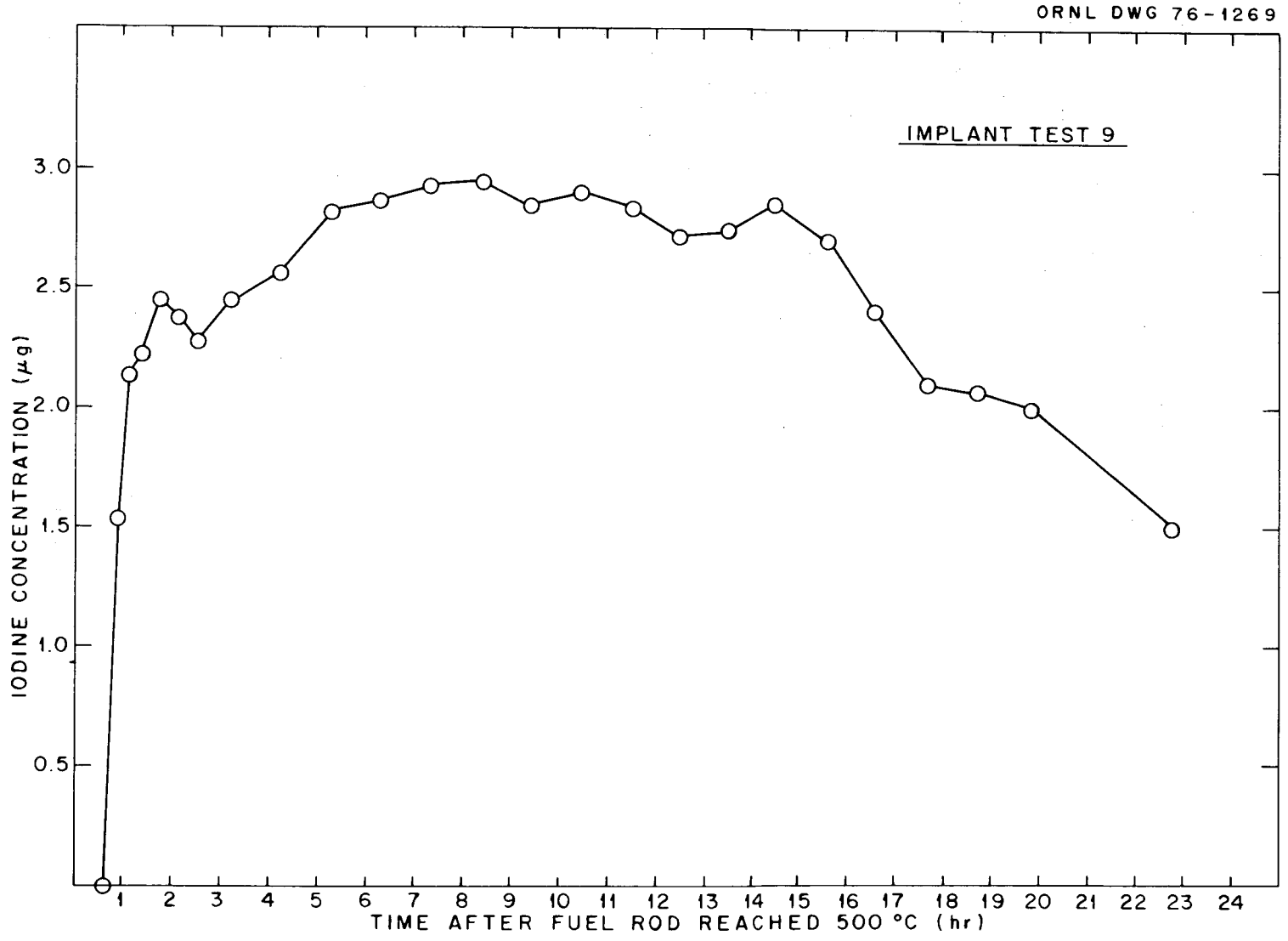

Fig. 47. Iodine deposition in the thermal gradient tube during Implant Test No. 9.

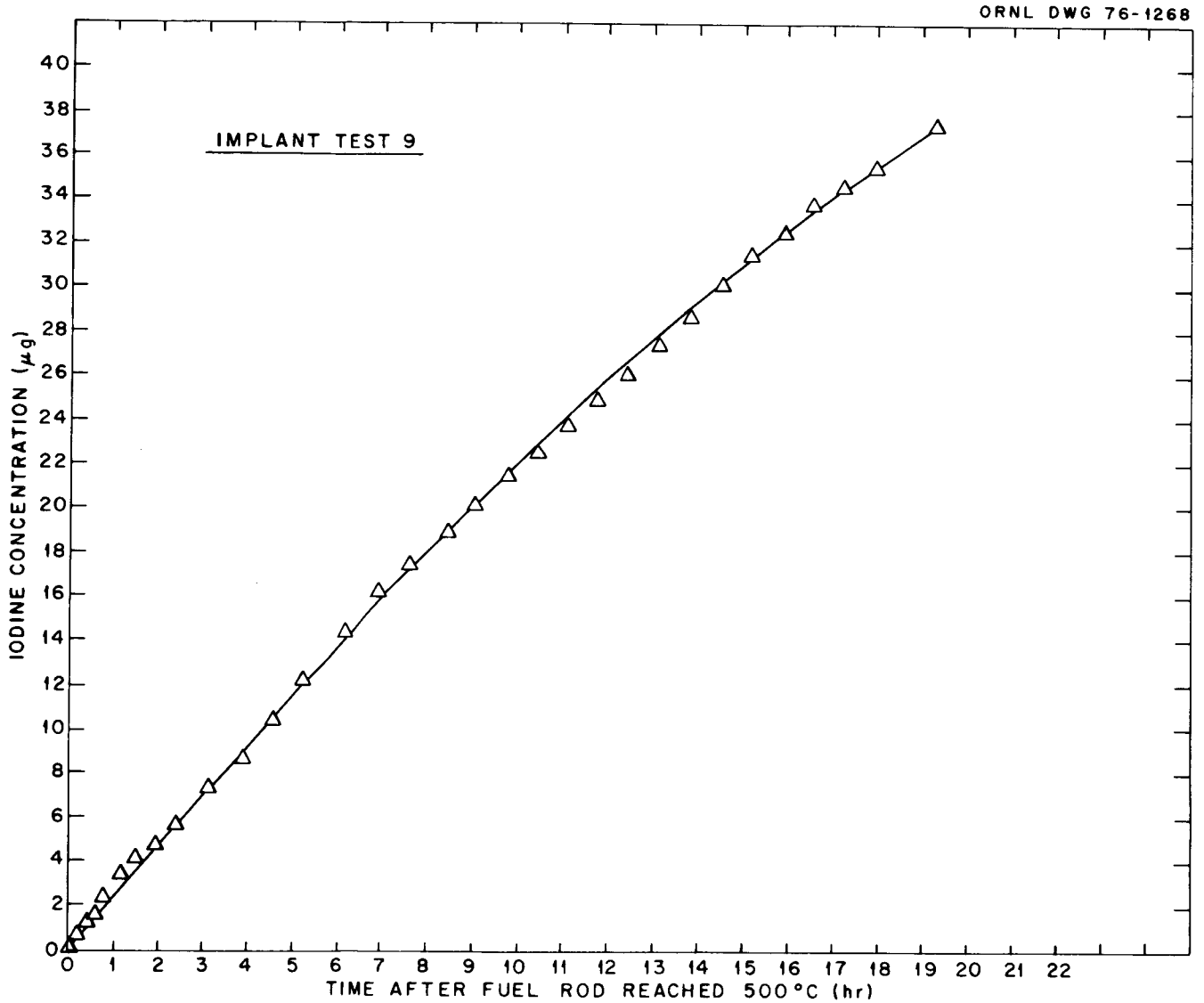

Fig. 48. Iodine deposition in the impactor-filter assembly during Implant Test No. 9.

Table 11. Distributions of cesium, iodine, and tellurium in Implant Test 10

Location	Temp. (°C)	Amount found in each location: Percent of total Cs	Percent of total I	Percent of total Te	μg Cs	μg I	μg Te
Fuel rod, total	700	(99.93)	(98.16)	(99.84)			
UO_2 pellets		42.02	40.22	18.05	2971.0	265.0	401.0
Zircaloy cladding		57.91	57.94	81.79	4094.0	382.0	1816.0
Quartz furnace tube	700	0.0	0.0	0.0			0.0
Thermal gradient tube	750 to 120	0.063	0.25	0.085	4.45	1.65	1.89
Orifice assembly	120	0.001	0.09	0.002	0.07	0.59	0.04
Impactor assembly	120						
Impactor housing		0.004	0.66	0.018	0.28	4.36	0.40
First-stage paper		0.0006	0.009	0.001	0.04	0.06	0.02
Second-stage paper		0.0	0.001	0.0		0.01	0.0
Third-stage paper		0.0	0.0	0.0		0.0	0.0
Fourth-stage paper		0.0	0.0	0.0		0.0	0.0
Fifth-stage paper		0.0	0.001	0.0		0.01	0.0
Filter assembly	120						
Filter housing		0.0	0.19	0.002		1.25	0.04
First filter paper		0.0	0.005	0.0		0.03	0.0
Second filter paper		0.0	0.01	0.0		0.07	0.0
Third filter paper		0.0	0.005	0.0		0.03	0.0
Silver screen No. 1		0.0	0.59	0.0		3.89	0.0
Silver screen No. 2		0.0	0.007	0.0		0.05	0.0
Silver screens Nos. 3 to 8		0.0	0.01	0.016		0.07	0.36
Adsorber assembly	120						
Adsorber housing		0.0	0.0	0.0		0.0	0.0
Charcoal No. 1a		0.0	0.015	0.023		0.10	0.51
Charcoal No. 1b		0.0	0.0005	0.0009		0.003	0.02
Charcoal No. 1c		0.0	0.0	0.0		0.0	0.0
Charcoal No. 1d		0.0	0.0	0.0		0.0	0.0
Charcoal No. 2		0.0	0.0	0.0		0.0	0.0
Charcoal No. 3		0.0	0.0	0.0		0.0	0.0
AgX		0.0	0.0	0.0		0.0	0.0
Condenser assembly	0						
Condenser housing		0.0	≤0.002	<0.004		≤0.02	≤0.08
Condensate		0.0	≤0.0004	≤0.0006		≤0.002	≤0.014
Freeze trap	-78	0.0	0.0	0.0		0.0	0.0
Cold charcoal trap	-78	0.0	0.0	0.0		0.0	0.0

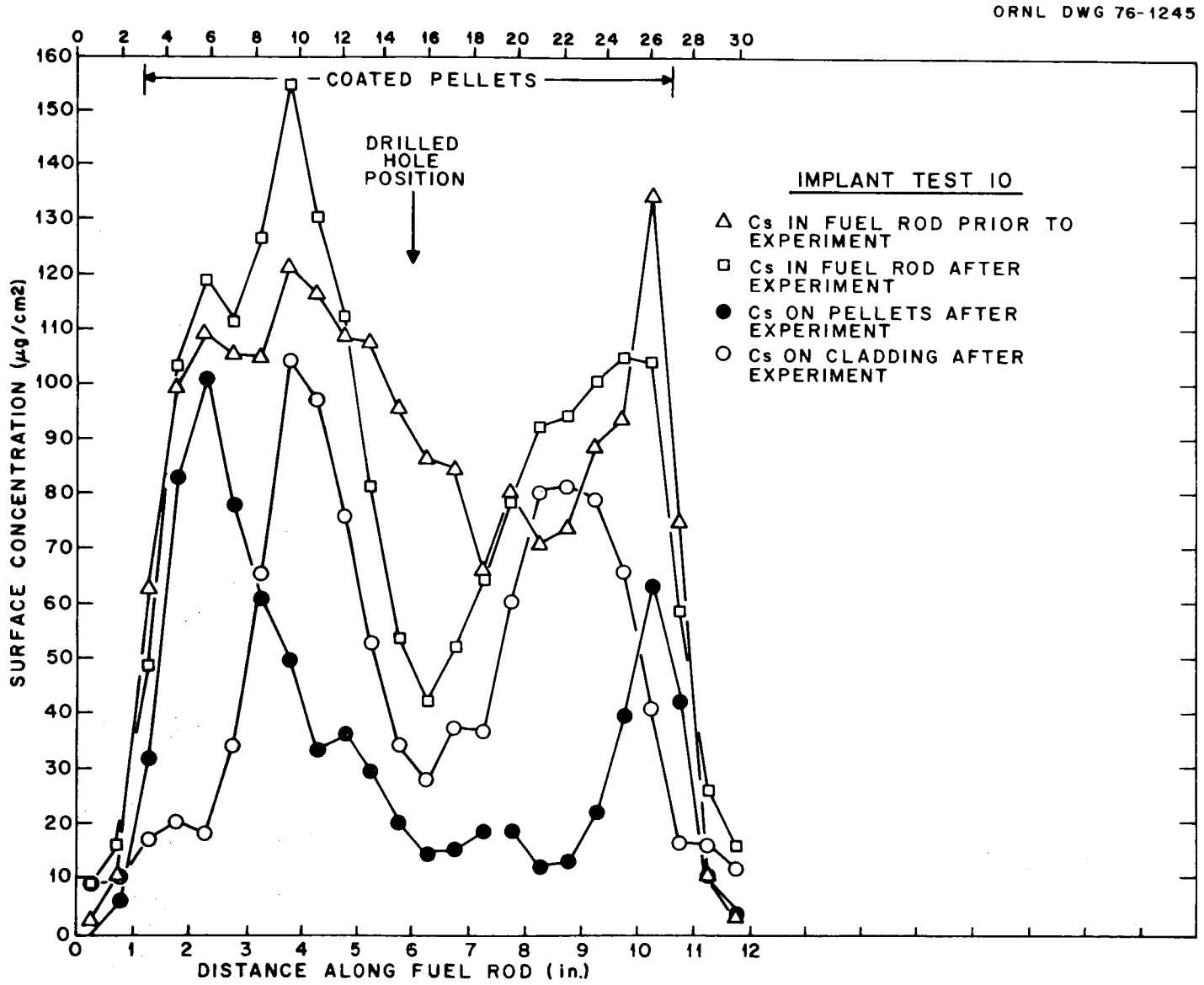

Fig. 49. Cesium distributions in the fuel rod of Implant Test No. 10.

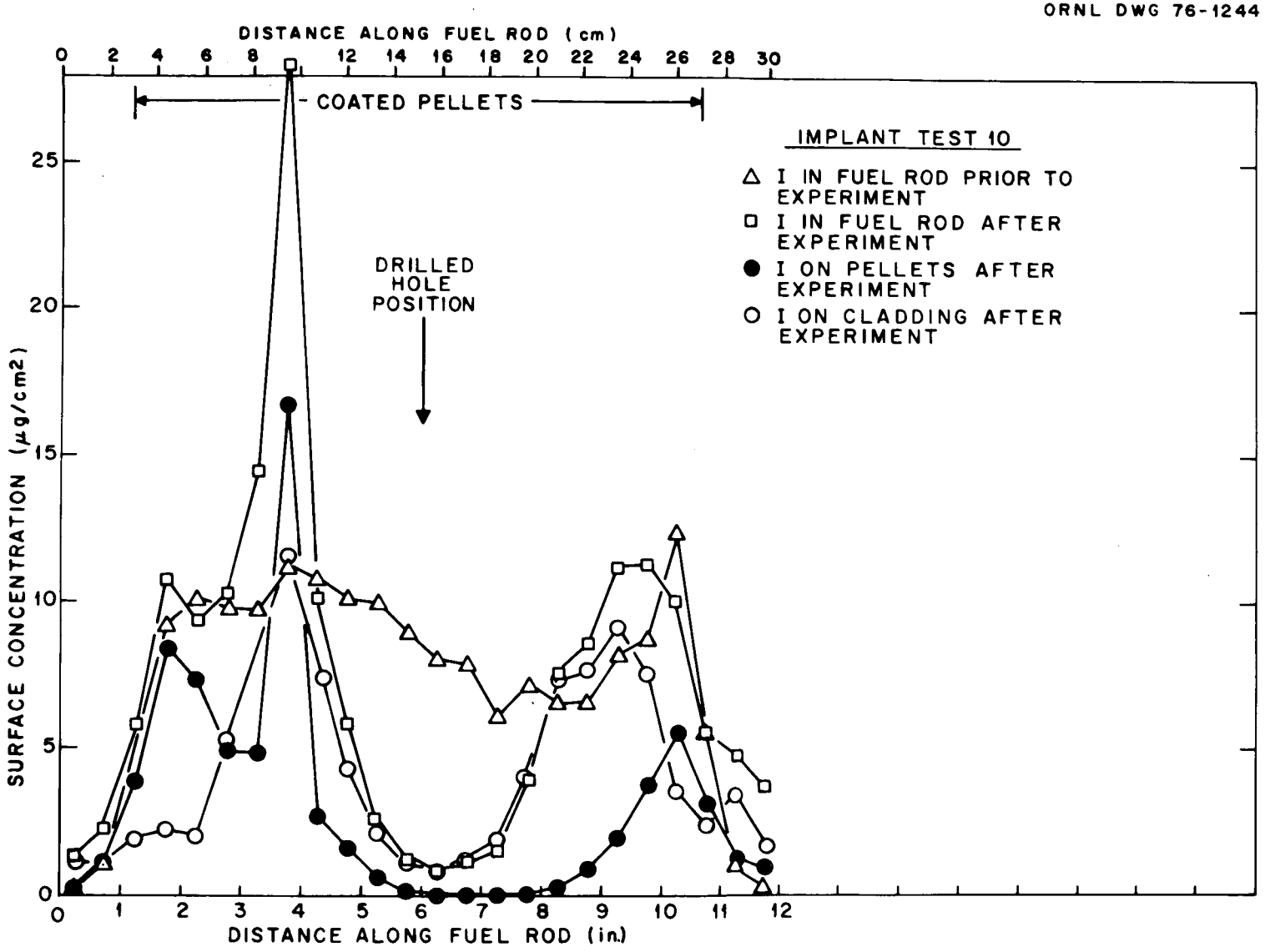

Fig. 50. Iodine distributions in the fuel rod of Implant Test No. 10.

of cesium and iodine in the vicinity of the drilled hole was caused more by migration to and deposition at the 3-3/4-in. location than by release from the hole.

As is apparent from the data in Table 11, releases of the simulants were small over the testing period; 0.07% of the cesium (5 μg), 1.84% of the iodine (12 μg), and 0.16% of the tellurium (3.5 μg) inventories were released.

About 1.5% of the iodine inventory was deposited on the impactor metal surfaces and silver screens as elemental iodine, and ∿0.25% of the original iodine was deposited in the thermal gradient tube as CsI. The rate of iodine deposition in the impactor and filter assembly is presented in Fig. 51. Unlike previous tests, in which some of the released nuclides were found in the quartz furnace tube, none were found in the furnace tube in this experiment.

The concentration profiles of the cesium and iodine which deposited along the thermal gradient tube are presented in Fig. 52. Continuous monitoring of the thermal gradient tube during the experiment revealed that most of the iodine deposition occurred in the first 10 min; little change in the concentration was noted at later time intervals.

Again, as in many of the previous implant tests, tellurium rings were clearly visible on the inner cladding surface at the pellet interfaces. Approximately 82% of the original tellurium was found on the cladding.

4.11 Behavior of Fission Product Simulant Mixture at 1300°C (Implant Test 11)

Implant Test 11 was conducted at 1300°C for 11 min; the fuel rod was actually at temperatures above 900°C for a 15-min period. Because of a leak at the fuel-rod inlet fitting, difficulty was encountered in obtaining rupture by application of internal argon pressure. (The fuel rod was unintentionally positioned within the induction heater in a manner that allowed the stainless steel inlet fitting to become overheated, thus

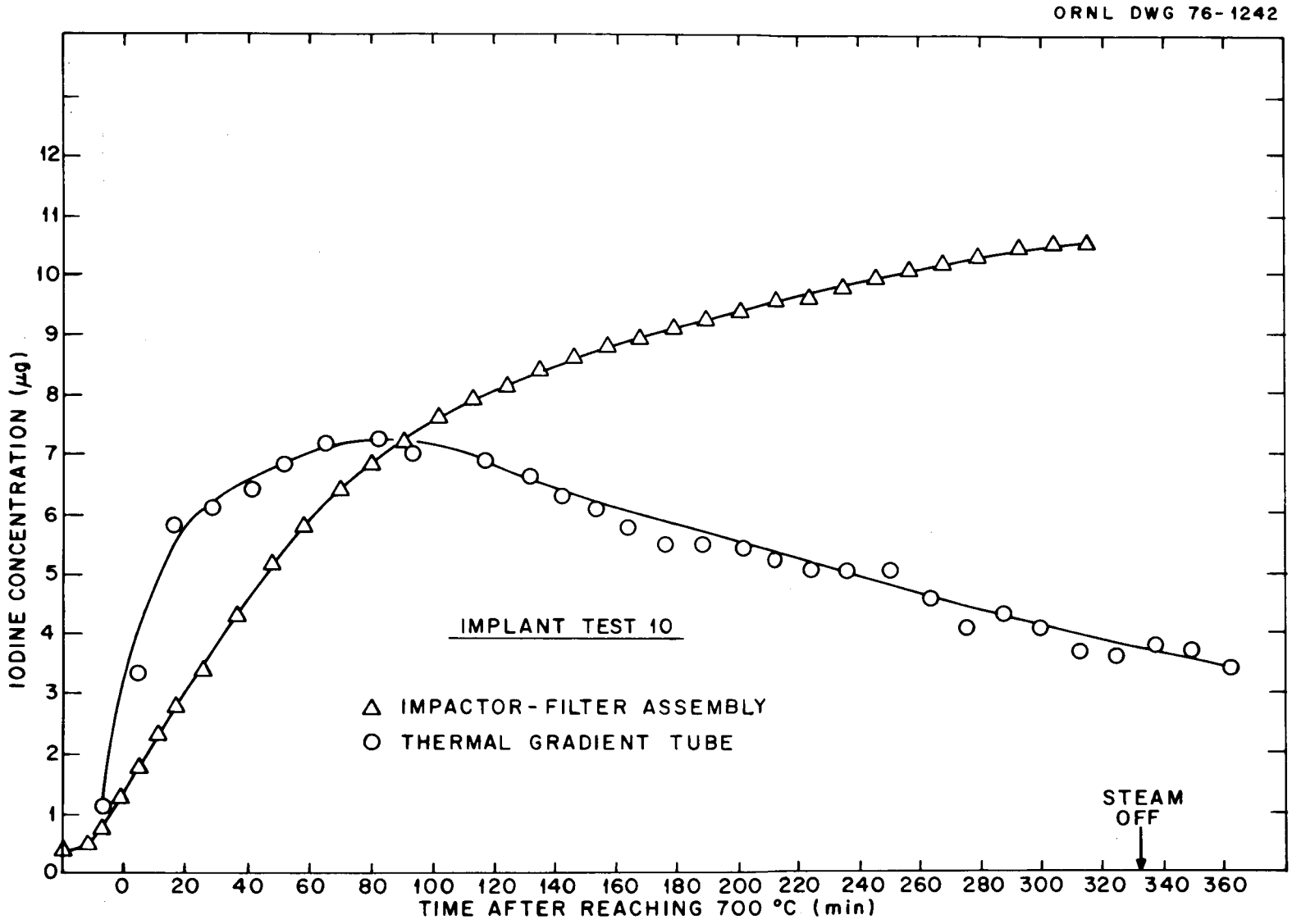

Fig. 51. Iodine deposition in the thermal gradient tube and the impactor-filter assembly during Implant Test No. 10.

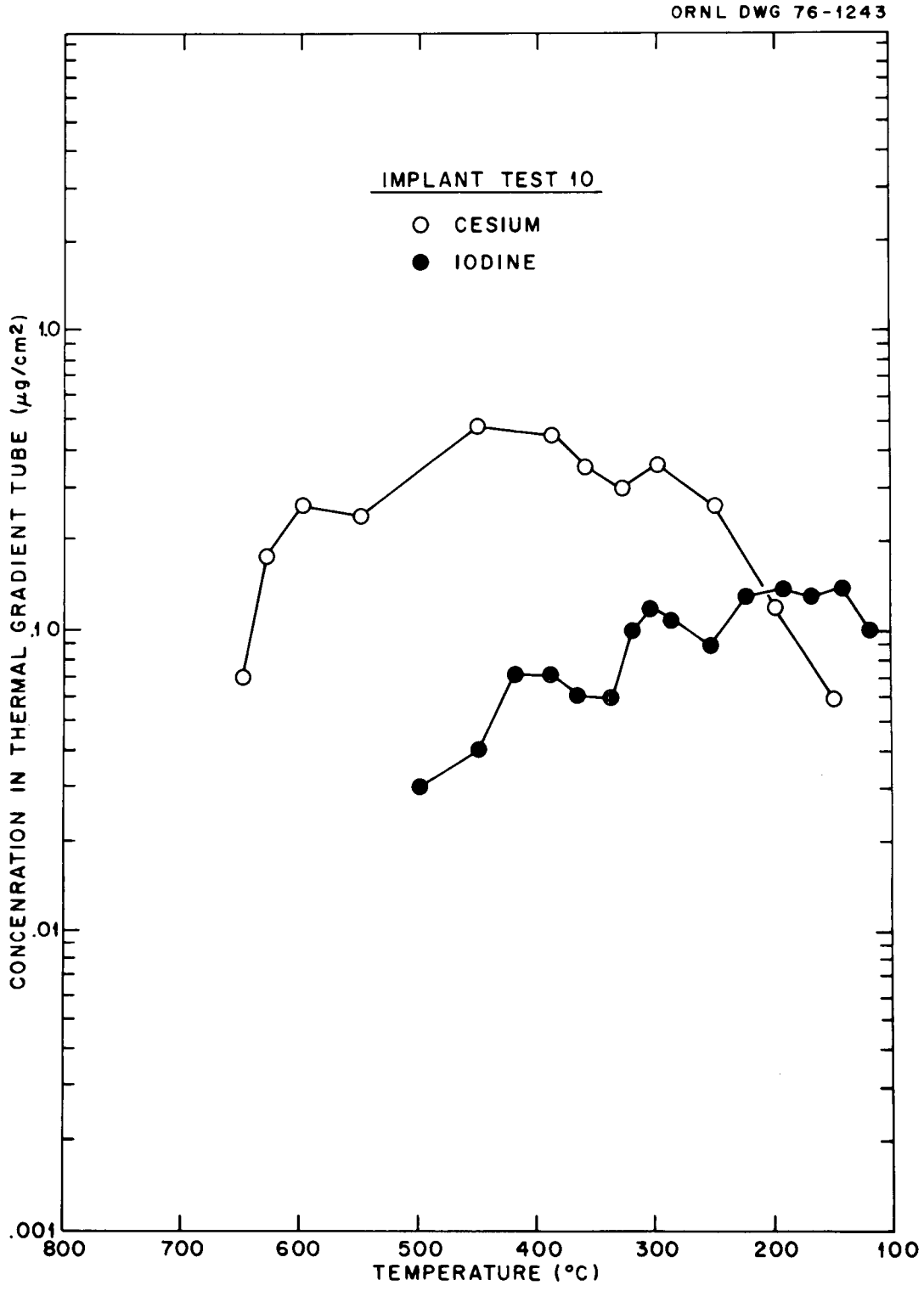

Fig. 52. Cesium and iodine concentration profiles in the thermal gradient tube of Implant Test No. 10.

causing the leak.) The rupture opening was 4 mm^2, but the ballooning effect normally experienced did not occur, therefore, the rupture pressure could not be measured. The experimental conditions are listed in Table 1, and the resulting nuclide distributions in the collection system are given in Table 12.

Post-test examination of the fuel rod indicated that the cladding was brittle. In addition, several pellets in the central portion of the rod appeared fused to the cladding. A photomicrograph of an affected region is shown in Fig. 53. Three horizontal layers can be seen: (1) the dark oxidized cladding at the top, (2) the unoxidized cladding (the light layer) in the middle, and (3) the dark fuel at the bottom. Such fuel-cladding interaction behavior has been observed previously but at somewhat higher temperatures.[10] This is not necessarily inconsistent behavior, however, because with induction heating, undesirable temperature irregularities frequently develop along the test capsule. Thus it is quite possible that portions of the cladding were significantly above 1300°C for at least short periods of time. The vertical streaks in the oxidized cladding layer in Fig. 53 were identified by x-ray analysis as tin. The tellurium-cladding reaction rings that have been seen at the pellet interfaces in previous tests were not visible; however, a gamma scan of a section of cladding indicated that the tellurium was primarily located at the interfaces.

Cesium and iodine distributions in the fuel rod are displayed in Figs. 54 and 55. As can be seen from the data presented, both species migrated to the cooler outlet end of the fuel rod.

The data listed in Table 12 indicate that 28% of the cesium (2320 μg), 4.5% of the iodine (26 μg), and 1% of the tellurium (18.6 μg) were released from the fuel rod. The values for iodine and cesium might have been significantly larger had the fuel rod been more centrally located within the induction heater. The relatively small rupture opening probably also restricted release. About 93% of the implanted tellurium was found on the cladding. Since there was neither axial migration nor significant release (1%) of the tellurium, it appears that the compound formed from the tellurium-cladding reaction is refractory at the upper temperature of this test.

Table 12. Distributions of cesium, iodine, and telluium in Implant Test 11

Location	Temp. (°C)	Amount found in each location: Percent of total Cs	Percent of total I	Percent of total Te	µg Cs	µg I	µg Te
Fuel rod, total	1300	(71.88)	(95.47)	(98.96)		553.7	
UO_2 pellets		49.88		5.63	4136.0		100.80
Zircaloy cladding		22.13		93.33	1835.0		1671.0
Quartz furnace tube	~200 to 900[a]	27.21	0.0	0.38	2256.0	0.0	6.8
Thermal gradient tube	750 to 185	0.44	3.24	0.47	36.5	18.8	8.4
Orifice assembly	140	0.006	0.004	0.005	6.50	0.02	0.09
Impactor assembly	140						
Impactor housing	140	0.19	0.86	0.132	15.8	4.99	2.36
First-stage paper		0.043	0.18	0.046	3.6		0.82
Second-stage paper		0.01	0.027	0.003	0.8	0.16	0.05
Third-stage paper		0.007	0.004	0.001	0.6	0.02	0.02
Fourth-stage paper		0.007	0.002	0.0005	0.6	0.01	0.01
Fifth-stage paper		0.005	0.001	0.001	0.4	0.001	0.02
Filter assembly	140						
Filter housing		0.025	0.08	0.0	2.1	0.46	0.0
First filter paper		0.038	0.04	0.006	3.2	0.23	0.11
Second filter paper		0.0006	0.01	0.001	0.05	0.06	0.02
Third filter paper		0.0	0.001	0.0002		0.01	0.004
Silver screen No. 1		0.0	0.06	0.0		0.35	
Silver screen No. 2		0.0	0.004	0.0		0.02	
Silver screen Nos. 3 to 8		0.0	0.01	0.0		0.06	
Adsorber assembly	115						
Adsorber housing		0.003	0.002	0.0	0.25	0.01	
Charcoal No. 1a		0.0	0.002	0.0		0.01	
Charcoal No. 1b		0.0	0.0006	0.0		0.003	
Charcoal No. 1c		0.0	0.0004	0.0		0.002	
Charcoal No. 1d		0.0	0.0004	0.0		0.002	
Charcoal No. 2		0.0	0.0009	0.0		0.005	
Charcoal No. 3		0.0	0.0007	0.0		0.004	
AgX		0.0	0.0002	0.0		0.001	
Condenser assembly	0						
Condenser housing		0.0	0.0	0.0			
Condensate		0.0	0.0	0.0			
Freeze trap	-78	0.0	0.0	0.0			
Cold charcoal trap	-78	0.0	0.0	0.0			

[a] Outlet end heated to minimize condensation of CsI.

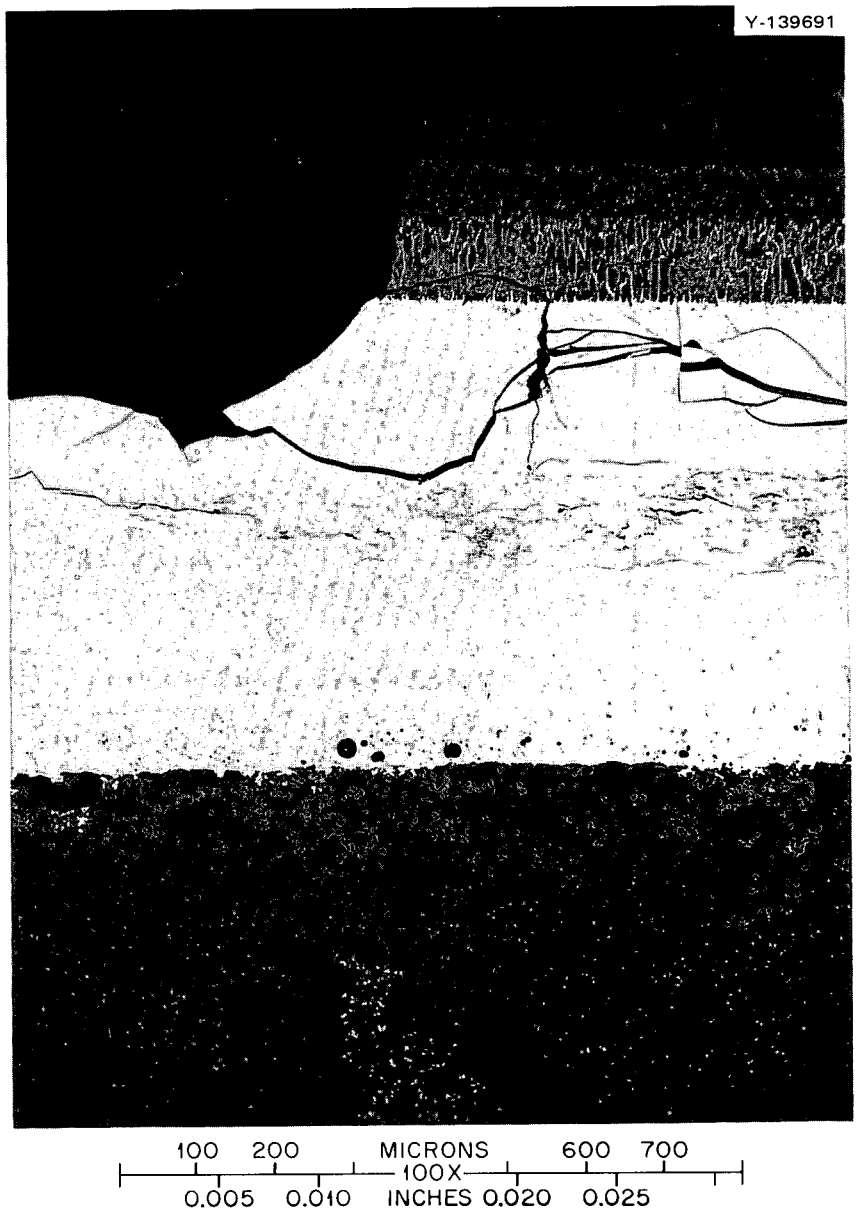

Fig. 53. A photmicrograph showing fuel-cladding interaction. The horizontal layers are: (1) the dark oxidized cladding at the top, (2) the unoxidized layer (the light layer) in the middle, and the dark fuel at the bottom.

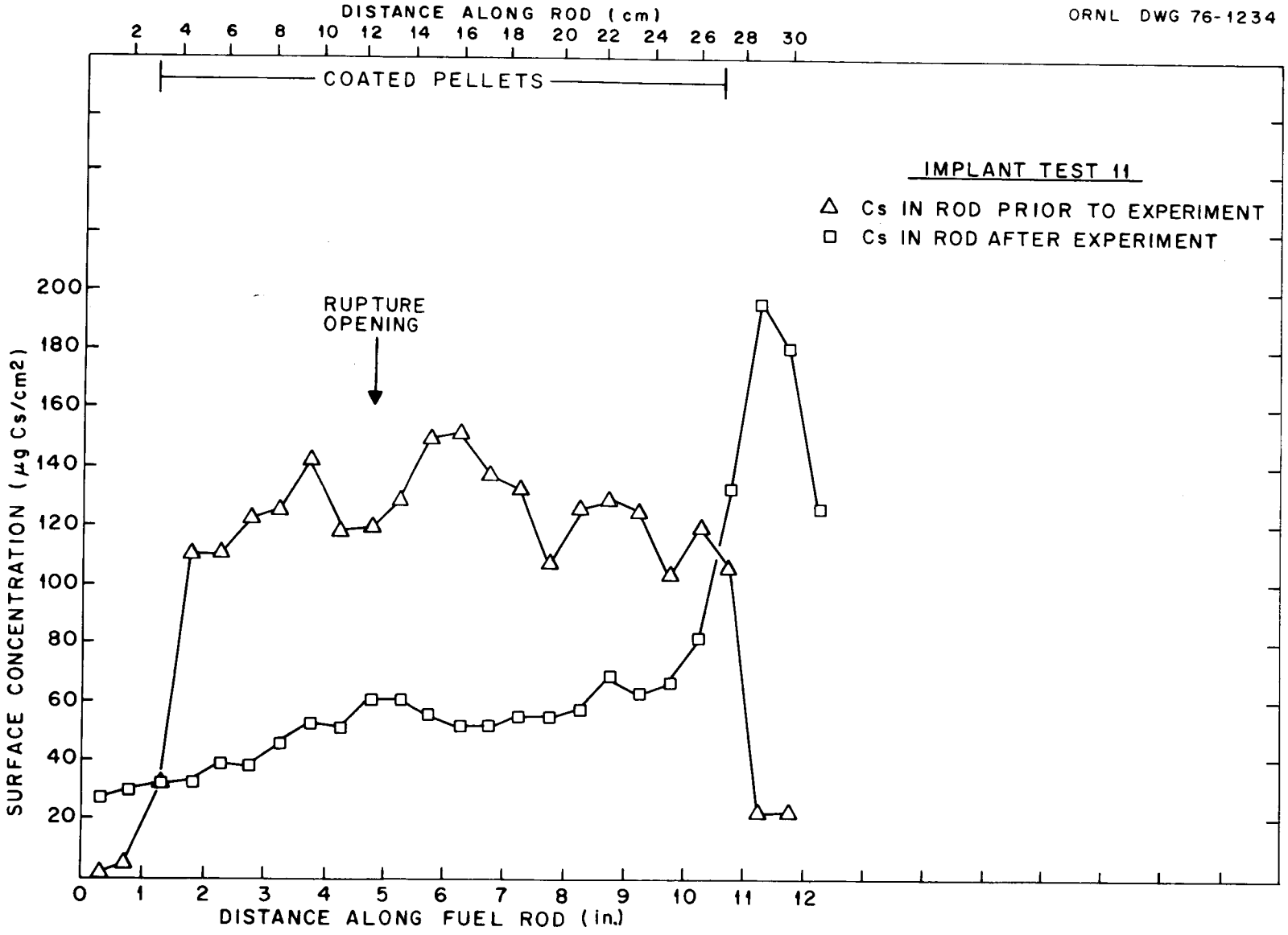

Fig. 54. Cesium distributions in the fuel rod of Implant Test No. 11.

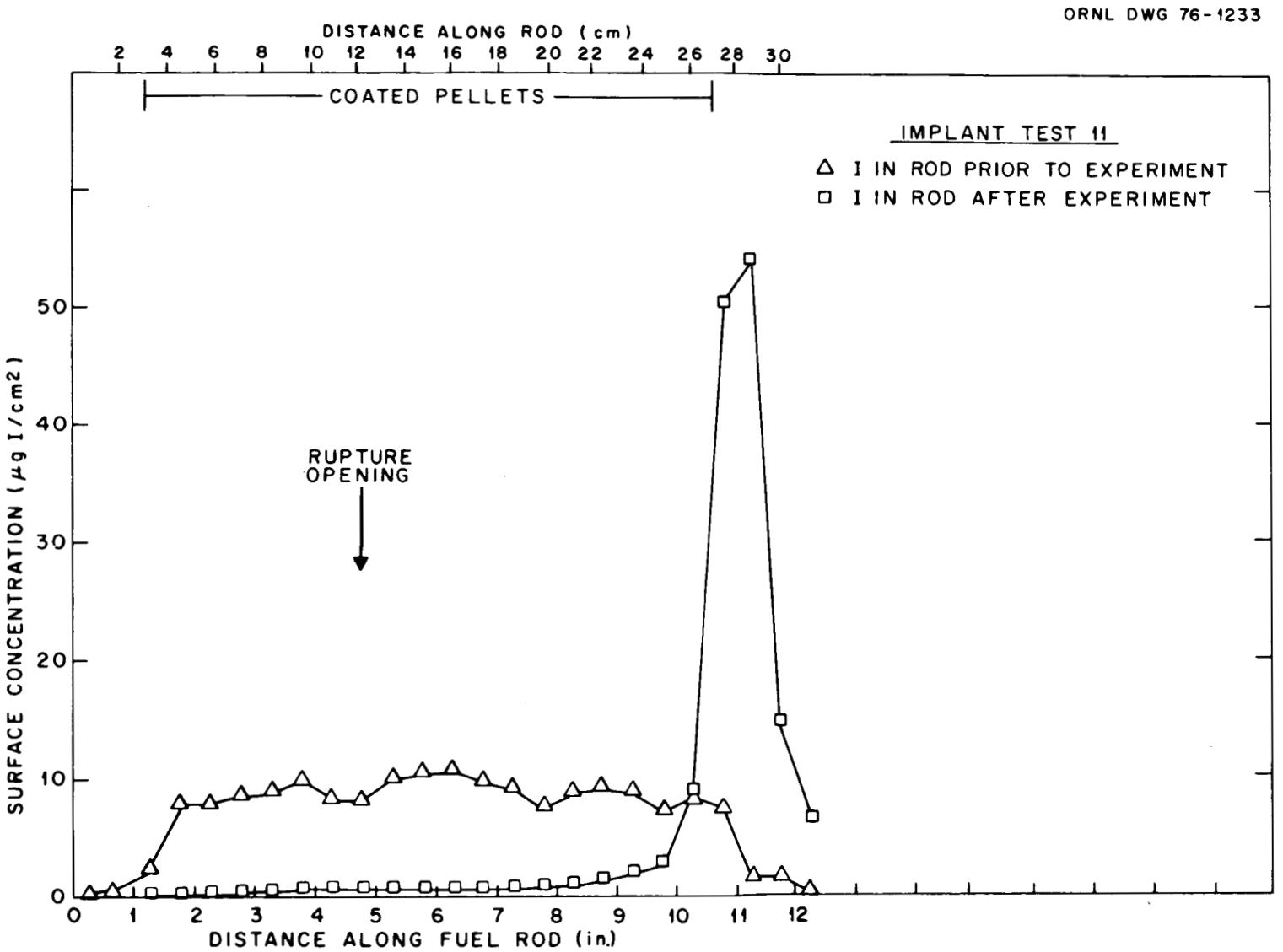

Fig. 55. Iodine distributions in the fuel rod of Implant Test No. 11.

Figure 56 indicates that most of the cesium released (27% of that which was implanted) was deposited in the quartz furnace tube, primarily on the surface adjacent to the rupture opening. No iodine deposition occurred in the furnace tube. The section of furnace tube between the end of the induction coil and the entrance to the thermal gradient tube was heated to a temperature of 600°C with an insulated heating tape; this minimized the condensation of CsI in that region. In addition, about half of the tellurium that was released was deposited in the same general area of the furnace tube as the cesium. As indicated by the data in Table 12, about 72% of the released iodine (or 3.24% of the implanted iodine) was condensed in the thermal gradient tube, probably as cesium iodide. However, twice as much cesium as iodine (on a mass basis) was deposited there. This additional cesium was probably cesium hydroxide.

The concentration profiles of cesium, iodine, and tellurium along the thermal gradient tube are presented in Fig. 57. The iodine and cesium peaks at 490°C are probably CsI and CsOH.

Releases of iodine, as deduced from separate measurements of ^{130}I activity in the thermal gradient tube and in the impactor-filter assembly, are presented graphically in Fig. 58. Little radioactivity was noted during the first 2 min after rupture, but as the temperature was raised from 900 to 1300°C during the following 3 min, a rapid increase in the activity was noted in the thermal gradient tube. Subsequently, a slight decline in activity was recorded for the remainder of the test. The increased activity in the impactor-filter assembly corresponds with a decrease in activity in the thermal gradient tube; this type of migration tends to wash out the profile structure in the thermal gradient tube. Most of the released iodine escaped from the rod within 2 min after reaching 1300°C. The iodine species was both highly volatile and mobile; no evidence exists to suggest that chemical reactions contributed to the stability. Cesium, on the other hand, was much more stable, as is shown by the final distribution within the rod (Fig. 54).

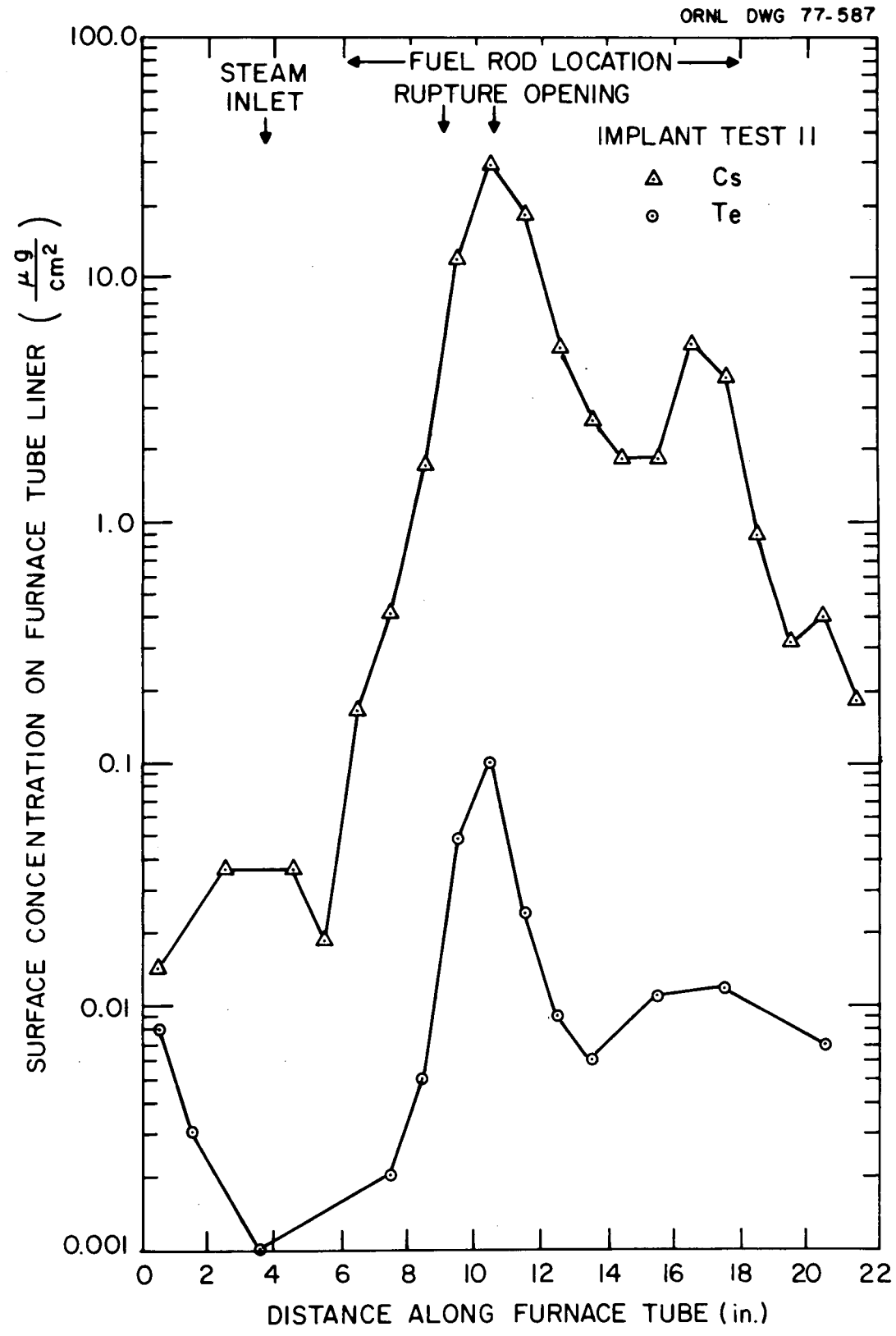

Fig. 56. Distributions of cesium and tellurium on the furnace tube liner of Implant Test No. 11.

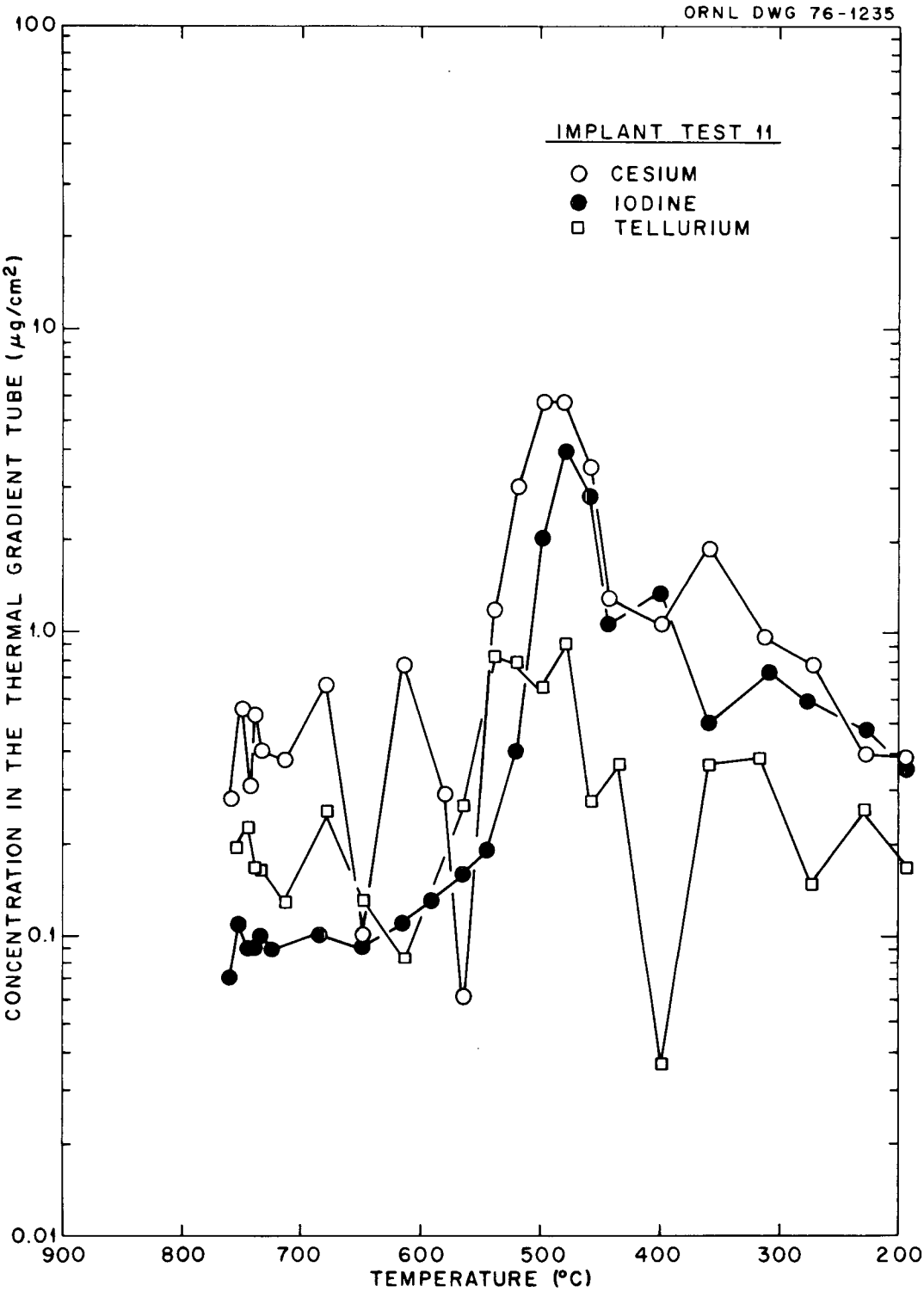

Fig. 57. Cesium, iodine, and tellurium concentration profiles in the thermal gradient tube of Implant Test No. 11.

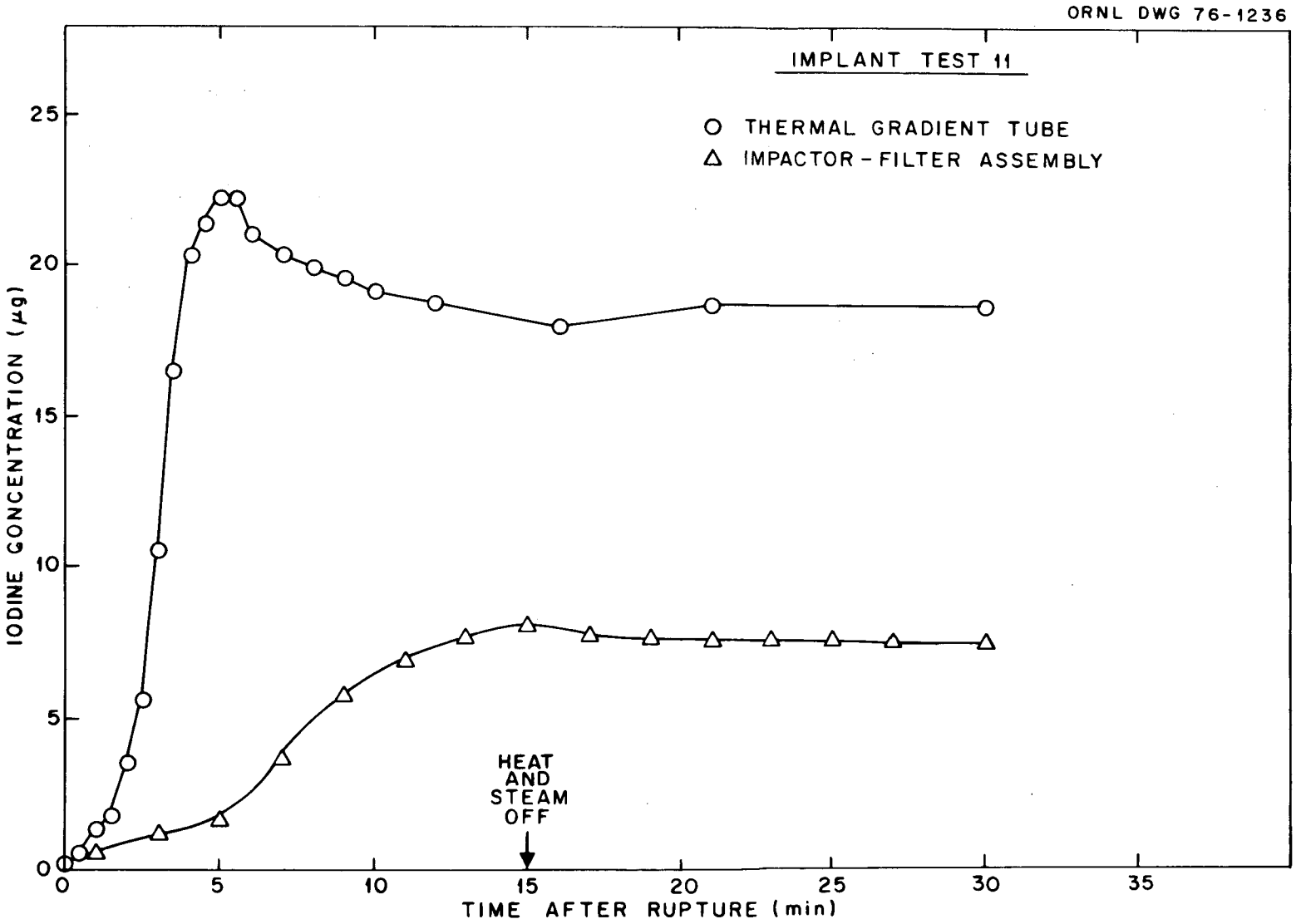

Fig. 58. Iodine deposition in the thermal gradient tube and the impactor-filter during Implant Test No. 11.

4.12 Behavior of Fission Product Simulant Mixture of Low Concentration at 900°C (Implant Test 12)

This test concluded the Implant Test Series. The operating conditions were different from those of Implant Test 3 only in the amounts of simulants used. About ten-fold decreases in the concentrations were to be present in both the pellet-cladding gaps of the low-burnup fuel capsules to be used in the Low-Burnup Test Series and in the gaps of the H. B. Robinson 12-in. fuel-rod sections to be used in the High-Burnup Test Series.

To minimize the likelihood of an argon pressurization leak like the one that developed in the previous test, a stainless steel "pellet" with a 1/16-in. hole through its center was substituted for the uncoated UO_2 pellet that normally would have been at the inlet end. The inlet portion of cladding was thereby sandwiched between the stainless steel ferrule fitting and the close-fitting stainless steel pellet, thus negating a potential leak that might have been caused by thermal expansion. The backup "pellet" also prevented creepdown of the Zircaloy tubing that loses strength rapidly at high temperatures.

Considerable swelling of the cladding occurred when the rod ruptured upon application of 250 psig of internal argon pressure (Fig. 59). The maximum circumferential change was 14.5 mm, and the rupture opening was $\sim$84 mm^2. A thick layer of flaky white zirconium oxide (probably caused by breakaway oxidation) is very evident along the inlet half of the fuel rod.

Distributions of cesium and iodine in the fuel rod before and after testing are presented in Figs. 60 and 61. Cesium migration toward the rupture opening can be noted, whereas iodine peaks appear at the cool ends of the rod as well as in the rupture region. Optical pyrometer measurements in the rupture location indicated that the temperature ranged from a low of 760°C at the rupture opening to a high of 1200°C at hot spots on both sides of the rupture opening. Although most of the rod was at 900°C during the test, the temperature variance at the rupture opening complicates an interpretation of the data. As mentioned previously,

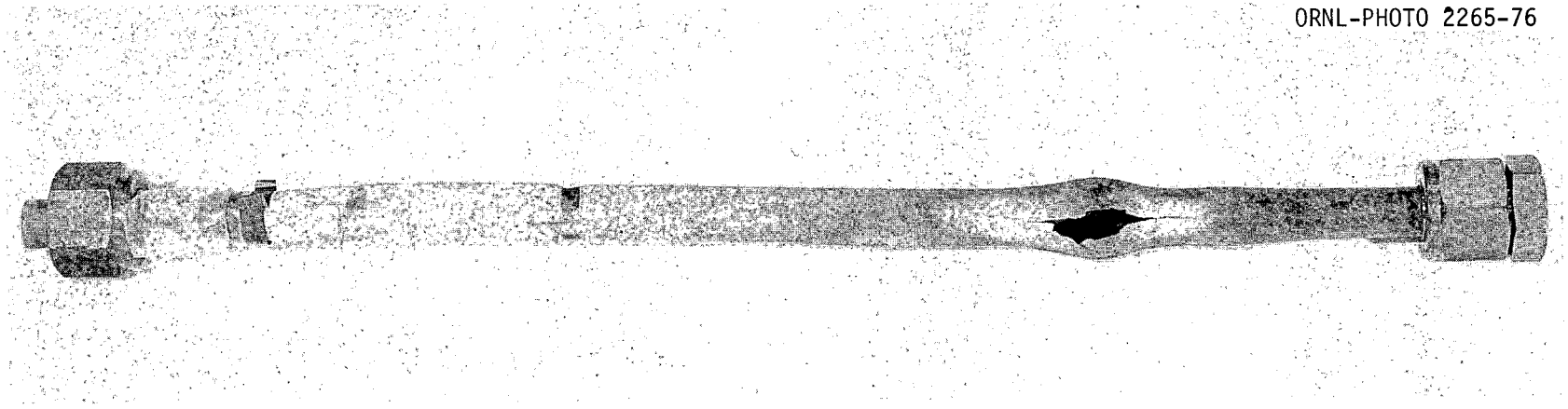

Fig. 59. Photograph of Implant Test No. 12 fuel rod.

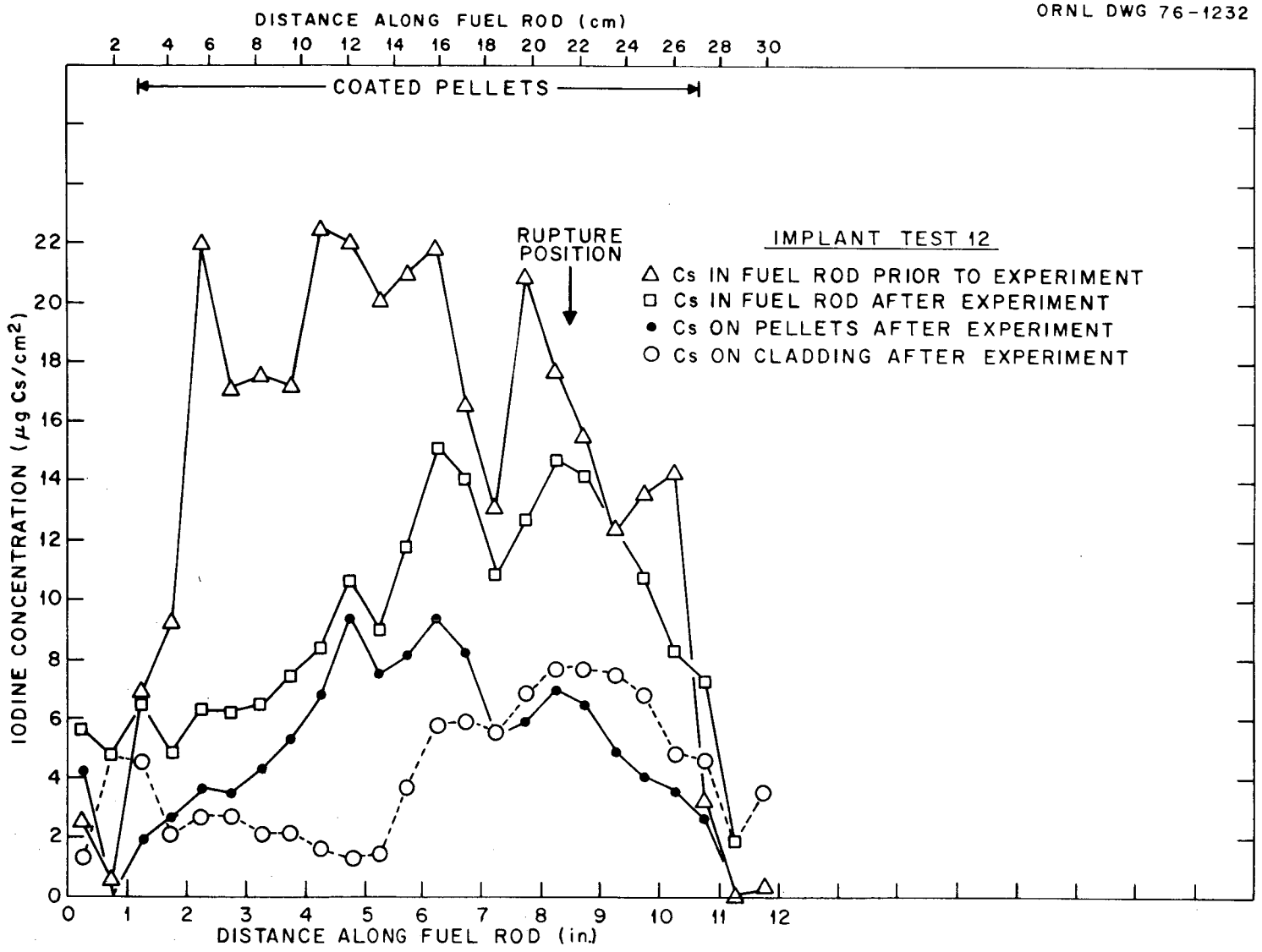

Fig. 60. Cesium distributions in the fuel rod of Implant Test No. 12.

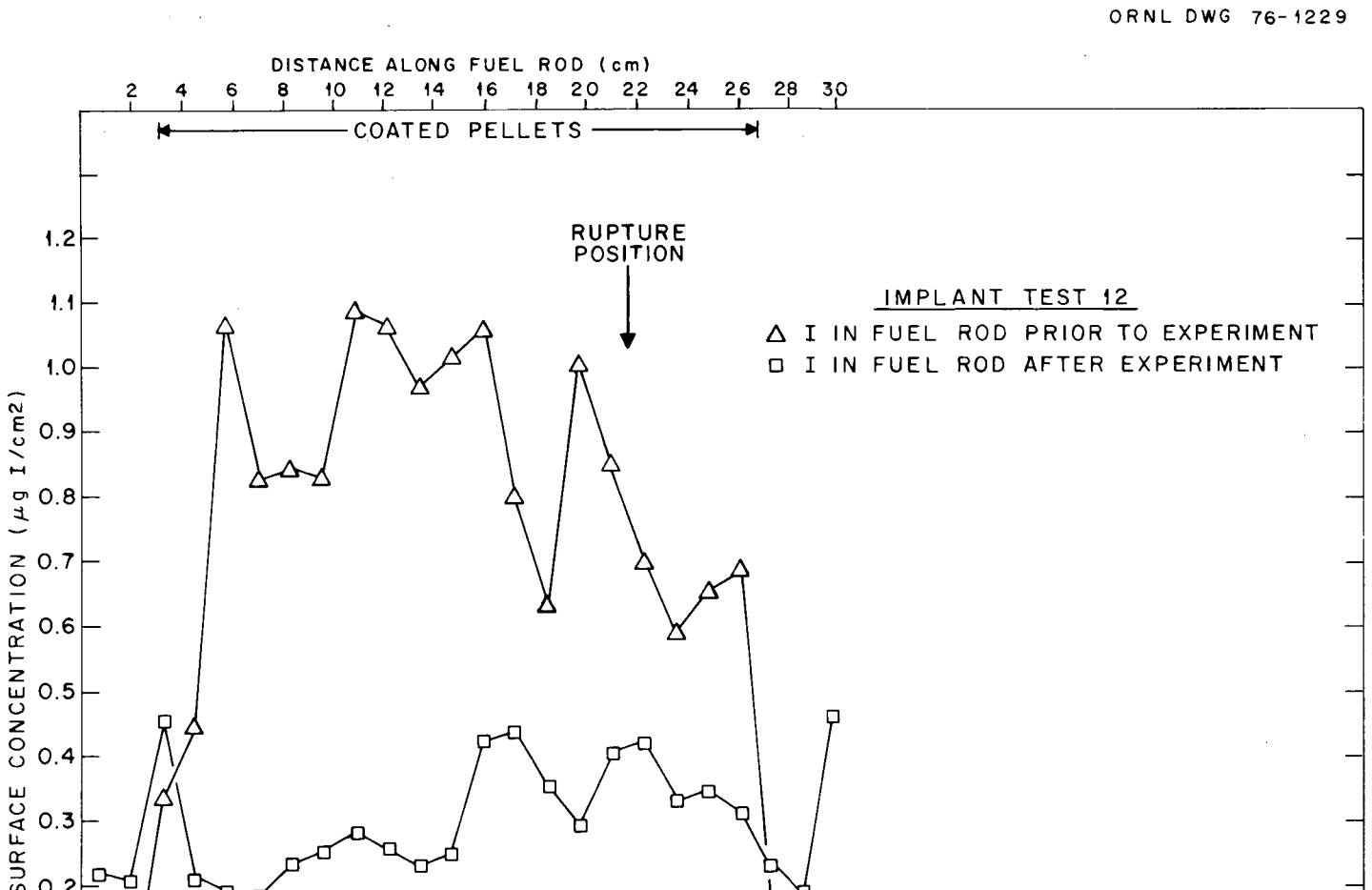

Fig. 61. Iodine distributions in the fuel rod of Implant Test No. 12.

coupling of the induction heater coil to the fuel rod is affected locally by axial splits in the tubing and by composition changes, such as conversion of Zr to ZrO_2.

The post-test distributions of cesium, iodine, and tellurium in the experimental apparatus are summarized in Table 13. About 25% of the cesium, 60% of the iodine, and 1.6% of the tellurium inventories were released. Most of the cesium released (21% of the implanted cesium) was deposited on the quartz liner opposite the rupture opening, as is displayed graphically in Fig. 62. If it is assumed that all of the released iodine was CsI, about 88% of the cesium released would have been collected as CsOH. However, since some of the iodine probably exited the rod as elemental iodine, this percentage of cesium as CsOH is a minimum value. Tracer analysis indicates that ∿15% of the implanted iodine was deposited in the collection system as elemental iodine.

Approximately half of the released iodine condensed in the thermal gradient tube as cesium iodide; this can be inferred from the nearly identical concentration profiles of cesium and iodine in the thermal gradient tube displayed graphically in Fig. 63. Moreover, an examination of the amount of iodine deposited in the thermal gradient tube with time (Fig. 64) indicates that most of the iodine was transported there in the first 4 min after rupture. The data presented in Fig. 64 also indicate that ∿64% of the iodine found in the impactor-filter assembly arrived in the first 10 min of the test.

Approximately 94% of the original tellurium deposited on the cladding at the pellet interfaces. Although the tellurium concentration was low, it was sufficiently high that the reaction rings were again visible.

5. BEHAVIOR OF IMPLANTED CESIUM IODIDE

5.1 General Behavior of CsI

Although CsI is the most stable iodide known, it was not found to be completely stable in the simulated LWR fuel-rod environments employed in our tests. In Implant Tests 1 and 2 (Sects. 4.1 and 4.2), 26 and 14% of

Table 13. Distributions of cesium, iodine, and tellurium in Implant Test 12

Location	Temp. (°C)	Amount found in each location					
		Percent of total			μg		
		Cs	I	Te	Cs	I	Te
Fuel rod, total	900	(75.12)	(39.67)	(98.45)			
UO_2 pellets		40.60	16.83	4.59	430.0	8.4	12.0
Zircaloy cladding		34.52	22.84	93.86	366.0	11.4	244.0
Quartz furnace tube	~200 to 700[a]	20.72	5.61	0.0	220.0	2.8	0.0
Thermal gradient tube	760 to 200	3.34	27.72	1.36	35.0	13.9	3.5
Orifice assembly	130	0.09	3.12	0.02	1.0	1.6	0.05
Impactor assembly	130						
Impactor housing		0.49	11.25	0.11	5.2	5.63	0.29
First-stage paper		0.08	3.87	0.007	0.9	1.94	0.02
Second-stage paper		0.02	0.08	0.0002	0.2	0.04	0.001
Third-stage paper		0.01	0.13	0.004	0.1	0.07	0.01
Fourth-stage paper		0.01	0.24	0.004	0.1	0.12	0.01
Fifth-stage paper		0.05	0.50	0.01	0.5	0.25	0.03
Filter assembly	130						
Filter housing		0.005	2.30	0.01	0.05	1.15	0.03
First filter paper		0.04	0.33	0.003	0.4	0.17	0.008
Second filter paper		0.001	0.24	0.0005	0.01	0.12	0.001
Third filter paper		0.001	0.12	0.002	0.01	0.06	0.005
Silver screen No. 1		0.01	3.83	0.002	0.1	1.91	0.005
Silver screen No. 2		0.0	0.48	0.0	0.0	0.24	0.0
Silver screen Nos. 3 to 8		0.0	0.25	0.0	0.0	0.13	0.0
Adsorber assembly	115						
Adsorber housing		0.002	0.04	0.007	0.02	0.02	0.02
Charcoal No. 1a		0.0009	0.149	0.0004	0.01	0.07	0.001
Charcoal No. 1b		0.0008	0.011	0.0	0.008	0.006	0.0
Charcoal No. 1c		0.0006	0.008	0.0032	0.006	0.004	0.01
Charcoal No. 1d		0.0002	0.003	0.0017	0.002	0.002	0.004
Charcoal No. 2		0.0001	0.007	0.0	0.001	0.004	0.0
Charcoal No. 3		0.0003	0.005	0.0017	0.003	0.003	0.004
AgX		0.0	0.004	0.002	0.0	0.002	0.01
Condenser assembly	0						
Condenser housing		0.0	0.005	0.0	0.0	0.003	0.0
Condensate		0.0	0.003	0.0	0.0	0.002	0.0
Freeze trap	-78	0.0	0.001	≤0.01	0.0	0.001	0.02
Cold charcoal trap	-78	0.0	0.0	0.0	0.0	0.0	0.0

[a]Outlet end heated to minimize condensation of CsI.

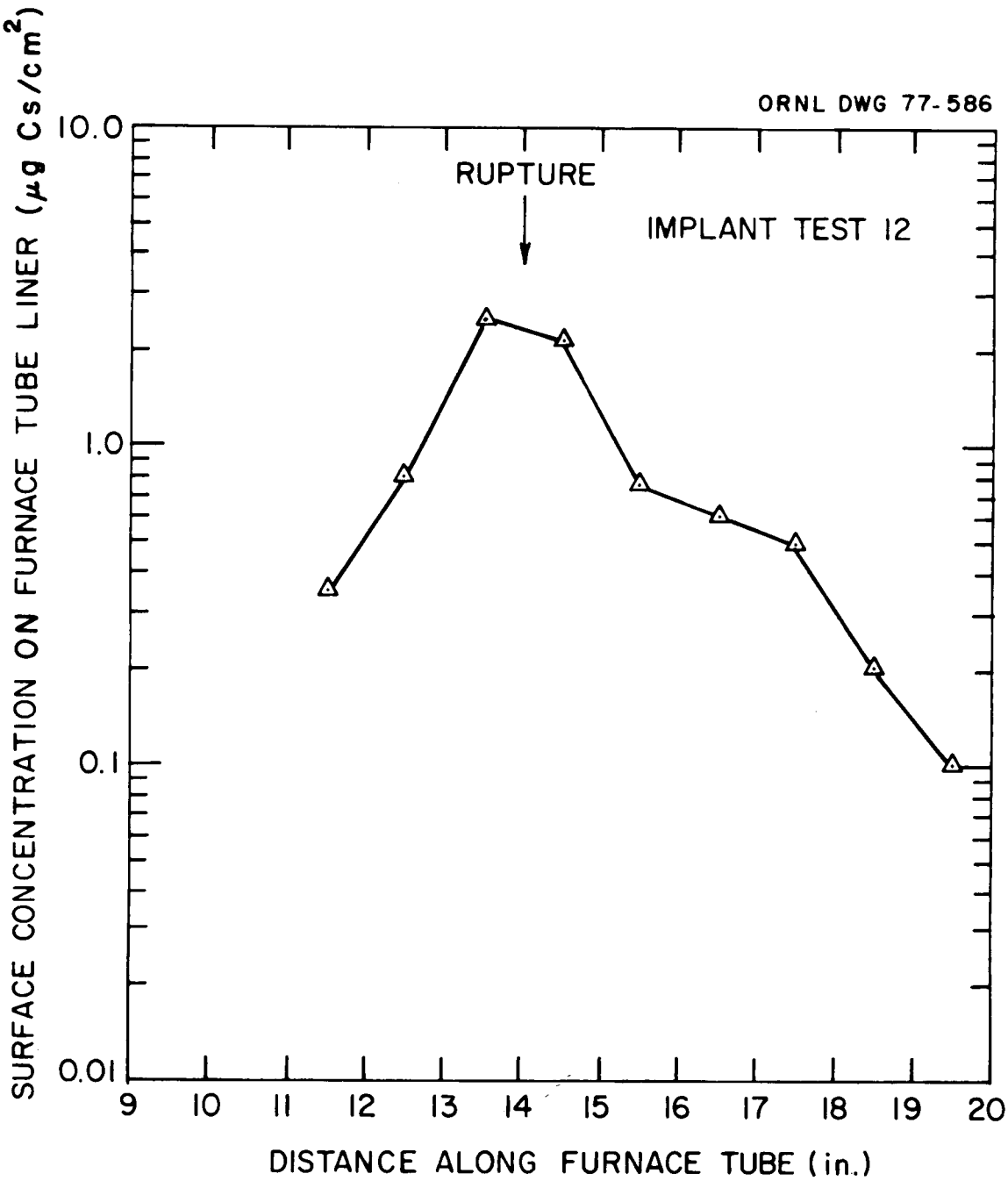

Fig. 62. Distribution of cesium on the quartz furnace tube liner of Implant Test No. 12.

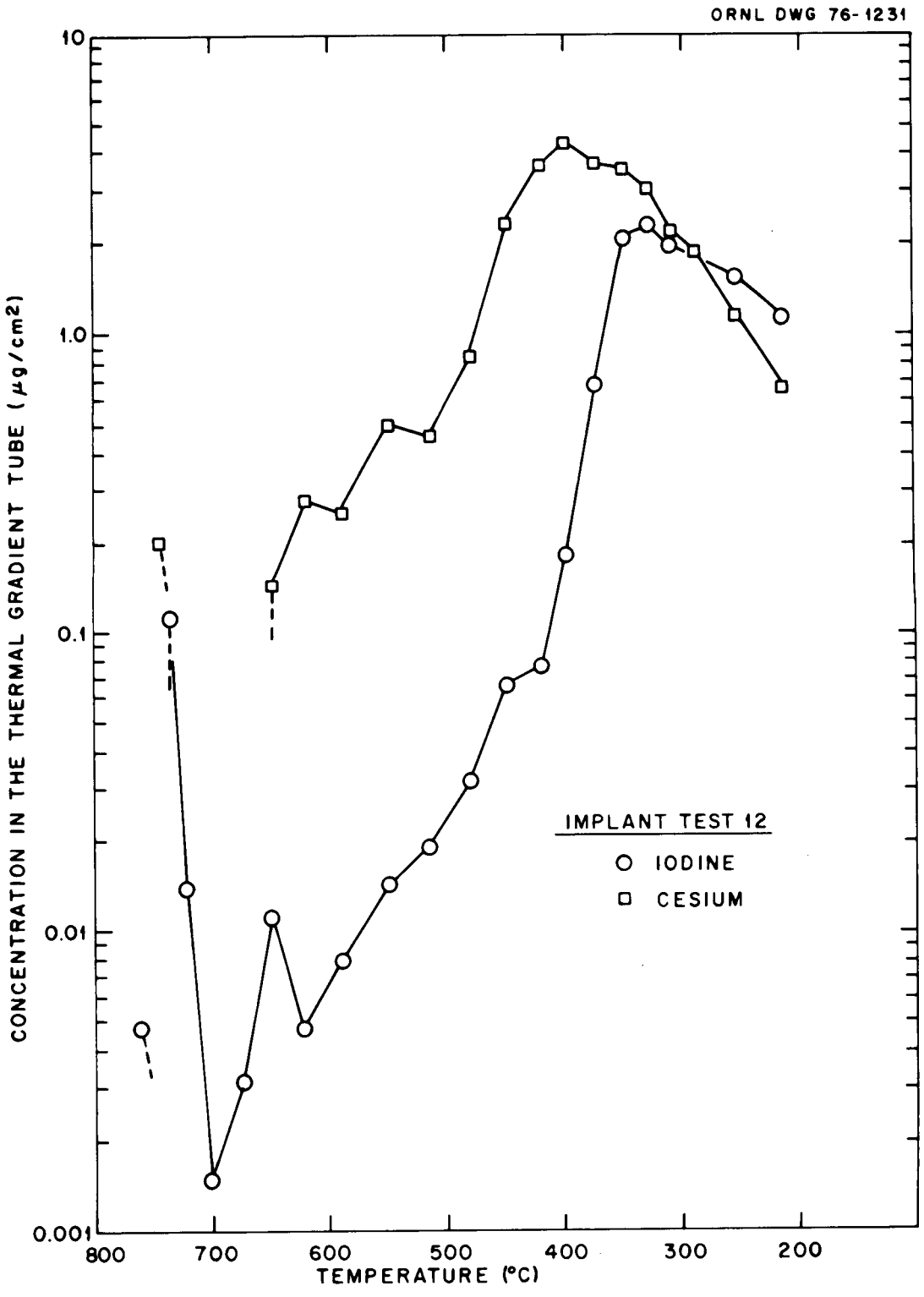

Fig. 63. Cesium and iodine concentration profiles in the thermal gradient tube of Implant Test No. 12.

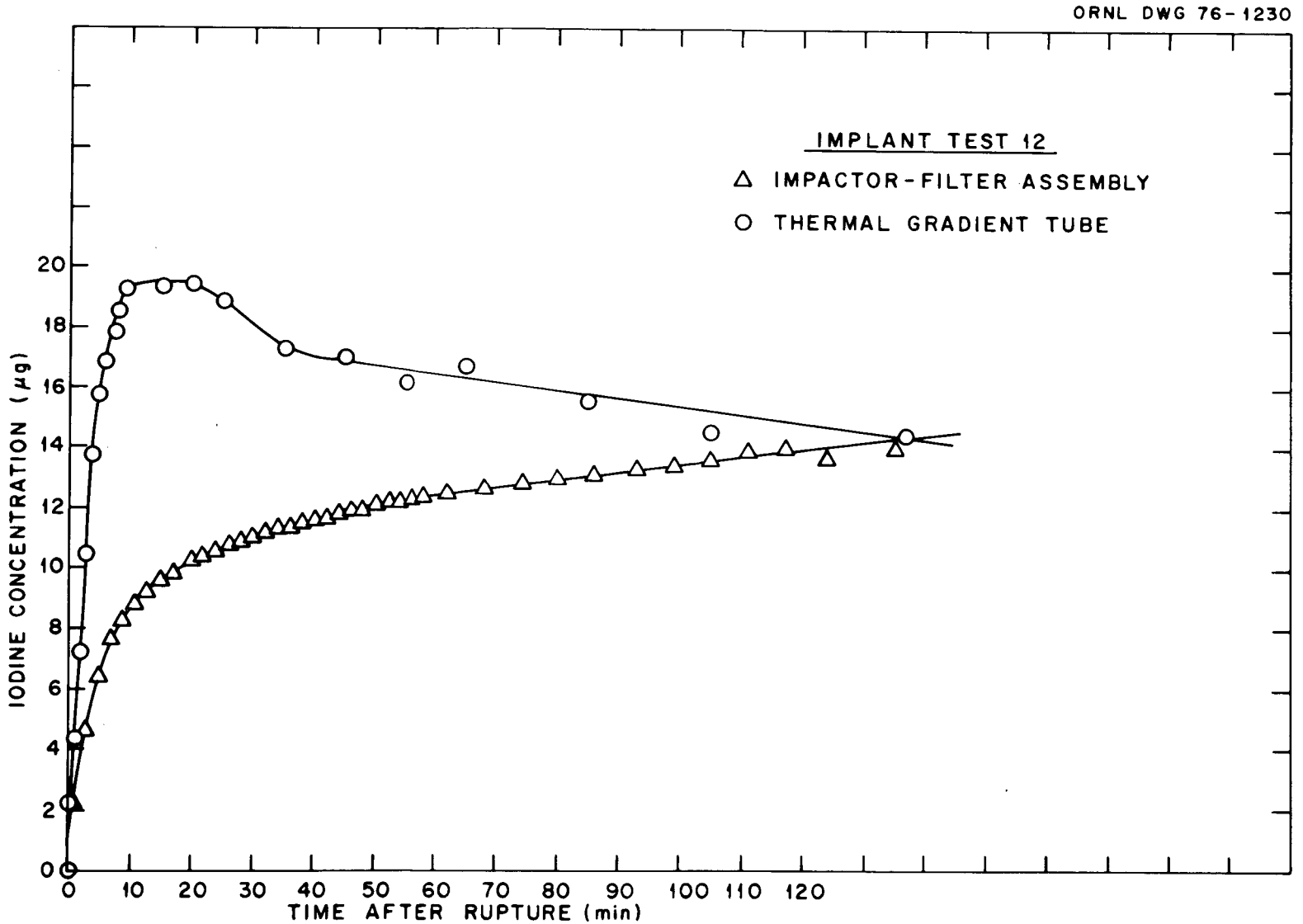

Fig. 64. Iodine deposition in the thermal gradient tube and the impactor-filter assembly during Implant Test No. 12.

the implanted CsI disproportionated respectively. These disproportion values were inferred from the presence of excess cesium on the pellets. The most plausible explanation is that some of the implanted CsI reacted with the hyperstoichiometric fuel (O/U ratio of 2.0004) to form a less-volatile cesium uranate and elemental iodine. (It is possible that the implantation procedure, Sect. 2, resulted in an even higher O/U ratio at the fuel surface.)

Approximately 55% of the liberated iodine in each of these tests was found associated with the Zircaloy cladding. Post-test scans of the 700°C experiments revealed that iodine did not migrate axially to the cooler ends of the capsules in these two experiments. Since elemental iodine has a high vapor pressure (bp = 183°C) at 700°C, it is likely that the excess iodine on the cladding probably reacted with the cladding to produce zirconium iodides[11] and/or oxyiodide compounds. Otherwise, the liberated elemental iodine would have been released. However, considering the low concentrations employed, some retention by sorption can be expected. A sample of material scraped from the inner surface (in a region 2 to 3 in. from the inlet end) of the Zircaloy cladding used in Implant Test 2 was found (by x-ray diffraction) to contain cesium zirconium iodate, $Cs_2(Zr(IO_3)_6)$. In a recent review by Epstein,[6] it was reported that CsI does not interact chemically with the fuel or other fission product compounds in hypostoichiometric fast-reactor fuel pins. Certainly our tests demonstrate the importance of the oxygen potential of the fuel in determining the stability of CsI when present at low concentration levels.

5.2 Axial Migration of CsI Within the Fuel Rod

Axial migration of iodine species to the cooler ends of the simulated fuel rod capsules was slow at 900°C but was rapid at temperatures of $\geq$1100°C. The axial temperature gradient was caused by induction heating of only the center 25 cm (10 in.) of the test specimen. For example, the ends of the capsule in Implant Test 8 (Sect. 4.8) were $\sim$800°C, while the 20-cm (8-in.) center was at 1100°C. By making use of a mobile (NaI) gamma scanner in Implant Test 8, it was determined that the iodine migration was essentially complete within 8 min after the temperature of the

capsule reached 900°C (4 min after it reached 1100°C). Because of the migration of iodine to the cooler outlet end of the capsule in Implant Test 11 (Sect. 4.11), a 1300°C test, the iodine release was significantly less. Little iodine was found on the cladding and pellets in the hot zones of the capsules in tests conducted at 1100°C and higher.

Our method of pressurization probably contributed to the movement of CsI toward the outlet end. Internal argon pressure was applied from the inlet end after the rod was heated to the desired temperature for rupture, thus pushing vaporized material toward the cool outlet end. Gamma scanning of the rod was not rapid enough to determine the amount of radioactive iodine movement coincident with pressurization. In all of the experiments in which the rod ruptured at 900°C (except in Implant Test 12), larger iodine peaks occurred at the outlet end. Implant Test 12, which used lower concentrations of implanted species, experienced relatively little iodine migration.

We can estimate the movement of vaporized implanted material as follows: the void space adjacent to the 24-cm length of coated pellets was $\sim$1.2 cm^3 (including dished ends and allowance for chipped pellets). At 900°C the vapor pressure of CsI is 0.025 atm, so the void spaces would contain $\sim$40 μg of iodine vapor as CsI (assuming no CsI decomposition) or 6.5% of a typical 620-μg iodine coating. This amount (and more if replenishment by vaporization occurred rapidly) could be pushed to the outlet end during the high-temperature pressurization where condensation would occur. Both the compression of the gas and the lower temperatures at the outlet end would promote condensation. Although this does not account for all of the iodine migration, it is true that the outlet-end peaks were consistently larger than the inlet-end peaks.

In the case of Implant Test 11, migration apparently occurred before rupture. This test rod was pressurized three times within 1.8 min while in the 900 to 950°C temperature range because a leak at the inlet Swagelok fitting prevented normal pressurization and rupture. (A length of restrictive capillary tubing between the pressure gauge and test rod was used to simulate pressure drop in the pellet-clad gap space of a full-length fuel

rod; this made it impossible to determine true pressure within the fuel rod if a sizable leak existed at the fuel rod end.) This multiple pressurization could have contributed to "compression migration."

In addition to migration caused by pressurization after heatup, migration can result from diffusion along the axial temperature gradient. The rate of diffusion to the cool ends can be calculated from the following equation:

$$\frac{dn}{dt} = D \frac{A}{L} \Delta C \ , \qquad (1)$$

where

$\frac{dn}{dt}$ = vapor flow rate (moles/sec),

D = diffusion coefficient (cm^2/sec),

A = cross-sectional area normal to the diffusion direction (cm^2),

L = length of diffusion path (cm), and

ΔC = change in concentration along the diffusion path (moles/cm^3).

The concentration gradient can be calculated from the CsI vapor pressure and the temperature gradient. Measured temperature distributions at the inlet end of implant test rods are shown in Fig. 65. At a rod temperature of 900°C, the inlet-end temperature drops to 675°C within 2 in. (L = 5.08 cm). Using the ideal gas law, the concentration of CsI at 900°C (0.025 atm vapor pressure) is 2.58×10^{-7} moles CsI/cm^3, and is 0.16×10^{-7} moles CsI/cm^3 at 675°C. The area is 0.034 cm^2 (for unexpanded cladding) and D is $\sim$0.89 cm^2/sec for CsI in argon at 900°C. If these values are inserted into Eq. (1), the rate of transport is calculated to be equivalent to 12.1 μg/min. For a typical coating of 620 μg of iodine, this amounts to 2.0%/min to each end (4.0%/min total). The possibility of natural convection enhancing migration along the gap space was not investigated.

These calculations suggest that pressurization while heated combined with axial diffusion may have caused significant migration of CsI at 900°C center temperature.

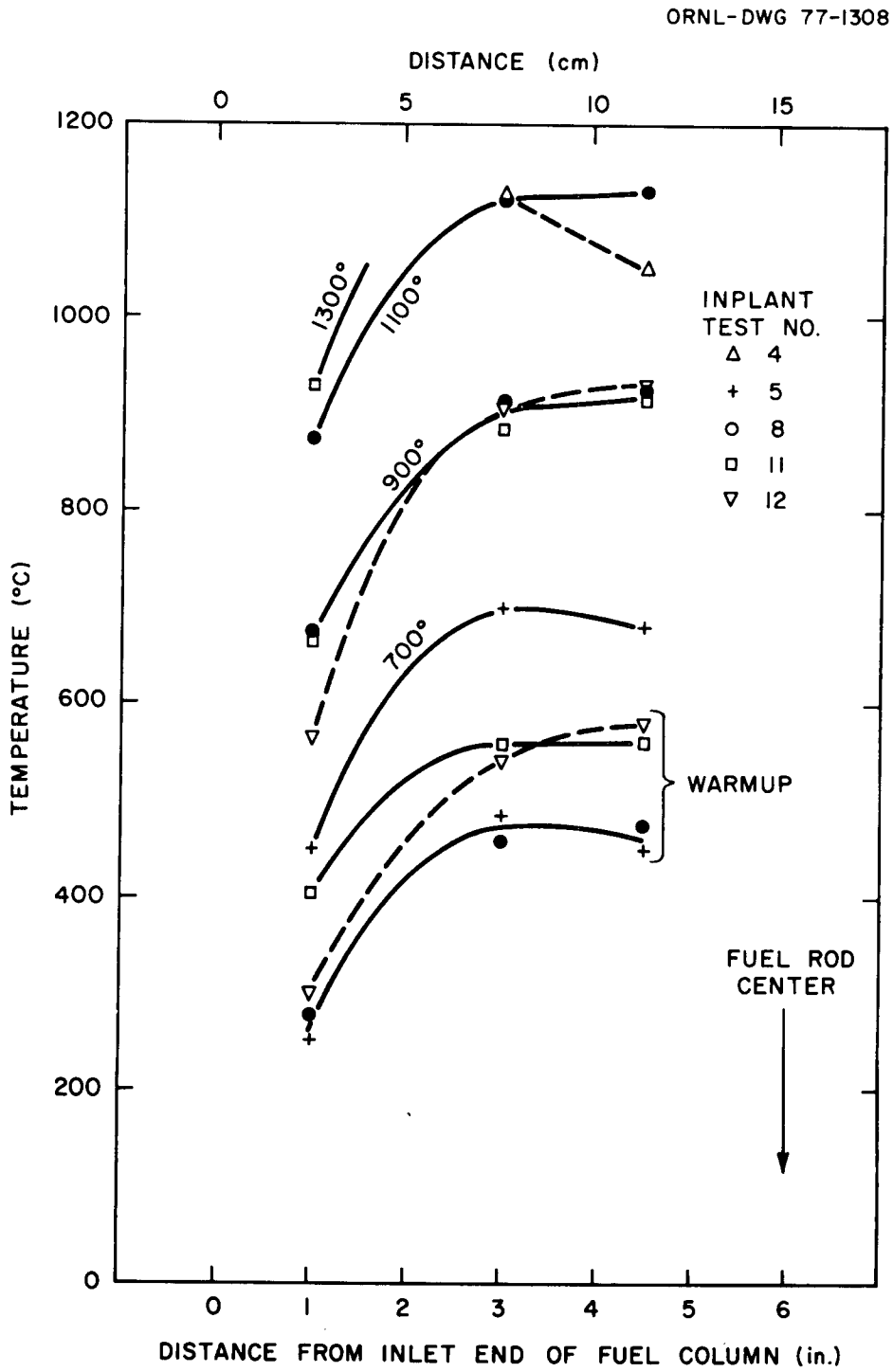

Fig. 65. Temperature profiles at inlet end of induction-heated fuel rods.

5.3 Characteristics of Released Iodine

Measurable quantities of iodine were released in each of the 12 experiments. Identification of the vapor species released from the capsules in some of the experiments was complicated by the tendency of the released CsI to react, in the presence of steam, with the hot surface of the quartz furnace tube liner to form cesium silicate and elemental iodine.[1] The problem of CsI reacting with hot quartz and stainless steel was also encountered by Collins et al.,[8] in their temperature gradient tube studies. Compared with inert atmospheres, they found that CsI was more readily decomposed by hot quartz and stainless steel in the presence of steam. They speculated that hydrolysis played a part in the reaction of CsI with both quartz and stainless steel.

The percentage of released iodine which was found deposited beyond the quartz furnace tube, and was indentified as elemental iodine is noted in Table 14. Because of the high vapor pressure of elemetal iodine, little would have deposited in the $\geq$200°C furnace tube. The values were obtained by assuming (1) that cesium found on a collection component was CsI, and (2) that any excess iodine was elemental iodine. Since CsOH could be present also, only minimum values are provided by this method. Generally, the data reveal that larger percentages of elemental iodine were obtained in the experiments conducted in air and under conditions where low mass releases resulted.

As mentioned previously, evidence exists for formation of I_2 from CsI both within the fuel rod and on the quartz surfaces. For experiments 7 and 9 conducted in air, the enhanced release of iodine (6 to 12 times greater) over comparable experiments conducted in steam suggest that the presence of air within the fuel rods contributed to the decomposition of CsI, resulting in the formation of cesium uranate and elemental iodine.

For experiments conducted in steam, it is likely that much of the formation of I_2 occurred after the release of CsI from the fuel rod. If I_2 formation occurred principally within the rod, we would expect some correlation with the mass of CsI implanted; such a correlation is not evident in the data presented in Table 14. Also, no temperature correlation is

Table 14. Amount of iodine collected as I_2

Implant Test No.	Test temperature (°C)	Atmosphere of test system	Mass of iodine implanted (μg)	Mass of iodine released (μg)	Mass found as elemental iodine (μg)	Percent of released iodine found as elemental iodine
9	500[a]	air	490	42.0	39.9	95.0
7	700[a]	air	640	74.0	70.3	95.0
2	700	steam	33	5.5	5.0	90.3
6	500[a]	steam	900	5.8	3.2	57.4
10	700[a]	steam	660	12.0	6.4	53.1
12	900	steam	50	30.0	8.6	28.8
8	1100	steam	610	401.0	33.3	8.3
1	700	steam	1600	360.0	27.0[b]	7.5[b]
4	1100	steam	440	145.0	9.0	6.2
11	1300	steam	580	26.0	0.5	1.8
3	900	steam	630	161.0	1.9	1.2
5	700	steam	610	109.0	0.5	0.5

[a]Defect made by drilling 0.0159-cm (0.0625-in.)-diam hole(s).

[b]A large surplus of iodine over cesium was found deposited in the furnace tube. (See Sect. 4.1 for details.)

obvious. (It should be remembered that at 1100°C and higher, the CsI remaining in the test rod rapidly migrated to the cooler ends, where temperatures were probably below 900°C.)

The mass-release data from Table 14 are plotted in Fig. 66; these data indicate that 7 of the 10 steam experiments exhibit a good correlation with release mass. The three off-line points may be in error because, as discussed above, our method of calculation determines a minimum amount of I_2 formed. Conversion of the mass-release data to average gas-phase concentrations provides a similar correlation.

The high percentage conversion to I_2 at low concentration could be the result of reaction with gas-phase impurities or reactive surface sites either available in limited number or consumed by competing reactions during the experiment. An example of the latter could be the reaction of CsOH with SiO_2 to form a cesium silicate. In such a case, more reactive sites would be available early in the run to allow reactions permitting formation of I_2 from CsI. We do observe more rapid appearance of I_2 early in the test, even when no burst release occurs. We also expect, and usually observe, greater release of CsI (appearing in the thermal gradient tube) early in the run.

The loss of several micrograms of iodine from the thermal gradient tube during the course of the experiment was often noticed. This was probably due to a loss of adsorbed I_2 (e.g., Implant Test 10).

The amount of organic iodide formed (collected in the absorber cartridges) did not correlate with any of the experiment parameters, such as the mass of iodine released, fuel-rod temperature, experiment duration, or atmosphere (steam or air). The median value for $\left(\frac{\text{mass I on adsorbers} \times 100}{\text{mass I released}}\right)$ is 0.5%, with variations of more than a factor of 10. This is in agreement with the amount of organic iodide found in other experiments, as described by Postma and Zavadoski.[5]

The distribution of iodine collected in the filter pack of several tests is shown in Fig. 67. The distribution is similar to that obtained during the Control Test Series.[1] As discussed in that report, all filter papers adsorb some I_2; in addition, the first filter paper collects the

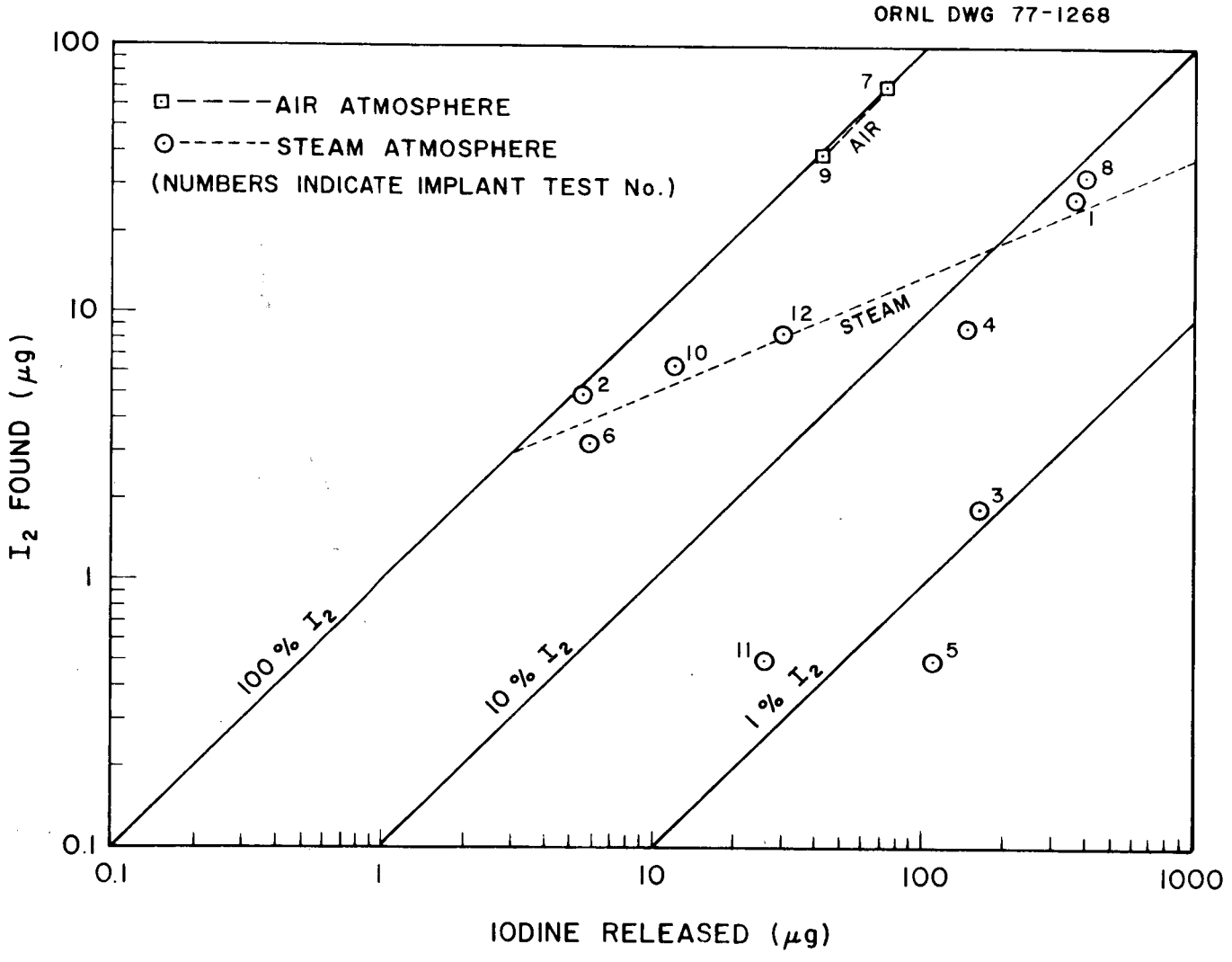

Fig. 66. Amount of elemental iodine formed during implant tests.

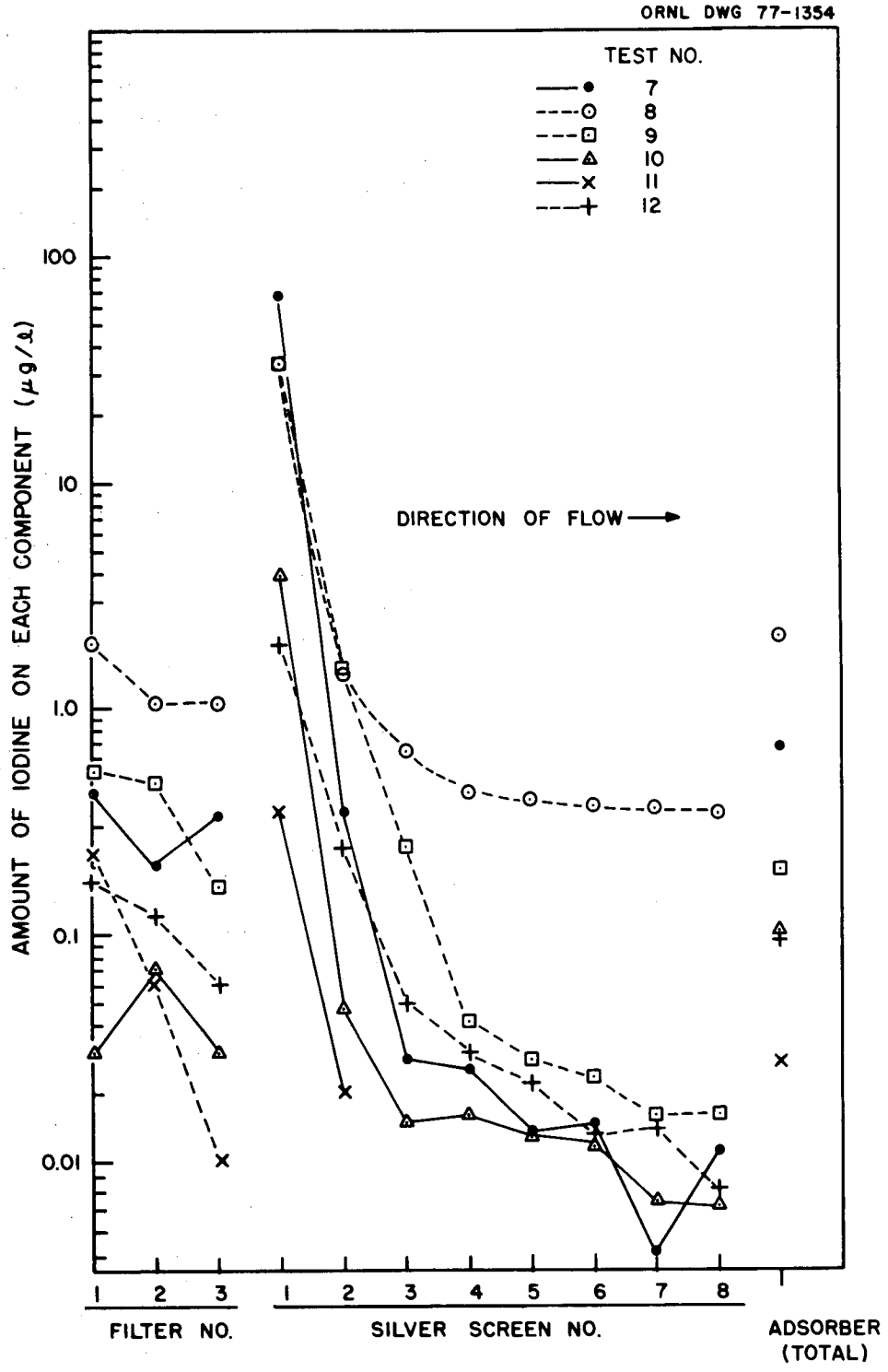

Fig. 67. Iodine retained on particulate filters and silver-plated screens.

particulate-associated iodine. As shown in Fig. 67, the amount of particulate iodine is not much greater than the adsorbed iodine and is much smaller than the amount of iodine that passed through the papers and was collected on the silver-plated screens. For the conditions of the Implant Test Series, the fraction of iodine adsorbed on the filter media appears to be significant only when the total mass of incident iodine is of the order of ≤ 1 μg.

The first four silver-plated screens accomplished nearly complete collection of the reactive forms of iodine (I_2 and probably HI). The source of iodine on the remaining screens is believed to be an unknown (and less reactive toward silver) iodine species. No reason is apparent for the larger amounts of iodine on these screens in Implant Test 8. Control Tests 5 and 10 (see ref. 1) leveled out at 0.2 μg of iodine per screen, a value similar to that of Implant Test 8. Kabat reported[19] that silver "adsorbs" a significant fraction of HOI.

The distribution of iodine adsorbed in the Implant Test Series is similar to that of the Control Test Series,[1] although the amounts are somewhat lower. The adsorber bed used in both test series was designed to have high efficiency of adsorption of methyl iodide; the small grain size (0.160-cm diam) and low relative humidity (<45%) ensured efficient operation. The large cartridges (Nos. 2, 3, and 4) were 1.59 cm in diam and 1.9 cm long and were filled with 1.9 g as-received charcoal or 3.4 g as-received type 13X zeolite, 95% silver exchanged. The superficial velocity was ∿20 cm/sec for operation both at low pressure (most experiments) and at atmospheric pressure (Tests 8 and 11). Beginning with Implant Test 8, cartridge No. 1 was subdivided into four parts, each 0.41 cm long (average depth), to provide greater detail of iodine distribution and to permit each separate subdivision to be irradiated in one exposure for ^{127}I and ^{129}I activation analysis.

Under the above conditions, the adsorption efficiency for methyl iodide provided a one-tenth thickness (the depth of the bed resulting in a decrease in iodine nuclide concentration of a fraction of 10) of approximately 0.80 cm. This is equivalent to a staytime of 0.04 sec removing 90% of the methyl iodide (decontamination factor of 10). As seen in Fig. 68, the silver-exchanged zeolite and charcoal adsorption efficiencies for the poorly sorbed iodine species were equivalent.

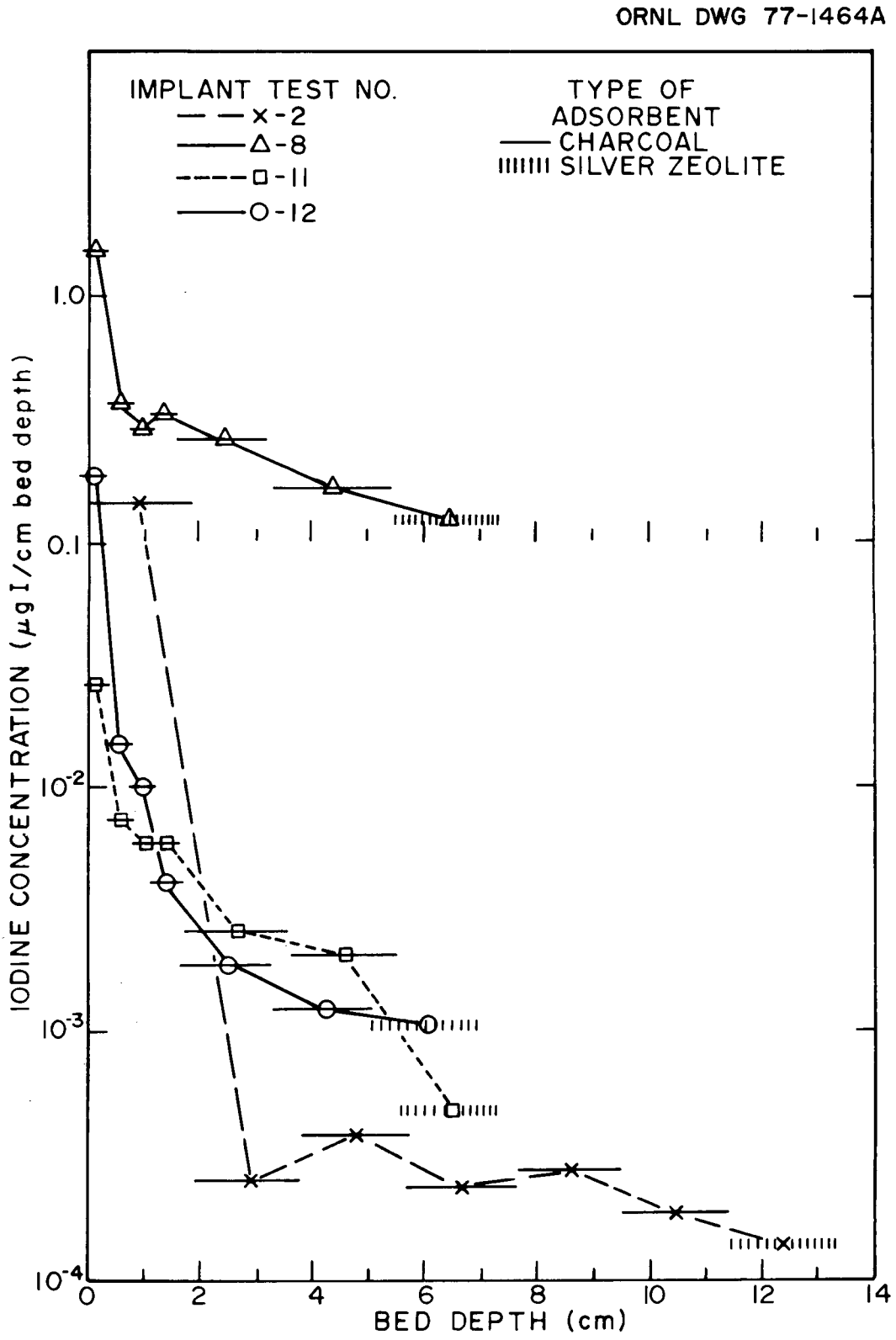

Fig. 68. Iodine distribution in adsorbent bed.

6. BEHAVIOR OF IMPLANTED CESIUM HYDROXIDE

The chemistry of CsOH, as related to our test environment, has been discussed in a previous report.[1] In our Knudsen cell-mass spectrometry work,[3] it was found that CsOH reacted with hyperstoichiometric fuel to form a less-volatile fuel compound(s), probably a uranate. Notable decomposition of the uranate occurred only at temperatures $\geq$925°C, and the primary decomposition product observed with the mass spectrometer was Cs^+. Cesium from the decomposed uranate would rapidly react with steam in our Implant Test Series experiments to form CsOH in the steam-argon atmosphere flowing through the furnace tube liner. In the Implant and Control Tests, cesium hydroxide has been shown to be extremely reactive with the quartz furnace tube liner at temperatures over a broad range (between 125 and 1000°C) forming less-volatile silicates.

Values for CsOH vapor pressure are given by the following equation (derived from JANAF data[12]):

$$CsOH_{(\ell)} = CsOH_{(g)} \tag{2}$$

$$\ln P_{atm} = -\frac{15315}{T} + 12.23 \quad (588 < T < 1263\ K). \tag{3}$$

In comparison with the vapor pressure of CsI, the vapor pressure of CsOH is between 10 to 30 times greater over the temperature range 700 to 1000°C.

In Table 15, the percent of total cesium (implanted as CsOH) that was collected as CsOH, and the percent of total cesium (implanted as CsI) that was collected as CsI for each of the tests are provided for comparison. An assumption was made that all of the iodine released in each experiment was collected as CsI, which is not completely true. However, it does allow the minimum collection of cesium as CsOH to be determined. In each of the tests where the capsule was pressure ruptured, measurable CsOH was collected. However, very little CsOH was collected in tests where the simulated defect was a predrilled hole. The fraction of cesium collected as CsOH in Test 5 was considerably larger than that collected in Test 10; both were conducted at 700°C. This variance in collection was probably due to the high burst pressure experienced in Test 5. Table 15 also shows that the implanted CsOH was more stabilized by the fuel-rod environment than was CsI.

Table 15. Amounts of cesium and iodine collected as CsOH and CsI

Implant Test No.	Test temperature (°C)	Time at test temperature (hr)	Atmosphere	Burst pressure[a] (psig)	Portion of total Cs (implanted as CsOH) collected as CsOH (%)	Portion of total Cs (implanted as CsOH) collected as CsOH (μg)	Portion of total Cs (implanted as CsI) collected as CsI (%)	Portion of total Cs (implanted as CsI) collected as CsI (μg)
8	1100	1	steam	425	33.7	2890	65.8	420
11	1300	1/4	steam	not measured	29.9	2294	4.4	27
4[b]	1100	1	steam	-	24.4	1088	33.0	152
12[c]	900	2	steam	250	23.0	232	63.0	33
3	900	2	steam	250	8.6	488	25.5	168
5	700	2	steam	500	4.3	275	17.7	113
6[d]	500	20	steam	-	0.3	32	0.6	6
10[d,e]	700	5	steam	-	-	-	0.7	5
7[d]	700	5	air	-	0.1[h]	8[h]	11.6	78
9[f,g]	500	20	air	-	-	-	3.9	20

[a]Tests 8, 11, 4, 12, and 3 were each ruptured at 900°C by applying internal argon pressure.

[b]Release was via a leak at inlet capsule fitting.

[c]A factor of about 7 times less cesium was employed in this test.

[d]Predrilled (1/16-in. hole) to simulate a defect.

[e]About 7 μg of iodine was released from the capsule as elemental iodine.

[f]Predrilled (three-1/16 in. holes).

[g]About 12 μg of iodine was released from the capsule as elemental iodine.

[h]Because of the dry air atmosphere, this cesium was probably collected as Cs_2O.

Table 16 indicates that at test temperatures of ≤900°C, the ratio of cesium on the pellets to cesium on the cladding is about 2:1. Considering the volatility of CsOH, it appears that CsOH is stabilized by both the fuel and cladding in this temperature range. (It should be remembered that 92% of the cesium inventory was originally CsOH.) In tests where the temperature is >900°C, such as in Tests 8 (1100°C) and 11 (1300°C), the ratio of cesium on the pellets to cesium on the cladding was about 2.3:1.

Table 16. Distribution of cesium between pellets and cladding

Implant Test No.	Temperature (°C)	Time at test temperature (hr)	Percent of total Cs excluding Cs as CsI		Ratio of Cs on pellets to Cs on cladding
			on pellets	on cladding	
6	500	20	61.55	29.02	2.12
5	700	5	54.89	32.20	1.70
7	700	5	58.84	32.52	1.80
3	900	2	55.84	28.71	1.95
8	1100	1	43.01	18.66	2.30
11	1300	0.25	46.68	19.66	2.30
12[a]	900	2	39.62	33.02	1.20

[a]Low-concentration test.

7. BEHAVIOR OF IMPLANTED TELLURIUM DIOXIDE

Tellurium dioxide is a stable compound with a melting point of 733°C and a boiling point of 1245°C. Values of TeO_2 vapor pressure are given by the following equations:[6]

$$TeO_{2(s)} = TeO_{2(g)};\ \Delta H_{sub} = 54.9 \text{ kcal/mole};$$

$$\log P_{atm} = 8.067 - \frac{12000}{T} \quad (846 < T < 1006 \text{ K}) \ . \tag{4}$$

$$TeO_{2(\ell)} = TeO_{2(g)};\ \Delta H_{vap} = 51.7 \text{ kcal/mole};$$

$$\log P_{atm} = 7.367 - \frac{11300}{T} \quad (1006 < T < 1211 \text{ K}) \ . \tag{5}$$

At temperatures above 1100°C, the dioxide dissociates in the gaseous state to form tellurium monoxide.[13]

In each of the experiments in this series, at least half of the implanted tellurium dioxide was transported to the Zircaloy cladding and was deposited. Furthermore, scans of tellurium activity along the cladding in each of the experiments revealed apparent rapid reaction with the cladding at pellet interface locations. In most of the experiments conducted at 700°C and above, reaction rings were evident at pellet interfaces as shown in Fig. 16. The reaction rings are an artifact of the implantation technique. If the TeO_2 had been initially distributed uniformly on the cylindrical surfaces of the pellets, we believe that the reaction with the Zircaloy would also have been uniform. The compound Te_3ZrO_5 was identified by x-ray diffraction in a sample of ring material. The product of reaction between the Zircaloy-4 and TeO_2 proved to be stable over the temperature range covered in these experiments (500 to 1300°C). A longitudinal cut through one such reaction zone, shown in Fig. 17 (Sect. 4.3), revealed a decidedly thinner oxide layer in this region.

The rate of transport of TeO_2 from the pellet dished ends to the cladding was found to increase with temperature. A first-order rate constant was calculated for the fraction transported to the cladding in each experiment. The results are shown in Fig. 69.

It can be seen from the data listed in Table 17 that <0.1% per hour of the total tellurium inventories were released in Tests 6, 10, 4, 9, and 7, where the capsules were predrilled to provide the simulated defect. In a steam atmosphere, tellurium dioxide can form an oxyhydroxide that is more volatile than the dioxide,[14] according to the following equation:

$$TeO_{2(s)} + H_2O_{(g)} \rightarrow TeO(OH)_{2(g)} \ . \tag{6}$$

The dimer Te_2 is considerably more volatile than the oxyhydroxide.

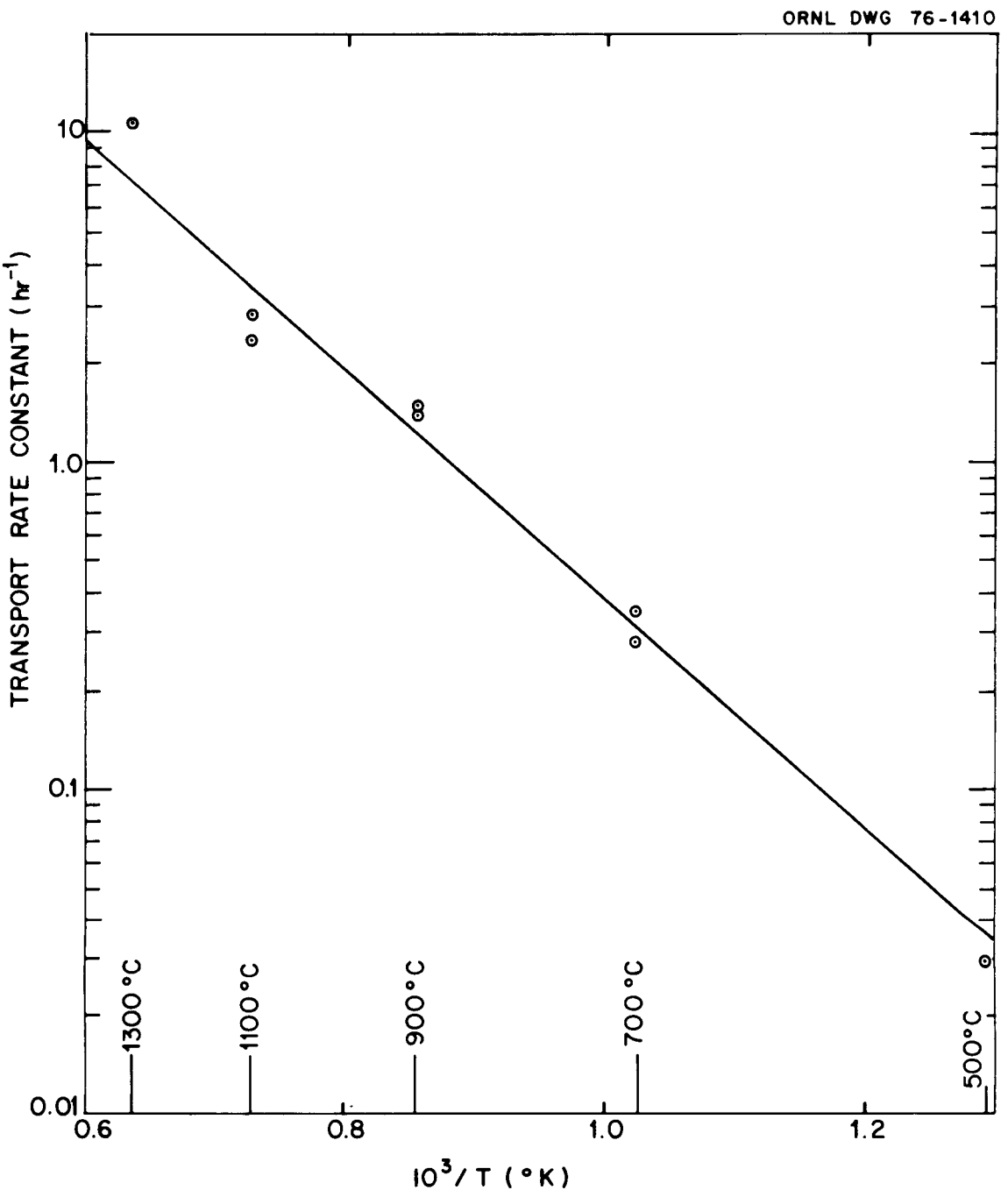

Fig. 69. Rate of transport of tellurium from pellet dished ends to Zircaloy cladding.

Table 17. Operating conditions affecting release of tellurium

Implant Test No.	Test conditions: Temperature (°C) At burst	Test conditions: Temperature (°C) During test	Test conditions: Atmosphere Steam argon	Test conditions: Atmosphere Dry air	Test conditions: Time at test temperature (hr)	Burst pressure (psig)	Percent of total Te released (%)
5	700	700	X	-	5	500	6.5
8	900	1100	X	-	1	425	3.3
12	900	900	X	-	2	250	1.6
3	900	900	X	-	2	250	1.6
11	900	1300	X	-	0.28	not measured	1.0
6	-	500	X	-	20	Predrilled (1/16-in. hole)	0.5
10	-	700	X	-	5	Predrilled (1/16-in. hole)	0.2
4	-	1100	X	-	1	Leak at inlet fitting	0.1
9	-	500	-	X	20	Predrilled (3) 1/16-in. holes	0.2
7	-	700	-	X	5	Predrilled (1/16-in. hole)	0.02

The mode of release in the predrilled tests was vapor diffusion. Table 17 indicates that the releases were larger in the tests (Nos. 5, 8, 12, 3, and 11) where the cladding was ruptured by internal application of argon pressure. The fuel-rod temperature appears to have had little influence on these releases; rather, the releases were more dependent upon burst pressure. The larger the burst pressure, the larger the release.

In both Implant Test 8 (1100°C) and 11 (1300°C), the distribution profile of tellurium in the quartz furnace tube liner was similar to that obtained for cesium, as shown in Figs. 37 and 56. Like cesium, tellurium was deposited primarily in the region near the rupture opening. At temperatures of 800°C and higher, tellurium reacts with quartz;[13,15] the maximum temperature of the quartz liner in these tests was probably higher than 800°C in the hot region, although the liner temperature was lower at the time of fuel-rod rupture.

Three side experiments were conducted in the laboratory to help explain the chemical behavior of the tellurium-Zircaloy system. These tests were conducted at 900°C for 1 hr with a flowing-argon carrier gas provided. In the first experiment, it was found that TeO_2 mixed with ZrO_2 reacted to form Te_3ZrO_5:

$$6\ TeO_2 + 2\ ZrO_2 = 2\ Te_3ZrO_5 + 3\ O_2\ . \qquad (7)$$

Agarwala et al.,[16] prepared Te_3ZrO_5 by heating a mixture of ZrO_2 and tellurium (taken in a ratio corresponding to one atom of zirconium to three atoms of tellurium) in air at 750°C for 48 hr.

In the second experiment, TeO_2 was mixed with metallic zirconium in an argon atmosphere at 900°C; the following reaction products, ZrO_2 and elemental tellurium, were obtained:

$$TeO_2 + Zr = ZrO_2 + Te\ . \qquad (8)$$

A large fraction of the liberated elemental tellurium was transported and condensed in a cool quartz tube that was downstream from the furnace tube. (The vapor pressure of tellurium is ∿200 torr at 900°C.[17])

Zirconium telluride (ZrTe) was obtained when elemental tellurium and zirconium were mixed and heated to 900°C in argon:

$$Zr + Te = ZrTe \ . \qquad (9)$$

When excess zirconium is present, the tellurium formed in accordance with Eq. (8) could also react to form the less-volatile ZrTe. In all three experiments, the reaction products were determined by x-ray diffraction.

Based upon the results of the Implant Tests and the three laboratory experiments, it is apparent that the "gettering" ability of Zircaloy for tellurium is the result of Eq. (7) when the oxide film is substantial and Eq. (9) when the oxide film is insignificant.

8. SUMMARY OF RELEASE DATA

8.1 Comparison of Amounts of Cesium and Iodine Released

Since the experiments were operated for different lengths of time, comparisons of the amounts of cesium and iodine released in the various experiments cannot be made directly. The release of the high specific activity ^{130}I (half-life, 12.4 hr) enabled essentially continuous monitoring of iodine released during most experiments, thus permitting a determination of release with time.

The amount of iodine released in the first hour of each experiment is displayed graphically in Fig. 70. Lines are drawn to show roughly the difference between release of iodine from test rods with predrilled hole defects and those ruptured by internal argon pressure. It is clear that the pressure-rupturing caused much greater release of iodine than occurred by undisturbed diffusion from the predrilled rods. The correlation for release from pressure-ruptured rods is presented in Sect. 8.2. Release of iodine from the predrilled rods was significantly less in the steam atmosphere than in dry air. As discussed in Sect. 5, 95% of the iodine released in dry air was in the elemental form (I_2) when collected. A summary of release by diffusion from the test rods is presented in Sect. 8.3.

The low specific activity ^{134}Cs (half-life, 2.06 years) employed in these tests could not be detected until the ^{130}I had decayed to a low level,

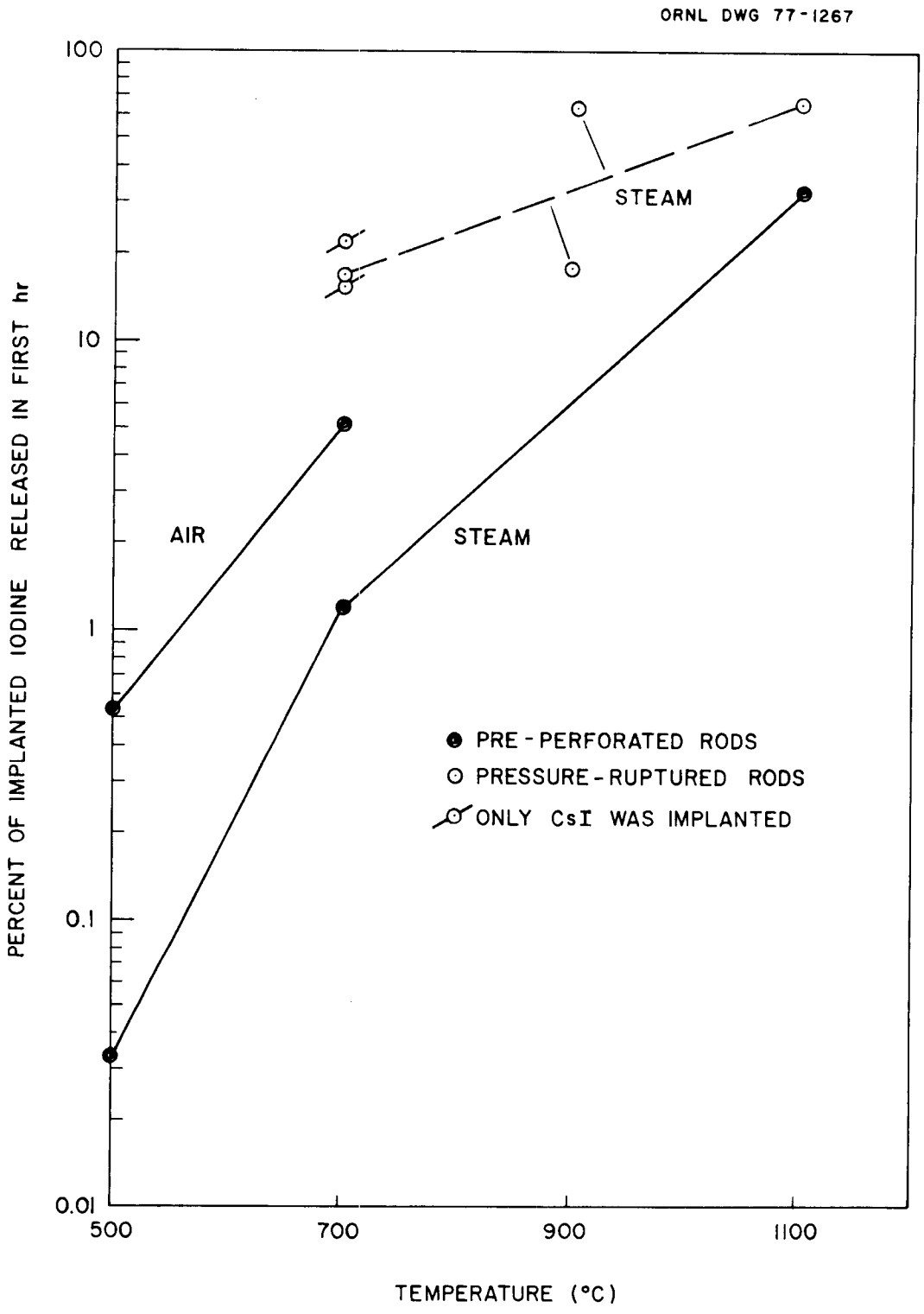

Fig. 70. Release of implanted iodine.

usually several days after the experiment. Therefore, interim release rates for cesium can only be inferred from the iodine release rates. Using iodine release as a guide, the amounts of cesium released during the first hour of each experiment have been estimated and are shown in Fig. 71.

The effects of experiment parameters on cesium release are similar to those of iodine. In all cases, however, the percentage of cesium released was less than for iodine. (The only exception was Implant Test 11, conducted in the 900 to 1300°C range, in which iodine apparently migrated to the cool ends of the test rod before rupture. See Sect. 5.2 for a discussion of migration behavior.) Athough the fractional release from cesium was consistently less than for iodine, the mass of cesium released in the higher temperature tests was greater than the mass of iodine. This is possible because of the higher mass loading of cesium in all tests except Nos. 1 and 2. The mass ratios of cesium-to-iodine release are plotted in Fig. 72. Although the data are scattered, a definite trend with temperature exists. The lower percentage releases of cesium are a clear demonstration that CsOH, more volatile than CsI, reacted with the fuel-rod components to form cesium compound(s) with significantly lower volatility. (See Sect. 6 for a discussion of the CsOH behavior.)

8.2 Release at Rupture — "Burst Release"

It is clear from Figs. 70 and 71 that a large amount of implanted material is released upon rupture. A logical mechanism for this "burst release" is the evaporation of implanted material as the pressurizing gas (plenum gas in a reactor fuel rod) flows along the pellet-cladding gap space and out of the rupture opening. By this mechanism the burst release is proportional to the partial pressure of the species and the volume of gas flowing out of the rupture opening. The partial pressure of each chemical species is determined by its ordinary vapor pressure (or possibly a chemical equilibrium as with $Cs_{(g)}$ over $Cs_2UO_{4(s)}$ modified by adsorption (at low concentration) and mass transfer from the solid to the gas phase during the blowdown. The volume of gas is a function of the amount of gas in the pelnum (and pellet-clad and pellet-pellet voids) and the

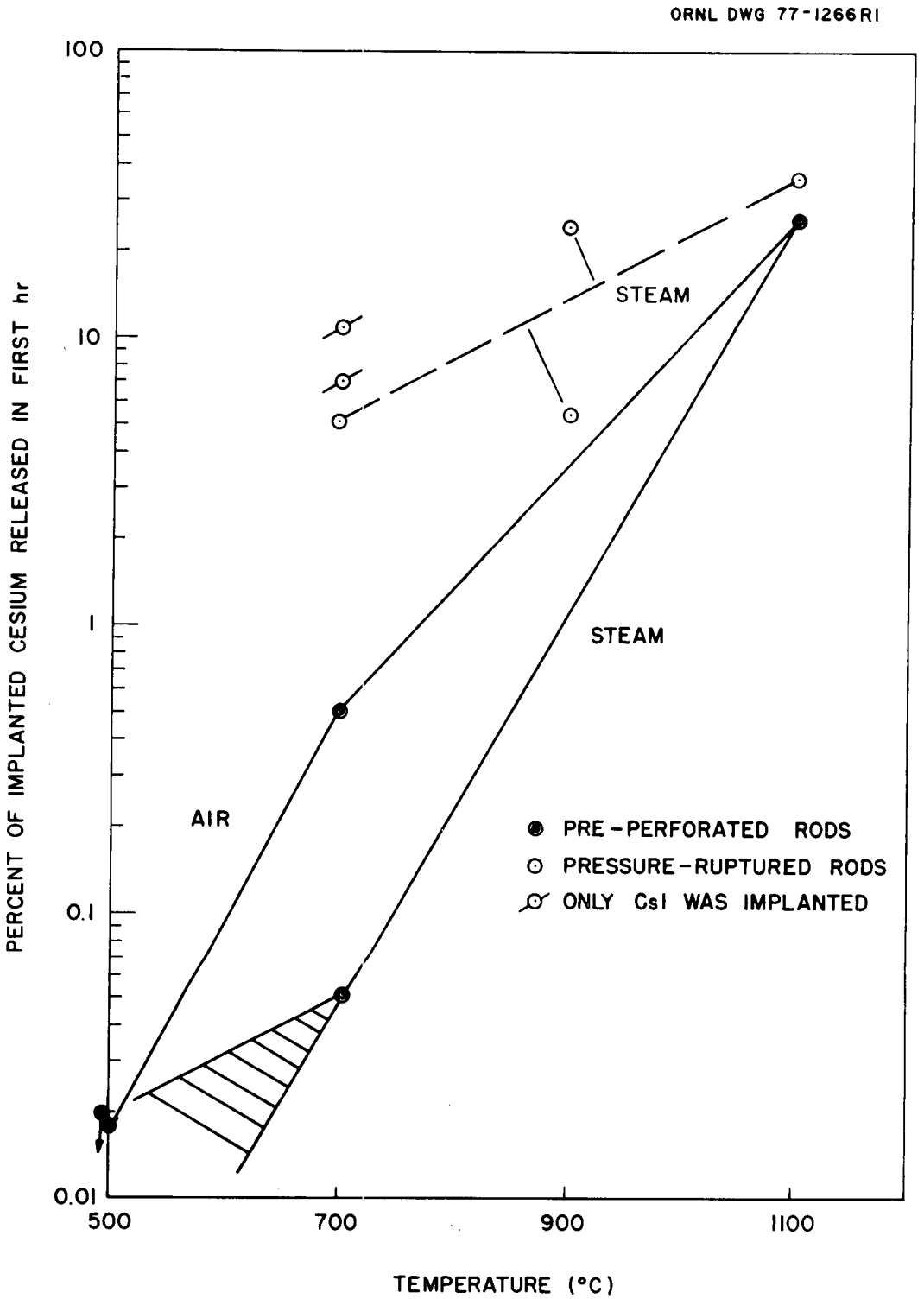

Fig. 71. Release of implanted cesium.

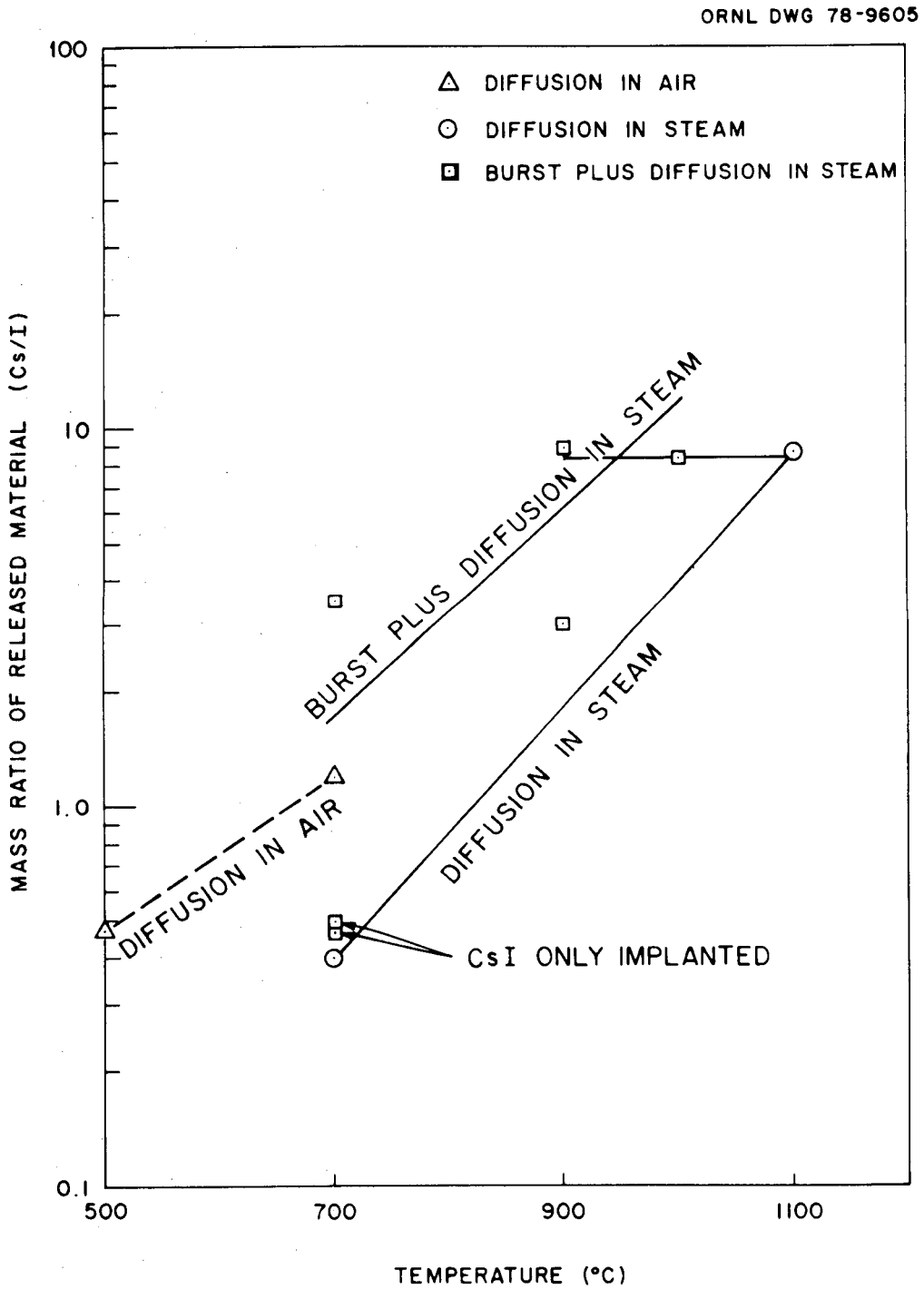

Fig. 72. The effect of temperature and atmosphere on the ratio of released cesium and iodine.

pressure at the location where the evaporation occurs. It must also be recognized that the plenum gas usually sweeps through only approximately half of the rod length.

The calculated amounts of gas vented at rupture, iodine and cesium mass released at rupture, and resulting concentrations of these elements in the vented gas are listed in Table 18. The gas "plenum" used in these tests consisted of small-diameter tubing, a pressure transducer, and a flow restrictor with a combined volume of 10.6 cm^3 which remained at ∿30°C during the test. The fuel rod contained 1.8 cm^3 volume, approximately half of which was heated to the rupture temperature while the remainder reached some intermediate temperature. The amount of gas vented at rupture was calculated from the pressure at rupture and the above volumes and temperatures. At rupture the plenum gas blowdown lasted several seconds because of the installed flow restrictor tubing.

The gas volumes and amounts of iodine and cesium released at rupture are only approximate. Continuous gamma monitoring of the radioiodine that was transported to the thermal gradient tube and filter pack was intended to differentiate between the amounts of iodine released at rupture and that released subsequently by diffusion. However, holdup of iodine species in the furnace tube interferred with this analysis, especially for tests conducted at 700°C. Therefore, the amount of iodine released at rupture at 700°C (and the amounts of cesium likewise released at 700 and 900°C) were calculated by subtracting diffusional release (Sect. 8.4) from the total release. For the iodine burst-release at 900°C, gamma monitoring of the released iodine was used.

The resultant concentrations of iodine and cesium in the vented gas are plotted in Fig. 73 as a function of the total element implanted. Four conclusions can be drawn from the data as plotted in this figure.

1. There is a strong dependence upon mass of implanted materials.
2. There is not much difference between cesium and iodine released in the burst. Agreement is roughly within a factor of 2.
3. Concentrations at 900°C are only 2 to 6 times greater than at 700°C.

Table 18. Iodine and cesium burst release

Implant Test No.	Temperature at rupture (°C)	Gas released at rupture (cm^3 He, STP)	Total iodine implanted (μg)	Total iodine released (μg)	Estimated iodine released at rupture (μg)	Estimated iodine released at rupture ($\mu g/cm^3$ He, STP)	Total cesium implanted (μg)	Total cesium released (μg)	Estimated cesium released at rupture (μg)	Estimated cesium released at rupture ($\mu g/cm^3$, He, STP)
2	700	221	33	5.3	4.9[a]	0.022	34	2.49	2.45[a]	0.011
5	700	340	610	109	103.0[a]	0.30	7050	381	378.0[a]	1.11
1	700	221	1600	362	356.0[a]	1.61	1680	180	179.5[a]	0.81
12	900	164	50	30	23[b]	0.14	1060	264	217[a]	1.32
8[c]	900	285	610	401	240[b]	0.84	9220	3311	1918[a]	6.73
3	900	164	630	162	65[b]	0.40	6340	486	290[a]	1.77

[a]Obtained by subtracting diffusional release from total release.

[b]Obtained from gamma monitoring of released iodine 5 min after rupture.

[c]Raised to 1100°C after rupture at 900°C.

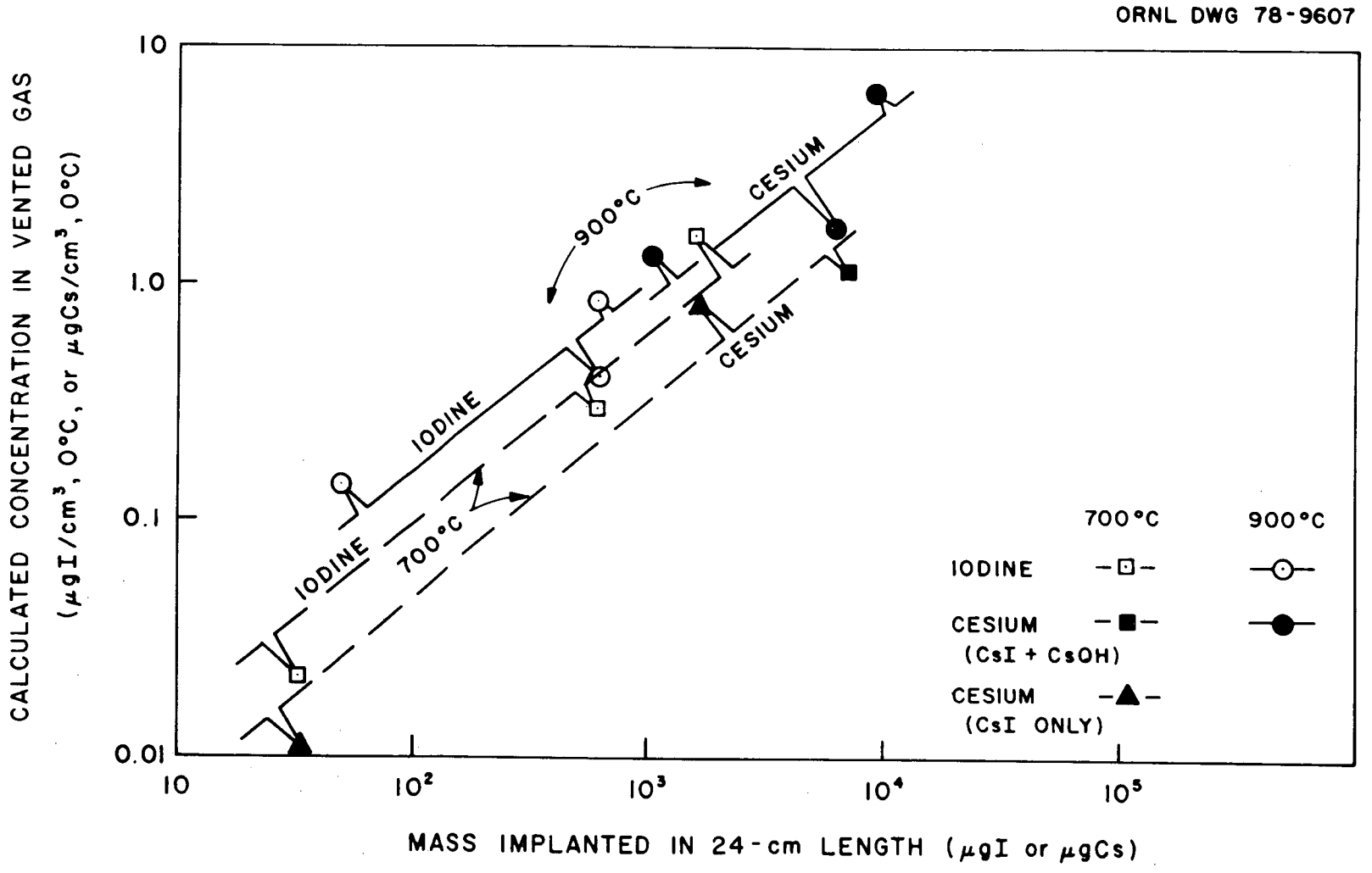

Fig. 73. The effect of mass of implanted cesium and iodine on their concentration in the vented gas.

4. The calculated concentrations are significantly lower than would occur with CsI vapor in equilibrium with CsI liquid, which are 6.2 μg I (or 6.5 μg Cs)/cm^3 (STP) at 700°C and 145 μg I (or 151 μg Cs)/cm^3 (STP) at 900°C.

It must be emphasized again that the calculated experimental concentrations of iodine and cesium in the vented gas are only approximate. Errors of a factor of 2 could easily occur since there was no accurate method for differentiating between amounts released at burst and later by diffusion. Even with this possible error, the calculated concentrations are well below those expected for CsI vapor at equilibrium with CsI liquid. Several mechanisms could explain why iodine implanted only as CsI would not behave as "ideal" CsI during the rupture blowdown: (1) at these low concentrations, sorptive forces can be quite strong, and the highest concentration of CsI implanted is equivalent to only several monolayers if one assumes equal distribution on pellet and cladding surfaces (with a roughness factor of 10 for these surfaces); (2) mass transfer inefficiency could inhibit the vaporization of the species present; and (3) chemical changes could have resulted in the formation of less-volatile species.

8.3 Release from Gap by Diffusion in Steam

Diffusion of fission products from the defect opening occurs following blowdown of the plenum gas. At this time, gas external to the fuel rod (usually steam) will diffuse into the gap space and may react chemically with fission products in the gap space. When steam is employed, significant amounts of hydrogen (0.01 to 20%) will be present in the steam outside of the fuel rod as a result of steam-zirconium reaction. Higher concentrations will be formed inside the gap space from steam diffusing into the rupture or drilled opening. Table 19 lists data from six tests for which diffusional release values were obtained. Tests 6 and 10 provided diffusion rates from cladding with a drilled 0.159-cm (0.0625-in.)-diam hole. Tests 3, 8, and 12 provided diffusion rates from fuel rods which experienced clad expansion and rupture at 900°C. A similar rupture was attempted in Test 4, but a leak that developed at the inlet-side

Table 19. Diffusional release of iodine and cesium in steam

Test No.	Temperature (°C)	Time (hr)	Iodine			Cesium		
			Amount implanted (µg)	Amount released by diffusion (µg)	Diffusional release rate (µg/hr)	Amount implanted (µg)	Amount released by diffusion (µg)	Diffusional release rate (µg/hr)
3	900	2.0	565[a]	97[a]	49	6050	196	98
4	1100	0.8	440	145	181	4920	1237	1547
6	500	20.0	900	5.76	0.29	10,270	<42	-
8	1100	0.96	370[a]	161[a]	168	7300	1393	1451
10	700	5.0	660	12.2	2.44	7070	4.84	0.97
12	900	2.0	27[a]	7.0[a]	3.5	843	47	23.5

[a]Amount obtained by subtracting estimated burst release from total release.

ferrule fitting prevented significant pressurization. Since it was observed that radioactive iodine was being released slowly, the test was continued and the results were treated as diffusional release.

The calculated diffusional release rates were plotted as a function of implanted mass in Fig. 74. The tests covered a wide temperature range with relatively little variation in implanted mass, yet the dependence is apparent. From this limited data set, it appears that the cesium release may vary with temperature more than iodine release.

Table 18 includes columns listing total release and estimated burst release. As noted in the table, the estimated burst release for most experiments was obtained by subtracting the estimated diffusional release (usually a small amount) from the total release (usually a much larger amount). The estimated diffusional release could only be obtained as very rough approximations from the data given in Fig. 68.

In spite of the limited amount of data, it is quite clear that the burst release, especially at 700°C, was much larger than release by diffusion at the same temperature.

8.4 Modeling Iodine and Cesium Release

Unfortunately, 12 experiments cannot supply sufficient data to formulate a comprehensive model for fission product release. However, we believe that the data presented in Figs. 73 and 74, which summarize the separate components for burst release and diffusional release, provide a basis for establishing such a model. The data shown in these figures were obtained only from simulated fission product compounds implanted in the gap space on UO_2 pellets. It is therefore recommended that these data be used in conjunction with fission product release measurements from highly irradiated LWR fuel in order to obtain the desired release model. The data shown in Figs. 73 and 74 are plotted as a function of inventory in the gap space, so that when comparing these data with release from irradiated fuel rods, an estimate of the irradiated-rod gap inventory (amount of cesium or iodine in the pellet-to-clad gap space) is required. For rupture into pressurized vessels, the volume of vented gas must be calculated at the system pressure

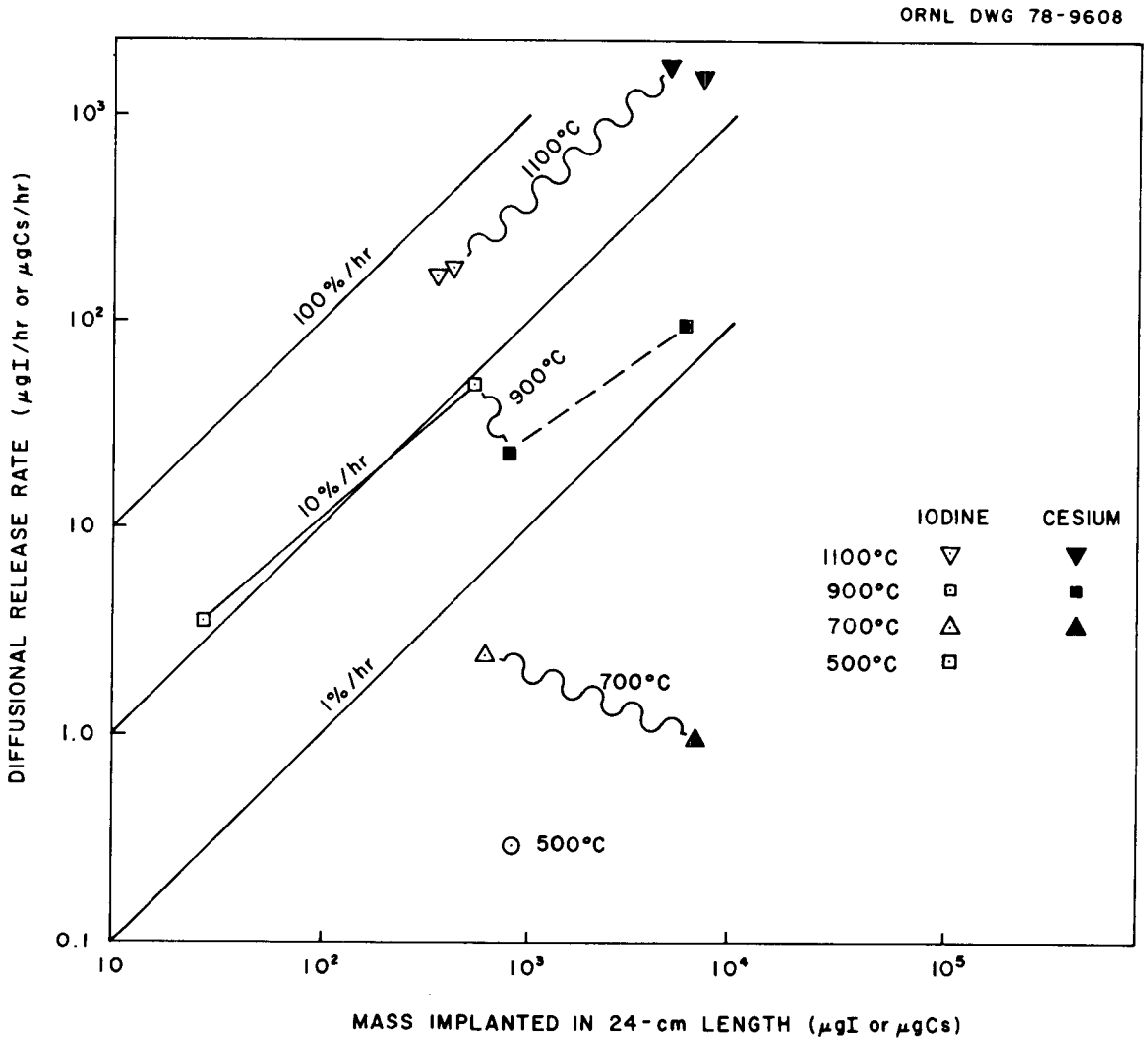

Fig. 74. The effect of mass of implanted cesium and iodine on their diffusional release rates from fuel rods defected in steam.

and reduced to 0°C in order to compare with data shown in Fig. 73. The diffusional release rates given in Fig. 74 are given for 0.1 MPa (atmospheric pressure); these release rates should be inversely proportional to absolute pressure.

8.5 Characteristics of Released Aerosol

The cascade impactor and high-efficiency filter media were used to collect and characterize the aerosol released during the implant tests. Although all of the flowing gas passes through the impactor, the amount of particulate material collected by the impactor stages and filter media is <100%. The larger particles tend to settle out in the furnace and thermal gradient tubes, and the smaller particles tend to deposit on equipment surfaces before entering the impactor.

The particulate material on the impactor collection papers and the first filter paper were analyzed for size distribution following the method of Parker and Buchholz.[18] The results are presented in Tables 20 and 21. The size particle collected by each stage depends upon particle density. The aerodynamic size assumed ρ = 1.0 g/cm^3; mass median sizes were calculated for ρ = 3.6 g/cm^3 (the density of CsOH) as well. The mass median diameter (MMD) for iodine-containing particles appeared larger and more scattered than for cesium-containing particles. The cesium MMD for the Implant Tests was very close to that found in the Control Test Series, as shown in Table 21.

Caution should be taken in making use of these size data. In addition to the large scatter, these sizes are unique to our apparatus and are not necessarily the same as might be found in a LOCA where the hot gas and the vapor which vented from a ruptured fuel rod would mix rapidly with a larger volume of relatively cool steam. This would tend to cause condensation of most cesium-containing species in the steam phase to form suspended particulates. In our test apparatus, by contrast, most of the vapors were forced to condense on the cool walls of the thermal gradient tube. As a typical value, only one-tenth of the cesium in our experiments passed through the thermal gradient tube and into the impactor assembly. No

Table 20. Characteristics of particulate material

Location	Implant Test 5 (700°C)			Implant Test 3 (900°C)			Implant Test 8 (900 to 1100°C)			Implant Test 11 (900 to 1300°C)		
	Aerodynamic cutoff diam, D_p (μm)	Amount at location Cs (%)	Amount at location I (%)	Aerodynamic cutoff diam, D_p (μm)	Amount at location Cs (%)	Amount at location I (%)	Aerodynamic cutoff diam, D_p (μm)	Amount at location Cs (%)	Amount at location I (%)	Aerodynamic cutoff diam, D_p (μm)	Amount at location Cs (%)	Amount at location I (%)
Stage 1	1.29	28.9	54.6	1.31	29.2	29.9	1.46	20.1	24.0	1.52	39.1	70.9
Stage 2	0.67	17.3	7.6	0.68	8.6	1.6	0.87	8.2	4.7	0.91	9.1	10.6
Stage 3	0.39	19.1	10.5	0.40	7.1	1.7	0.57	7.4	6.6	0.60	6.4	1.6
Stage 4	0.24	22.7	18.3	0.24	25.1	12.0	0.38	11.9	8.8	0.40	6.4	0.8
Stage 5	0.10	5.2	4.6	0.10	15.0	49.5	0.20	8.6	25.6	0.21	4.6	0.8
First filter	-	6.7	4.4	-	15.0	5.3	-	43.9	30.3	-	34.6	15.7

Table 21. Mass median diameter of particulate material

	Implant Test 5 500°C		Implant Test 3 900°C		Implant Test 8 900 to 1100°C		Implant Test 11 900 to 1300°C		Median of four implant experiments		Median of four control experiments
	Cs	I	Cs	I	Cs	I	Cs	I	Cs	I	Cs
Aerodynamic mass median diam (assumed density 1.0 g/cm^3)	0.60	1.8	0.33	0.22	0.33	0.22	0.87	1.8	0.44	0.77	
Mass median diam (assumed density 3.6 g/cm^3)	0.24	0.76	0.11	0.067	0.13	0.13	0.41	0.85	0.18	0.31	0.16

obvious size difference was observed between pressure-rupture and predrilled-defect experiments. The higher steam flow used in Tests 8 and 11 did appear to carry more aerosol and vapor through the thermal gradient tube.

As mentioned previously, the distribution of visible material collected on the impactor collection papers did not usually correspond to the distributions of cesium and iodine. Cesium iodide was identified by x-ray diffraction only on the fifth stage of Implant Test 8 and Control Test 10 (see ref. 1); $CsOH \cdot H_2O$ was found in a variety of stages in many different experiments.

9. MATERIAL BALANCE

Material balances were calculated for ^{130}I ($t_{1/2}$ = 12.4 hr) and ^{134}Cs ($t_{1/2}$ = 2.06 years) following each experiment. The ^{130}I balance was determined by comparing the activity of ^{130}I in the assembled fuel rod before the experiment with the sum of ^{130}I found on the system components after the experiment. The results are shown in Table 22. The mean value was 99.8% with a standard deviation (S.D.) of 5.6%.

Table 22. Material balances

Implant Test No.	Percent of implanted iodine found	Estimated percent of implanted cesium found
1	105	87
2	104	79
3	110	74
4	102	73
5	91	87
6	100	100
7	102	101
8	100	94
9	98	93
10	99	98
11	91	96
12	95	87
	Mean = 99.75 S.D. = 5.56	Mean = 89.1 S.D. = 9.7

Determination of the initial amount of ^{134}Cs was made indirectly. As described previously, the tracer isotopes were prepared by direct neutron activation of CsI before each experiment, resulting in an initial specific activity of ^{130}I approximately 70 times greater than ^{134}Cs. We therefore could not measure the amount of ^{134}Cs before the experiment with the NaI scintillation crystal but obtained a calculated initial amount by determining the ratio of ^{134}Cs to ^{130}I in an aliquot of the implantation solution. The amount of ^{134}Cs initially in the fuel rod was then determined by multiplying the initial ^{130}I by the above ratio. The results shown in Table 22 gave a mean value for the cesium material balance of 89.1%, with a S.D. of 9.7%. We believe that this slightly low number is the result of the method for calculating the initial amount of ^{134}Cs and a systematic error in counting geometries.

Similar balances were performed for the ^{123m}Te tracer, but the scatter was large because of the low energy and low specific activity of the ^{123m}Te employed. The total mass of each implanted chemical species was determined by weight. Neutron activation provided an independent verification of the mass in each experiment.

The accuracy of the release values was affected by the counting statistics and geometry. For data shown in Figs. 70 and 71, we estimate the following accuracy: for 10% release, ±1%; for 1% release, ±0.2%; for 0.1% release, +0.05%, -0.03%; and for 0.01% release, +0.02%, -0.01%. Additional scatter occurred because of lack of reproducibility in experiment parameters such as rupture hole size, amount of clad expansion, and axial thermal gradients. Application of these data to full-length fuel rod behavior would increase the possible amount of error.

10. CONCLUSIONS

10.1 The Effect of the Fuel Rod Gap Environment on the Volatility of Implanted CsOH and CsI

The partial pressure of cesium-containing species calculated to exist in the gas vented at rupture (Table 18) was more than a factor of 100 lower than the vapor pressure of CsOH,[22] the chemical form in which

90% of the cesium was implanted in Tests 3, 5, 8, and 12. This difference, shown graphically in Fig. 75, must be attributed principally to a chemical reaction between the CsOH and UO_2 to form a less-volatile cesium species such as Cs_2UO_4.

A similar decrease in cesium volatility was observed in the Knudsen cell tests[3] when Cs_2CO_3 was mixed with UO_2 powder. Furthermore, a mixture of CsOH and UO_2 powder displayed the same low cesium volatility as for the Cs_2CO_3-UO_2 mixture.

When cesium was implanted only as CsI (Test 1 and 2, Table 18), the calculated cesium partial pressures were a factor of 8 or more less than would occur with CsI[23] (see Fig. 75). Since iodine was implanted in all tests only as CsI, the calculated iodine partial pressure was a factor of 4 or more lower than that for CsI vapor in equilibrium with condensed CsI. These moderately lower experimental partial pressures for cesium and iodine implanted as CsI should not be interpreted as resulting from chemical changes. As discussed in Sects. 8.2 and 8.3, the volatility of cesium and iodine in these tests was found to depend upon the amount of material implanted, an observation which suggests that sorption forces were important at the low concentrations employed. Mass transfer inefficiency and difficulty in distinguishing the amounts released at rupture might also have contributed to the low partial pressures.

Sorption and mass transfer limitations would also contribute to the low cesium partial pressure observed when CsOH was implanted, but most of the large reduction must be attributed to compound formation. Although we did not positively identify any specific Cs-U-O compound, a recent thermodynamic analysis provides grounds for the existence of Cs_2UO_4 in the gap space of LWR fuels.[6]

10.2 Modeling Cesium and Iodine Gap Escape

The 12 implant tests were insufficient in number to develop a comprehensive release (gap escape) model. The data as presented in Figs. 73 and 74 do provide the basis for such a model. Separate, additive, releases can be calculated for burst release (that amount carried out with plenum

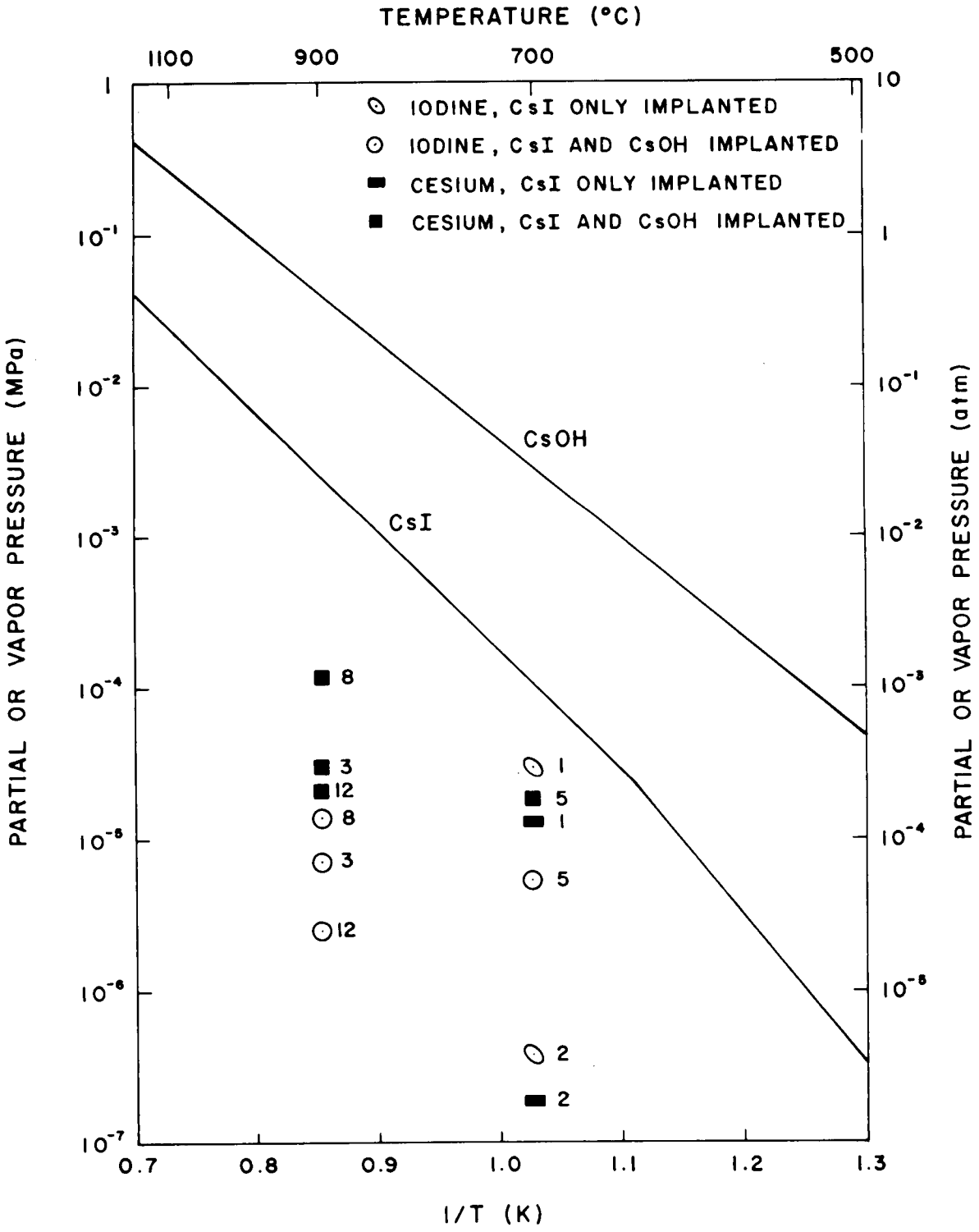

Fig. 75. Comparison of the partial pressures of cesium and iodine species vented from ruptured fuel rods with the vapor pressures of CsI and CsOH.

gas vented at rupture), and for diffusional release (the amount released following the blowdown of plenum gas while the fuel rod remains heated), as discussed in Sect. 8.4.

10.3 Iodine Behavior in Steam-Atmosphere Tests

At 900°C and higher, significant axial migration of the implanted CsI was observed (Sect. 8.2). When only CsI was implanted (Tests 1 and 2, Sects. 4.1 and 4.2), chemical changes occurred at 700°C so that the UO_2 pellets became rich in cesium and the cladding rich in iodine. It is believed that the hyperstoichiometric fuel reacted with the implanted CsI. Although I_2 was collected in every experiment, the percentage of the released iodine in the elemental form was usually greatest when the released mass was low, as shown in Fig. 66. The compound $Cs_2(Zr(IO_3)_6)$ was identified on the cladding of Test 2 by x-ray diffraction.

10.4 Cesium Behavior in Steam-Atmosphere Tests

Cesium in the flowing steam, after release from the fuel rod, existed mainly in two chemical forms: CsOH and CsI (any elemental cesium or cesium oxide exposed to steam would form CsOH). The CsOH reacted rapidly with the quartz furnace tube liner (see Fig. 56 for a typical distribution), but some was carried into the thermal gradient tube. Some of the CsI sorbed or condensed on cooler parts of the quartz furnace tube liner where a portion may have reacted with the quartz. Beginning with Test 8, the outlet end of the furnace tube was heated so that a higher percentage of the CsI was transported into the thermal gradient tube where condensation occurred in the 300 to 500°C temperature range.

10.5 Tellurium Behavior in Steam-Atmosphere Tests

As described in Sect. 7, tellurium, implanted as TeO_2, migrated to the cladding where reactions occurred that minimized release from the defected fuel rod. The reaction product(s) proved to be stable in the testing temperature range of 500 to 1300°C. It was determined by x-ray diffraction that the major constituent in a sample of the reaction

material was Te_2ZrO_5. Although not identified, zirconium telluride could also have been formed. The rate of transport of TeO_2 from the coated pellet interfaces to the cladding increased with temperature. Tellurium release from the fuel rod appeared to be more a function of rupture pressure than test temperature.

10.6 Iodine, Cesium, and Tellurium Behavior in Dry-Air-Atmosphere Tests

Iodine release was approximately a factor of 10 greater in dry-air tests than in steam. The iodine was collected almost exclusively as I_2. Cesium release was also significantly greater in dry air atmosphere, but the tellurium release was less.

11. REFERENCES

1. R. A. Lorenz, M. F. Osborne, J. L. Collins, and S. R. Manning, Behavior of Iodine, Methyl Iodide, Cesium Oxide, and Cesium Iodide in Steam and Argon, ORNL/NUREG/TM-25 (July 1976).
2. A. P. Malinauskas, "Use of Simulants for Fission Product Release," paper presented at the Second Light Water Reactor Safety Research Information Meeting, Sept. 19, 1974. See Nucl. Saf. 16, 19 (1975).
3. J. L. Collins, M. F. Osborne, A. P. Malinauskas, R. A. Lorenz, and S. R. Manning, Knudsen Cell-Mass Spectrometer Studies of Cesium-Urania Interactions, ORNL/NUREG/TM-24 (June 1976).
4. J. L. Margrave, The Characterization of High-Temperature Vapors, p. 503, Wiley, New York, 1967.
5. A. K. Postma and R. W. Zavadoski, Review of Organic Iodide Formation Under Accident Conditions in Water-Cooled Reactors, WASH-1233 (October 1972).
6. B. D. Epstein, A Review of the Literature Pertinent to Fission-Product Migration and Interaction in Fuel Rods, GA-A13423, UC-77, p. 13 (June 1975).

7. J. R. Soulen, P. Sthapitanoda, and J. L. Margrave, "Vaporization of Inorganic Substances: B_2O_3, TeO_2, and Mg_2N_3," paper presented at the Symposium on High-Temperature Chemical Reactions at the 126th Meeting of the American Chemical Society, New York, Sept. 15, 1954.

8. D. A. Collins, R. D. Collins, R. Taylor, A. E. McIntosh, and W. B. Roys, The Temperature-Gradient Tube Technique for Characterization of Released Fission Products, TRG Report 1332(W) (January 1967).

9. V. J. Tennery, pp. 23-32 in Voloxidation-Removal of Volatile Fission Products from Spent LMFBR Fuels, ed. J. H. Goode, ORNL/TM-3723 (January 1973).

10. M. Fischer, paper presented at the Third Water Reactor Safety Information Meeting, Gaithersburg, Md., September 1975.

11. Horst Feuerstein, Behavior of Iodine In Zircaloy Capsules, ORNL-4543, (August 1970).

12. D. R. Stull, ed., JANAF Tables of Thermochemical Data, Dow Chemical Co., Midland, Mich., 1965.

13. E. A. Buketov, L. I. Mekler, E. G. Nadirov, A. S. Pashinkin, and L. D. Trofimova, "Investigation of the Tellurium-Tellurium Dioxide System," Russ. J. Inorg. Chem. 9(1), 123-24 (January 1964).

14. A. P. Malinauskas, J. W. Gooch, and J. D. Redman, "The Interaction of Tellurium Dioxide and Water Vapor," Nucl. Appl. Technol. 8, 52 (1970).

15. J. Duchesne and B. Rosen, "Spectra of Bent Triatomic Molecules," J. Chem. Phys. 15, 641 (1947).

16. R. P. Agarwala, E. Govindan, and M. C. Naik, Crystallographic Data 32(6), 729 (May 1960).

17. R. C. Weast, Handbook of Chemistry and Physics, 55th ed., p. D-166, CRC Press, Inc., Cleveland, Ohio, 1974.

18. G. W. Parker and H. Buchholz, Size Classification of Submicron Particles by a Low-Pressure Cascade Impactor, ORNL-4226 (June 1968).

19. M. J. Kabat, "Selective Sampling of Hypoidous Acid," p. 506 in Proceedings of the Fourteenth ERDA Air Cleaning Conference, Aug. 2-4, 1976, CONF-760822 (February 1977).

20. J. G. Wilhelm and J. Furrer, "Head-end Iodine Removal from a Reprocessing Plant," p. 464 in Proceedings of the Fourteenth ERDA Air Cleaning Conference, Aug. 2-4, 1976, CONF-760822 (February 1977).

21. R. A. Lorenz, S. R. Manning, and W. J. Martin, "The Behavior of Highly Radioactive Iodine on Charcoal in Moist Air," pp. 323-52 in Proceedings of the Fourteenth ERDA Air Cleaning Conference, Aug. 2-4, 1976, CONF-760822 (February 1977).

22. R. Lide, Jr., ed., "JANAF Thermochemical Tables, 1974 Supplement," J. Phys. Chem. Ref. Data 3(2), 416-17 (1974).

23. R. C. Feber, Thermodynamic Data for Selected Gas Impurities in the Primary Coolant of High-Temperature Gas-Cooled Reactors, LA-NUREG-6635 (April 1977).

NUREG/CR-0274
ORNL/NUREG/TM-154
Dist. Category R3

INTERNAL DISTRIBUTION

1. R. E. Blanco
2-4. J. L. Collins
5. D. E. Ferguson
6. T. B. Lindemer
7-9. R. A. Lorenz
10-19. A. P. Malinauskas
20. F. R. Mynatt
21-23. M. F. Osborne
24. G. W. Parker
25. H. Postma
26. C. D. Scott
27. D. B. Trauger
28. R. P. Wichner
29. R. G. Wymer
30. Document Reference Section
31. Central Research Library
32. Laboratory Records — RC
33. Laboratory Records Department
34. ORNL Patent Section
35. E. L. Gaden (Consultant)
36. L. J. Colby (Consultant)
37. L. E. Swabb (Consultant)
38. K. D. Timmerhaus (Consultant)
39. G. R. Choppin (Consultant)

EXTERNAL DISTRIBUTION

40-44. Director, Division of Reactor Safety Research, Nuclear Regulatory Commission, Washington, DC 20555
45. Director, Research and Technical Support Division, DOE, ORO
46. J. Sisler, Division of Environmental Control Technology, DOE
47. K. Campe, Office of Nuclear Reactor Regulation, NRC
48. W. Lahs, Office of Nuclear Regulatory Research, NRC
49. D. Hopkins, Office of Standards Development, NRC
50. W. B. Murfin, Gesellschaft für Kernforshung, 7500 Karlsruhe Postfach 3640, West Germany
51-348. Given distribution as shown in category R-3
349-362. Special distribution by NRC

☆ U.S. GOVERNMENT PRINTING OFFICE: 1977-748-189/249